博士論文

Structural basis of the Rho effector recognition

(低分子量 G 蛋白質 Rho による標的蛋白質の認識機構の構造的基礎)

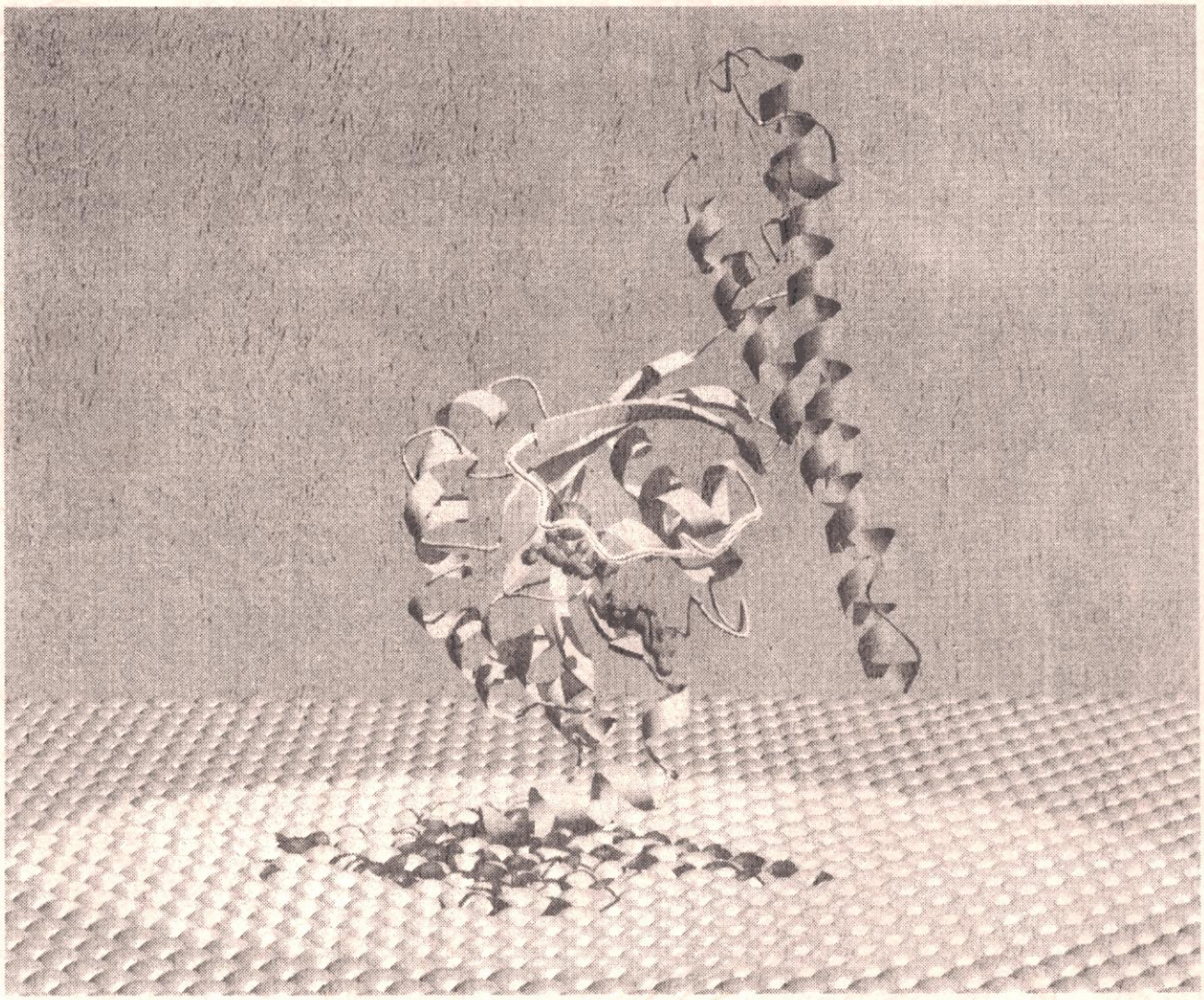

前崎　綾子

奈良先端科学技術大学院大学
バイオサイエンス研究科　生体高分子構造学講座
平成１４年　３月

バイオサイエンス研究科　博士論文要旨

所属 （主指導教官）	生体高分子構造学講座　　（箱嶋　敏雄）		
氏名	前崎　綾子	提出	平成　１４年　１月　８日
題目	Structural basis of the Rho effector recognition (低分子量 G 蛋白質 Rho による標的蛋白質の認識機構の構造的基礎)		

要旨

The Rho family small GTP-binding proteins such as Cdc42, Rac, and Rho participate in regulation of actin cytoskeleton and cell adhesion through specific target proteins. Rho-binding domains of these effector proteins have been classified into at least two motifs, class 1 and 2. The class 1 motif is characterized as a polybasic region followed by a leucine-zipper-like motif. The other motif, class 2, has a putative coiled-coil motif. To understand the molecular mechanisms of the Rho effector recognition, I determined the crystal structure of RhoA bound to the N-terminal effector domain of human protein kinase N (PKN) which has a class 1 Rho-binding motif. In addition, to obtain insights into the class 2 of Rho-binding motifs, I also determined the crystal structure of the Rho-binding region from Rho-kinase.

The crystal structure of the RhoA/PKN complex reveals that PKN has a novel effector domain for Rho, which is distinct from the other effector domains such as the CRIB domains for Cdc42 and Rac. The PKN effector domain binds to RhoA at switch I, β-sheet B2/B3, and the C-terminal α-helix A5. These binding regions are different from those for Cdc42 and Rac.

The interactions between switch I of RhoA and the effector domain of PKN shows how RhoA binds PKN in a GTP dependent manner. Thus, the present structure shows the various ways that the Rho family members interact with their effector proteins. Moreover, the present structure suggests that multiple effector domains may interact different molecular surfaces on the G protein.

The structure of the Rho-binding domain from Rho-kinase reveals parallel coiled-coil motif with long consecutive helices extending to about 97 A. The presence of long coiled-coil motif suggests that Rho-kinase is present in an oligomerization form in solution.

博士論文番号：9981035

Structural basis of the Rho effector recognition

(低分子量G蛋白質Rhoによる標的蛋白質の認識機構の構造的基礎)

前崎　綾子
奈良先端科学技術大学院大学
バイオサイエンス研究科　生体高分子構造学講座
（箱嶋　敏雄　教授）

平成１４年１月８日提出

Contents

I. Introduction

Rho is a small GTP-binding protein (small G protein) that has been identified as the gene product of the ras homologous gene. The Rho family of small G proteins, which have been purified from both mammalian tissue membrane (Yamamoto et al., 1988) and cytosol (Morii et al., 1988) fractions, have emerged as key regulators of several events in eukaryotic cells (Van Aelst and D'Souza-Schorey, 1997; Hall, 1998; Kaibuchi et al., 1999). Three members of the mammalian Rho family, Rho, Rac and Cdc42, have been well characterized in the context of cytoskeleton, cell adhesion and cytokinesis. Rho is implicated in the cytoskeletal responses to extracellular stimuli such as lysophosphatidic acid and bombesin, which result in the formation of stress fibers and focal adhesion in fibroblast cells (Ridley and Hall., 1992). Rac and Cdc42 are also involved in regulating the organization of actin cytoskeleton, whereas the cell morphological effects induced by these members are clearly different in appearance. Activation of Rac by platelet-derived growth factor, epidermal growth factor, or insulin leads to lamellipodium formation and membrane ruffling (Ridley et al., 1992), Cdc42 activated by bradykinin regulates filopodium formation (Kozma et al., 1995; Nobes and Hall, 1995) (Fig.1).

Rho has three mammalian isoforms, RhoA, RhoB and RhoC, that exhibit high sequence homology with 83% identities. Rac and Cdc42 share a significant homology with ~68% identities and, actually, bind to some common effector proteins for activation. However Rho exhibits relatively little similarity to both Rac and Cdc42 (~45% identities). These differences

in similarity are thought to be essential for the specific activation of several downstream effector proteins by each small G protein, although we do not yet understand the molecular mechanism defining the specificity.

Like other small G proteins, the Rho family members function as molecular switches, cycling between an inactive GDP-bound form and an active GTP-bound form. At least 10 candidate effector proteins for Rho have been identified so far. These proteins bind to Rho in a GTP-dependent manner. The Rho-binding domains of the effector proteins consist of less than 100 residues and have been classified into at least two motifs (Fujisawa et al., 1996; Bishop and Hall, 2000). The class 1 of the Rho-binding motif is characterized by a polybasic region followed by a leucine-zipper-like motif and is found in PKN, PRK2, Rhophilin and Rhotekin. Rho-kinase/ROKα, p160ROCK/ROKβ/ROCKII and Citron-kinase make up another class of the Rho-binding motif, class 2, that has a putative coiled-coil motif located at the C-terminus of the segment that is similar to myosin rod. Some proteins such as Bni1p or p140mDia are not yet classified (Fig. 2). Recently two protein serine/threonine kinases, Rho-kinase (Matsui et al., 1996), PKN (Amano et al., 1996a; Watanabe et al., 1996), whose kinase activities are activated by the Rho binding, have attracted a lot of attention.

PKN, which is identical to PRK1 and has an isoform PRK2 (Palmer et al., 1995a), is a serine/threonine protein kinase with a catalytic domain highly homorogous to that of protein kinase C (Nishizuka, 1995), and its kinase activity is enhanced by unsaturated fatty acids such as arachidonic acid (Mukai and Ono, 1994; Kitagawa et al., 1995). The N-terminal region of PKN contains a repeat of leucine zipper-like motifs, which have been suggested to be

involved in protein-protein association (Mukai et al., 1994; Kitagawa et al., 1995) (Fig.3). Moreover, a close inspection of the PKN sequence indicates that there are two additional regions homologous to the effector domain in the following to the N-terminal effector domain of PKN with spacers from 15 to 20 residues. This tandem repeat is unique among several effector proteins of small G proteins but is largely uncharacterized. PKN phosphorylates neurofilament proteins (Mukai et al., 1996), actin cross-linking protein α-actinin (Mukai et al., 1997), intermediate filament proteins such as glial fibrillary acid protein and vimentin (Matsuzawa et al., 1997). In addition, it interacts with a neural antigen PCD17 which is recognized by characteristic antibodies of patients with paraneoplastic cerebellar degeneration (Takanaga et al., 1998). These data suggest that PKN plays a specific role in the pathology of Alzheimer's disease (Kawamata et al., 1998). Recent biochemical studies have shown that PKN is also involved in apoptosis through proteolytic activation of its kinase activity by caspase-3 or related proteases (Takahashi et al., 1998). Moreover, Drosophila PKN has been found to be required for dorsal closure during embryogenesis (Lu and Settleman, 1999).

Rho-kinase, which has been purified from bovine brain, has a catalytic domain highly homologous to that of myotonic dystrophy kinase. Rho-kinase is composed of the N-terminal catalytic domain, a coiled-coil domain, the Rho-binding domain, and the C-terminal PH domain (Matsui et al., 1996) (Fig 4). The arrangement of these domains has also been observed in myotonic dystrophy protein kinase (DMPK) (Bush et al., 2000), myotonic dystrophy kinase-related Cdc42-binding kinase (MRCK) (Tan et al., 2001), citron kinase, and citron (lack of kinase domain) (Madaule et al., 1998). A model for the actin polymerization

and stress fiber formation is proposed in which Rho-kinase controls the phosphorylation of myosin light chain of myosin II by direct phosphorylation and by the inactivation of myosin phosphatase through the phosphorylation of MBS (Kimura et al., 1996; Amano et al., 1996b).

It is of considerable interest how Rho proteins recognize these types of effector domains that have no apparent homology each other. These domains have no sequence similarity to those of the Cdc42-effector domain of the activated Cdc42Hs-associated kinase (ACK) (Manser et al., 1993), the Rac1/Cdc42-effector domain of the p21 (Cdc42/Rac1)-activated protein kinase (PAK) (Manser et al., 1994) or the Ras-effector domain of Raf-1 (Fabian et al., 1994).

To understand the molecular mechanisms of the Rho effector recognition, I have determined the crystal structure of RhoA bound to the N-terminal effector domain of human PKN, which has a class I Rho-binding motif. In addition, to obtain insights into the class 2 of Rho-binding motifs, I have also determined the crystal structure of the Rho-binding region of Rho-kinase.

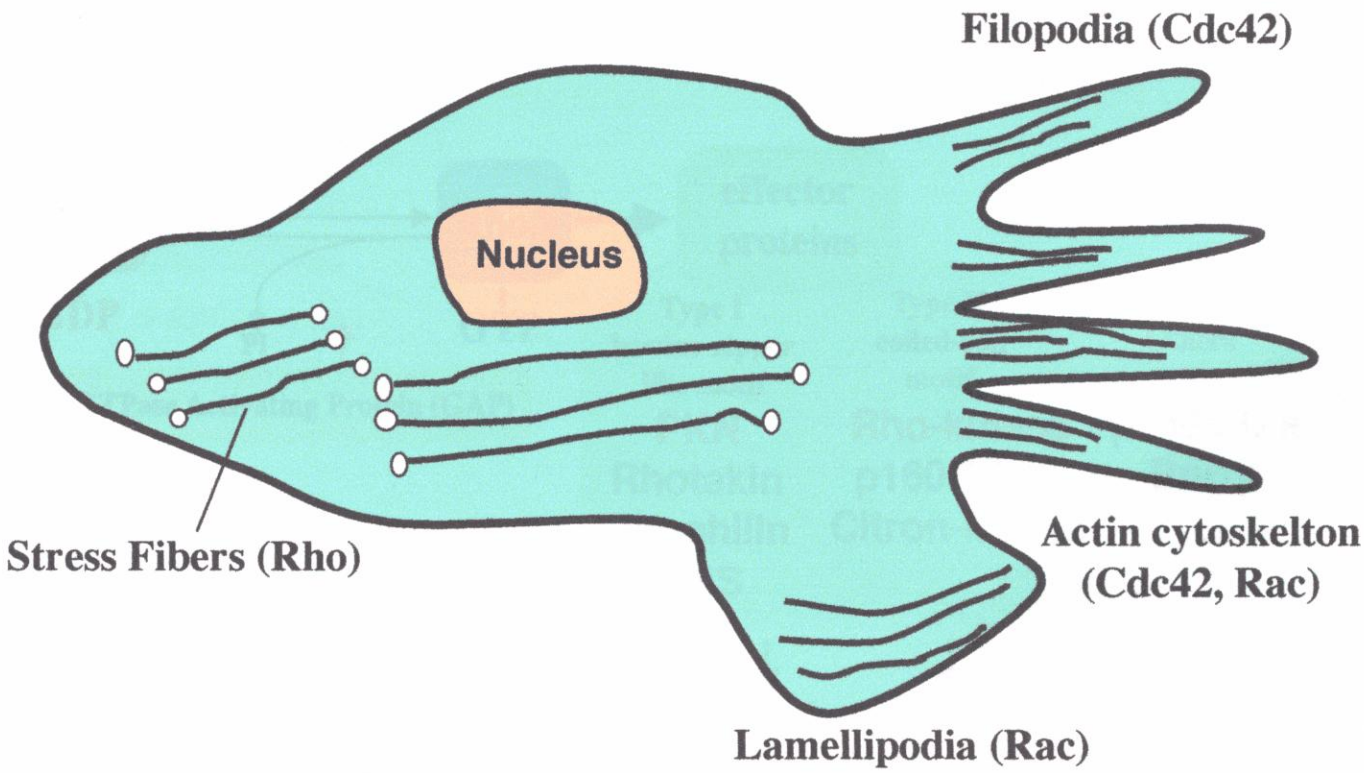

Fig.1. Rho family Small G Proteins

The Rho family Small G proteins are involved in regulating the organization of actin cytoskeleton and the cell adhesion molecules.The Rho and the Rac subfamily members induce different cell morphologies. RhoA, RhoB, and RhoC regulate the formation of focal adhesions and stress fibers. Rac1, Rac2, and Cdc42 regulate the formation of lamellipodia, filopodia and focal complexes.

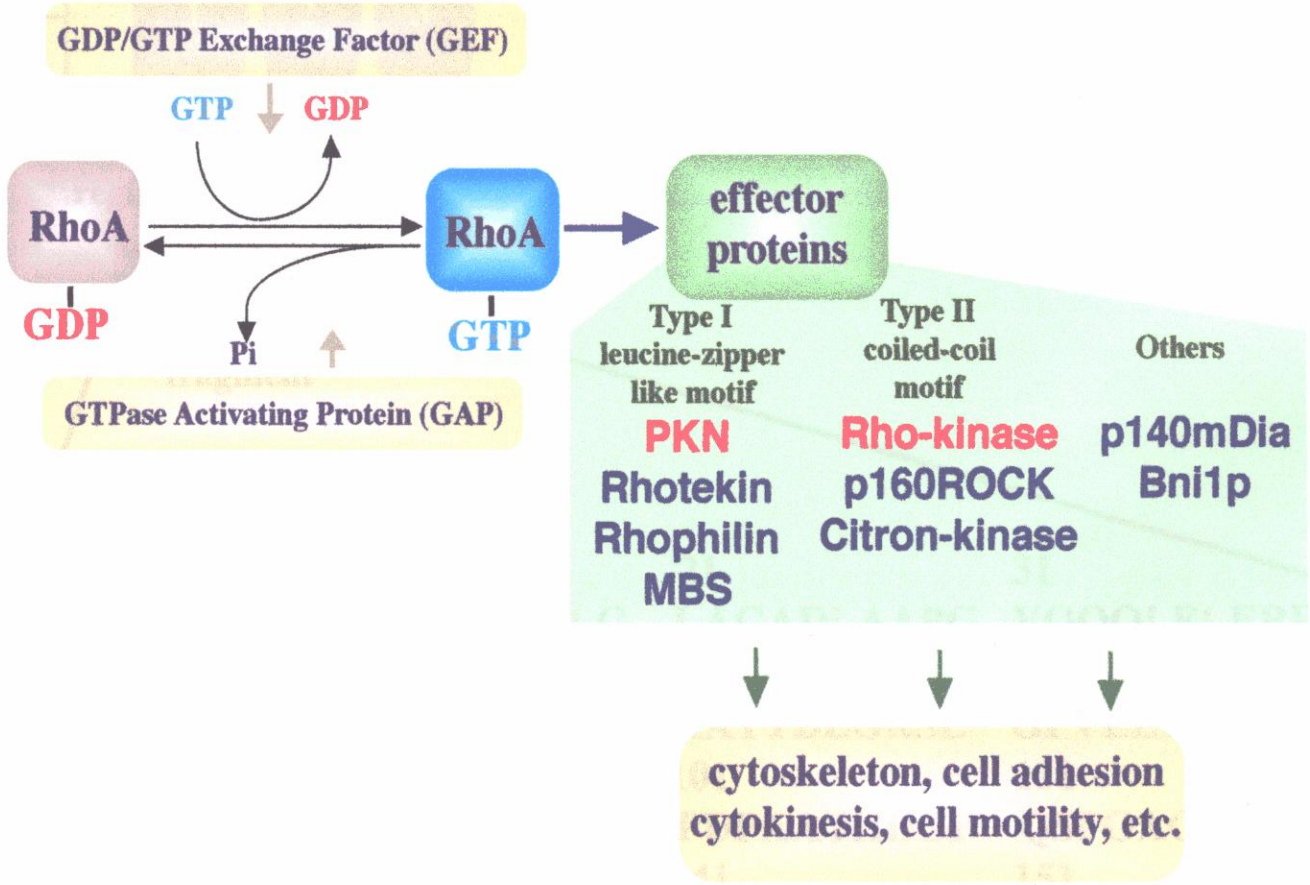

Fig.2. Small G Protein Rho and its Effector Proteins

Rho functions as molecular switches, cycling between an inactive GDP-bound form and an active GTP-bound form. Usually, this cycle is regulated by GDIs, GEFs, and GAPs. The GTP-bound form can interact with their downstream effector proteins. The effector proteins that bind to Rho in a GTP-dependent manner have at least two different Rho binding motifs.

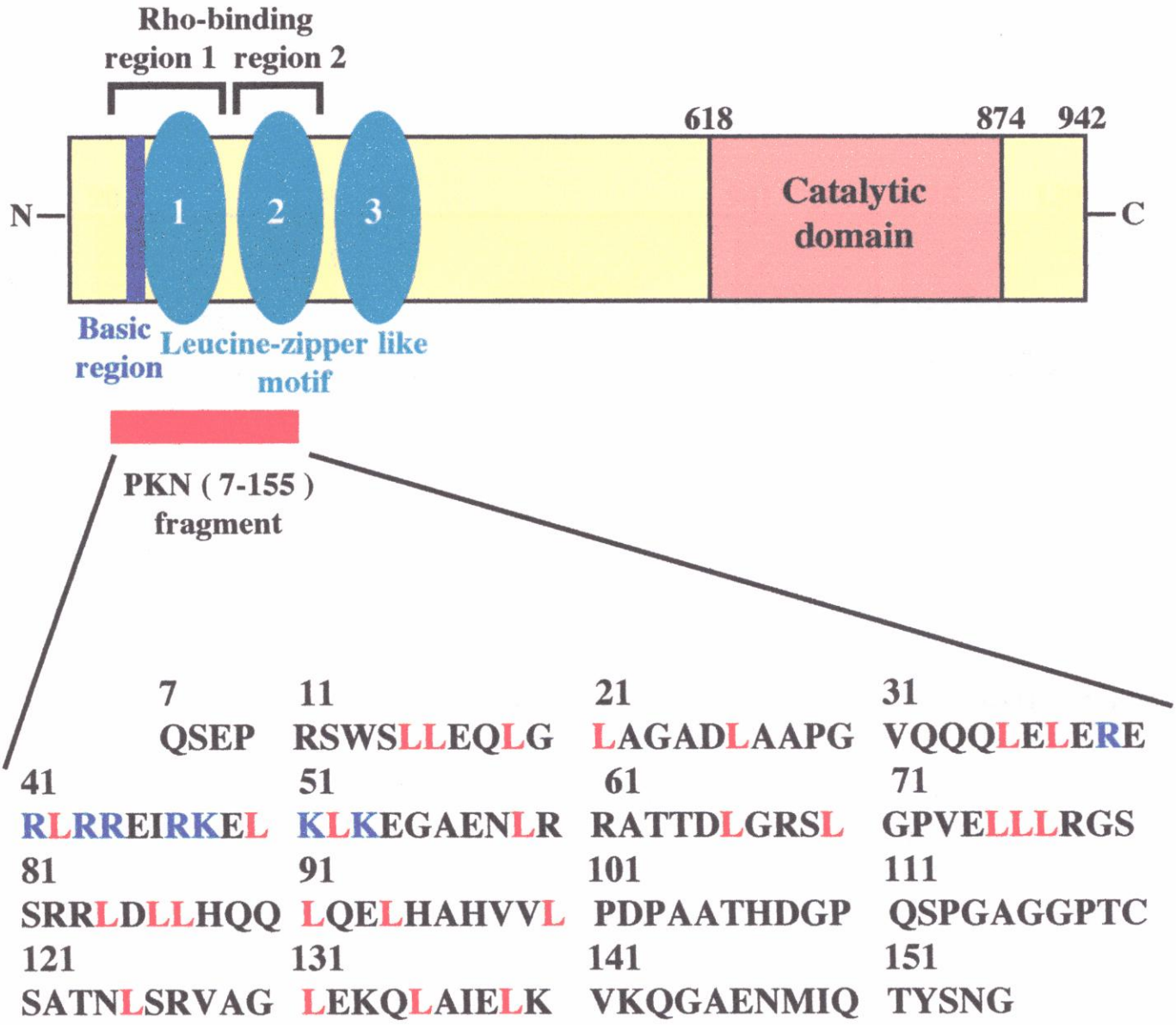

Fig.3. Domains of PKN

The N-terminal basic region (blue), three leucine zipper-like motifes (green), and the catalytic domain (rose) are indicated. The red bar under the diagram indicates the PKN (7-155) used for the present work. In the sequence of PKN (7-155), the leucine repeats and the basic amino acids in the N-terminal region are colored in red and blue respectively.

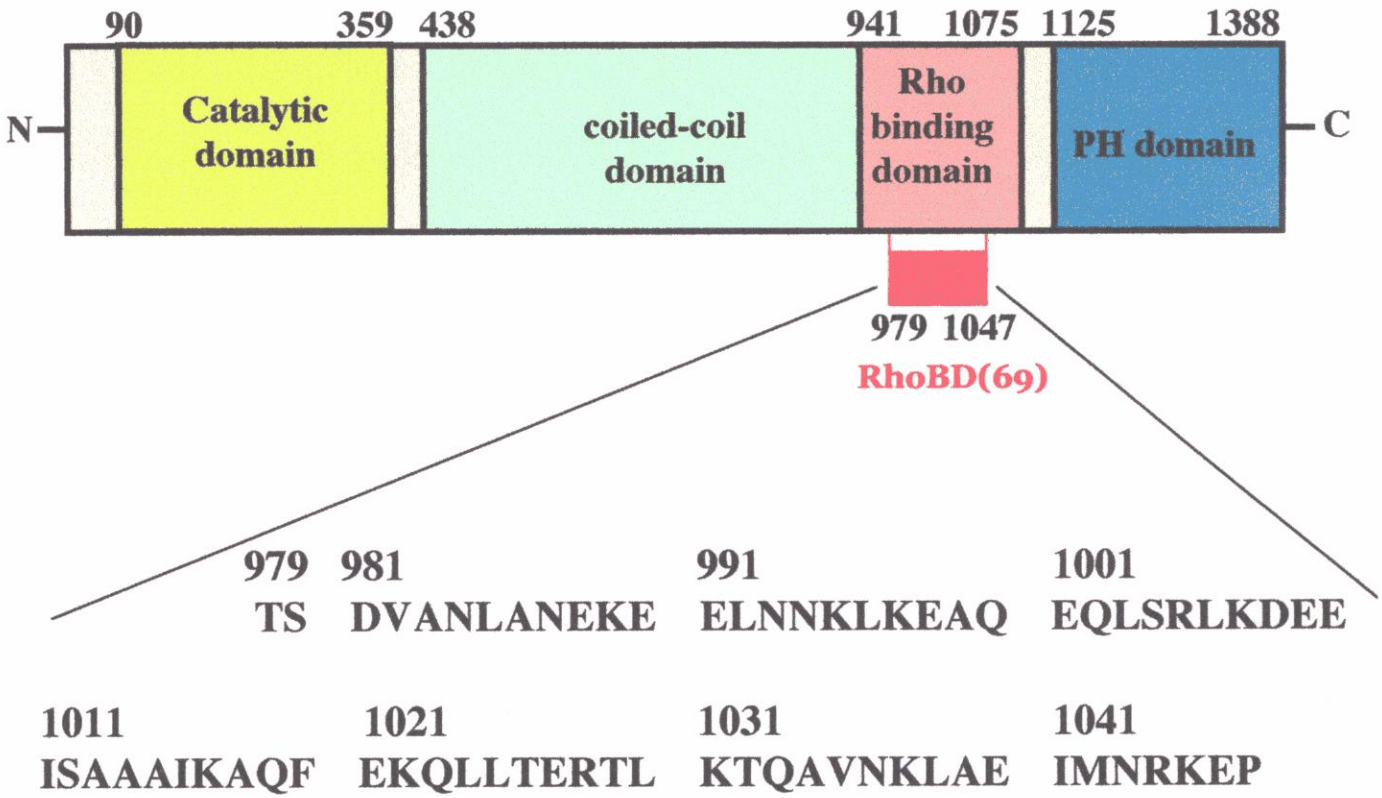

Fig.4. Domains of Rho-kinase

The N-terminal catalytic region (yellow green), coiled-coil domain (light green), the Rho binding domain (rose), and the PH domain (green) are indicated. The red bar under the diagram indicates the RhoBD(69) used for the present work.

II. Crystal Structure of the RhoA/PKN Complex

1. Materials and Methods

Expression and Purification

PKN have unique N-terminal regulatory regions that contain a tandem repeat of three leucine zipper-like sequences with ~25% identities and a basic region adjacent to the first repeat (Fig.3). The basic region plus the first repeat are sufficient for binding to RhoA in a GTP-dependent manner (Shibata et al., 1996). In fact, residues 7-155, showed an almost full binding activity in a GTP dependent manner (Amano et al., 1996a). Therefore we used PKN(7-155) for our biochemical and structural studies.

PKN(7-155) was subcloned into pGEX-2T (Amersham Pharmacia Biotech), and the glutathione-S-transferase (GST)-fused protein was expressed in *E.coli* DH5α cells. The GST-fused protein was purified over two steps of column chromatography, using glutathione Sepharose 4B and Mono-Q (Amersham Pharmacia Biotech). The purified GST-PKN(7-155) was cleaved by human thrombin (Sigma) with 6 units/ml for 3 hours at 4℃. Then, 5 mM p-amidino-phenyl-methanesulfonyl fluoride was added to stop the proteolytic reaction. The resultant PKN(7-155) was purified over three steps of column-chromatography, using glutathione Sepharose 4B, Hitrap SP, and Sephacryl S-100 (Amersham Pharmacia Biotech). The purified samples used in this study were verified with matrix-assisted laser desorption/ionization time-of-flight mass spectroscopy, MALDI-TOF MS (JMS-ELITE, PerSeptive Inc) and N-terminal analysis (M492, Applied Biosystems). The molecular weight of the purified PKN(7-155) observed by MALDI-TOF MS was 16,510 Da, which is virtually

the same as its calculated value (16,508 Da).

Like H-Ras and other small G proteins, the C-terminal tail of RhoA is hydrophobic and contains a Cys residue which is post-translationally modified by geranyl-geranylation to localize it to membrane. This region is believed to have no effect on intrinsic molecular function, while it is essential for the partitioning between membrane and cytosol. Actually, no changes in GTPase activity, effector binding, or activation of effector proteins have been reported for small G proteins truncated at the C-terminal tails. Moreover, the crystal structure of truncated H-Ras proteins was essentially the same as that of a full length form that displayed the disordered C-terminal tail (Milburn et al., 1990). To avoid unfavorable interference of the unstructured tail on crystallization, the C-terminal tail (residues 182-193) were truncated from RhoA. I chose a dominantly activated form with substitution of Gly-14 by valine ($RhoA^{V14}$), which exhibits about ten times lower GTPase activity to the wild type one, but does not affect the binding to PKN and other effector proteins. Since this dominantly activated form of RhoA still has residual GTPase activity, which may be significant for the crystallization time-scale, we used a nonhydrozylable GTP analog, guanosine 5'-3-*O*-(thio)-triphosphate (GTPγS). A truncated (residues 1-181) $RhoA^{V14}$ was subcloned into pRSET B (Amersham Pharmacia Biotech), and expressed in *E.coli* DH5α cells as His-tagged protein. The His-tagged proteins were purified over two steps of column chromatography, using Ni-NTA-agarose (QIAGEN Inc.) and MonoQ (Amersham Pharmacia Biotech). During the purification, 1 mM $MgCl_2$ was added to the purification buffers. The purified protein was a mixture of GDP and GTP form. Excess amounts of ethylene diamine-N,N,N',N'-tetraacetic

acid (EDTA) and GTPγS were added to a solution of the purified protein and gel-filtrated to remove unbound GDP, GTP, and GTPγS. The purified samples used in this study were verified with MALDI-TOF MS and N-terminal analysis. These results showed the spontaneous truncation of N-terminal His-tag during the preparation and one additional serine residue at the N-terminus. At room temperature, GTPγS bound to $RhoA^{V14}$ was stable for one month.

Binding assay and RhoA/PKN Complex Preparation

Analyses of the interactions between $RhoA^{V14}$ and PKN(7-155) were performed by both electrophoretic mobility shift assay (EMSA) on 6% polyacrylamide gel and gel filtration using a Superose 12 equipped FPLC system (Amersham Pharmacia Biotech) or Sephacryl S-100 columns attached to a HiLOAD system (Amersham Pharmacia Biotech). For EMSA, 4 ul of 30 μM-120 μM purified $RhoA^{V14}$ and PKN(7-155) were loaded in a stoichiometric range from 1:0.5 to 1:3. Mixtures of the GTPγS-bound form of $RhoA^{V14}$ and PKN(7-155) produced each shift band for the complex on EMSA gels, whereas the GDP-bound form of $RhoA^{V14}$ mixed with PKN(7-155) gave no shift band (Fig.5), indicating the binding of $RhoA^{V14}$ to PKN(7-155) is GTP-dependent. These results are consistent with the previous data using other methods such as affinity chromatography, two-hybrid assay, and ligand-overlay assay (Amano et al., 1996; Watanabe et al., 1996; Shibata et al., 1996). Interestingly, the band for unbound $RhoA^{V14}$ was observed when a 1:1 mixture of $RhoA^{V14}$- GTPγS and PKN(7-155) was loaded, suggesting that $RhoA^{V14}$ and PKN(7-155) form a complex with 1:2 stoichiometry in a

GTP-dependent manner. For gel filtration, Superose 12 was equilibrated with 20 mM HEPES buffer (pH 7.5) containing 5 mM $MgCl_2$ and 10 mM β-mercaptoethanol with 50 mM, 140 mM, or 500 mM KCl. For each gel filtration experiment, 200μl of a mixture solution of the purified $RhoA^{V14}$ and PKN(7-155) were loaded with 1:1 or 1:2 stoichiometry. The $RhoA^{V14}$ / PKN(7-155) complex was eluted from a Superose 12 gel filtration column at a position distinct from that of $RhoA^{V14}$ or PKN alone. The elution profile of a 1:1 mixture gave a peak for unbound $RhoA^{V14}$, which contained roughly half of the loaded $RhoA^{V14}$ (Fig.6A). The elution profile also contained a peak for the complex with 55 kDa which was obtained from a calibration curve. This obtained molecular weight was virtually the same as the calculated value (55.3 kDa) of the 1:2 complex, while the calculated value of 1:1 complex is 38.8 kDa. The 1:2 complex was also indicated by SDS-PAGE for the fractions of the complex peak. For crystallization, the $RhoA^{V14}$/PKN(7-155) complex formed by incubating PKN(7-155) and $RhoA^{V14}$ with 1:2 stoichiometry was purified using Sephacryl S-100. The elution profile contained a peak corresponding to the 1:2 complex without any significant peak for residual proteins (Fig.6B).

Crystallization

The best crystals of the complex were obtained in 5 μl of microbatch containing 2 mg/ml $RhoA^{V14}$/PKN(7-155) complex with 50 mM Bis-tris (pH6.5), 15 mM $Ca(CH_3COO)_2$ and 15% polyethylene glycol (PEG) 300 and maintained for a week at 4℃. Prismatic crystals with maximum size of 0.3×0.2×0.1 mm were obtained in a week (Fig.7A). Crystals were

thoroughly washed and dissolved in buffer, and then the solution was analyzed with MALDI-TOF MS and SDS-PAGE. These results indicated that crystals contained two proteins with observed peaks of 16,583 Da and 22,372 Da, which correspond to the calculated values of 16,508 Da for PKN(7-155) and 22,328Da for $RhoA^{V14}$, respectively. This was also verified by SDS-PAGE (Fig.7B).

Data Collection

Crystals of the truncated $RhoA^{V14}$ bound to GTPγS and Mg^{2+} complexed with the N-terminal effector domain of PKN (in the following referred to as $RhoA^{V14}$/PKN complex) were obtained by the microbatch method and were flash frozen in liquid nitrogen for data collection. X-ray diffraction data were collected at 2.2A resolution (Fig.8) using a Rigaku R-Axis IV on a rotating anode generator (Rigaku FR-C) operating at 50 kV and 60 mA with Cu-K_α radiation (λ = 1.54178 A) at 100K using a Rigaku Cryosystem. The focus size of the X-ray beam was 100 μm, and the beam was focused using a Supper double-focusing mirror (Charles Supper, USA). The distance from a crystal to an imaging plate was 150 mm. The data of 300° rotation were collected at a rate of 2° per 30 min for each image. All data were processed using the programs DENZO and SCALEPACK (Otwinowski & Minor, 1997) (Table 1). Each intensity, *I(h k l)*, was evaluated from the imaging plates and transformed to the amplitude of structure factor, *F(h k l)*, where *h*, *k*, and *l* are the reciprocal lattice points. The crystals belong to the tetragonal space group $P4_12_12$ or $P4_32_12$, with unit cell dimensions $a = b = 66.90$ A, $c = 149.54$ A. A total of 696,854 independent measurements were merged to obtain 17,568

unique reflections. The R_{merge} value based on intensity data (1.0 σ cutoff) was 9.0% with a completeness of 95.7% (in the highest-resolution shell of 2.28 - 2.20 A with an R_{merge} of 31.2% and a completeness of 85.7%). The I/σ(I) ratio is 24.0 for all data and 2.8 in the highest shell (Table 2). The reliability of data, R_{merge}, is defined by,

$$R_{merge} = \frac{\sum_{hkl}\sum_{i}\left|I_i(hkl) - \langle I(hkl)\rangle\right|}{\sum_{hkl}\sum_{i} I_i(hkl)} \times 100,$$

for n independent reflections and i observations of a given reflection. $<I(hkl)>$ is the average intensity of the i observations. The typical value of R_{merge} is under 10%.

The number of molecules per unit cell, Z, can be estimated by a V_m value which is the ratio of the unit cell volume and the molecular weight (Matthews, 1968). The V_m value can be calculated by,

$$V_m = \frac{V_{cell}}{M_r Z} \quad ,$$

where V_{cell} is the volume of the unit cell, and M is the molecular weight of the protein. V_m values usually range between 1.7 and 3.5 A^3/Da for protein crystals. The solvent content of the crystal, V_{solv}, is calculated from V_m values by,

$$V_{solv} = \left(1 - \frac{1.23}{V_m}\right) \times 100,$$

Assumption of one 1:1 complex of $RhoA^{V14}$/PKN(7-155) in the asymmetric unit gives a V_m value of 2.2 A^3/Da (a solvent content of 44 %), which is within commonly found values. In contact, assumption of one 1:2 complex of $RhoA^{V14}$ / PKN(7-155) in the asymmetric unit gave a V_m value of 1.5 A^3/Da and a solvent content of 22%, which is too small for a protein crystal.

The 1:1 stoichiometry was also verified by SDS PAGE (Fig.7B) and MALDI-TOF MS of a solution in which the crystals were dissolved.

Phasing with Molecular Replacement Method

The electron density $\rho(x\ y\ z)$ of the crystal is calculated with structure factors, $\mathbf{F}(h\ k\ l)$, by,

$$\rho(xyz) = \frac{1}{V}\sum_{h}\sum_{k}\sum_{l}\mathbf{F}(hkl)e^{-2\pi i(hx+ky+lz)},$$

$$\mathbf{F}(hkl) = F(hkl)e^{i\alpha(hkl)},$$

and,

$$|F(hkl)|^2 = I(hkl),$$

where x, y, and z are relative coordinates in the real space unit cell, and h, k, and l are the reciprocal lattice points. The X-ray diffraction experiments give only the intensities, $I(h\ k\ l)$, yielding to the amplitudes of structure factors, $F(h\ k\ l)$. To obtain the electron density, the phase angles of structure factors, $\alpha(h\ k\ l)$, are needed. There are several techniques to obtain protein crystal phases using heavy atom isomorphous replacement method, anomalous scattering method, or molecular replacement method.

The molecular replacement method (Rossmann and Blow, 1962) can be applied if the structure of the protein or homologous proteins was already established. In our studies the initial phases were calculated by the molecular replacement method with the program AMoRe (Navaza, 1994) using a search model based on the human $RhoA^{V14}/GTP\gamma S/Mg^{2+}$ structure (Ihara et al., 1998). The orientation and position of the molecule in the target unit cell were determined using rotation and trunslation functions (Crowther and Blow, 1967; Crowther,

1972).

Reliability of the solutions in the molecular replacement method are judged by calculating an *R*-factor, *R*, and the correlation coefficient, *Cc*, defined as,

$$R = \frac{\Sigma \left| |\mathbf{F}_{obs}| - k|\mathbf{F}_{calc}| \right|}{\Sigma |\mathbf{F}_{obs}|},$$

$$k = \frac{\Sigma |\mathbf{F}_{obs}| \, |\mathbf{F}_{calc}|}{\Sigma (|\mathbf{F}_{calc}|)^2},$$

and,

$$Cc = \frac{\Sigma (|\mathbf{F}_{obs}|^2 - \overline{|\mathbf{F}_{obs}|^2})(|\mathbf{F}_{calc}|^2 - \overline{|\mathbf{F}_{calc}|^2})}{\left[\Sigma (|\mathbf{F}_{obs}|^2 - \overline{|\mathbf{F}_{obs}|^2})^2 \Sigma (|\mathbf{F}_{calc}|^2 - \overline{|\mathbf{F}_{calc}|^2})^2\right]^{1/2}}$$

Both schemes gave the agreement index between calculated structure factors, $\mathbf{F}_{calc}$, and observed structure factors, $\mathbf{F}_{obs}$. The *R*-factor includes a scale factor *k* for the intensities, while the correlation coefficient is scaling insensitive. In the refinement, the *R*-factor has to be minimized and the correlation coefficient has to be maximized.

Several searches using different ranges of intensity data and integration radii resulted in a unique solution. After calculations of possible eight space groups, *P*422, *P*42$_1$2, *P*4$_1$22, *P*4$_1$2$_1$2, *P*4$_2$22, *P*4$_2$2$_1$2, *P*4$_3$22, *P*4$_3$2$_1$2, the highest correlation coeficient and the lowest R-factor were obtained when the crystal belong to *P*4$_1$2$_1$2. A summary of the solutions of rotation and translation function by AmoRe is given in Table 3, Table 4. Rigid body refinements of the search model performed with the program CNS (Brunger et al., 1998), resulted in a correlation coefficient of 0.669 and *R*-factor of 44.8% in *P*4$_1$2$_1$2. The resultant initial map shows clear electron densities for most of RhoA^{V14}, and residual densities for the PKN

effector domain, exhibiting typical features for helices in a coiled-coil form.

Structure Refinement

The models were built and refined through alternating cycles using the programs O (Jones et al., 1991) and CNS, respectively. Two regions of the PKN effector domain were poorly defined in the resulting map. The first is at the six N-terminal residues, and the second is at the 60 C-terminal residues that are followed by helix 3. After several cycles of refinement, I could not define these regions that have uninterpretable densities that imply complex disorder. The final model, which was refined with a crystallographic R_{value} of 21.4% (free R_{value} of 26.8%) for all intensity data at 2.2 resolution, includes 86 residues of the PKN effector domain (spanning residues 13-98), $RhoA^{V14}$ (residues 1-181), one GTPγS molecule, one magnesium ion, and 115 water molecules. A summary of the refinement statistics is given in Table 5. The PKN effector domain may have two rotamers of the His-88 side chain in the imidazole ring plane, which could not be determined in the current analysis. There is no residue in disallowed regions of the Ramachandran plots as defined in PROCHECK (Laskowski et al., 1993) (Fig.10). The structure was inspected using the programs QUANTA (Molecular Simulators Inc.), GRASP (Nicholls et al., 1991), MOLSCRIPT (Kraulis, 1991) and raster3d (Merritt EA et al., 1994).

The atomic coordinates and structure factors (code 1cxz) were submited to the Protein Data Bank, Research Collaboratory for Structural Bioinformatics.

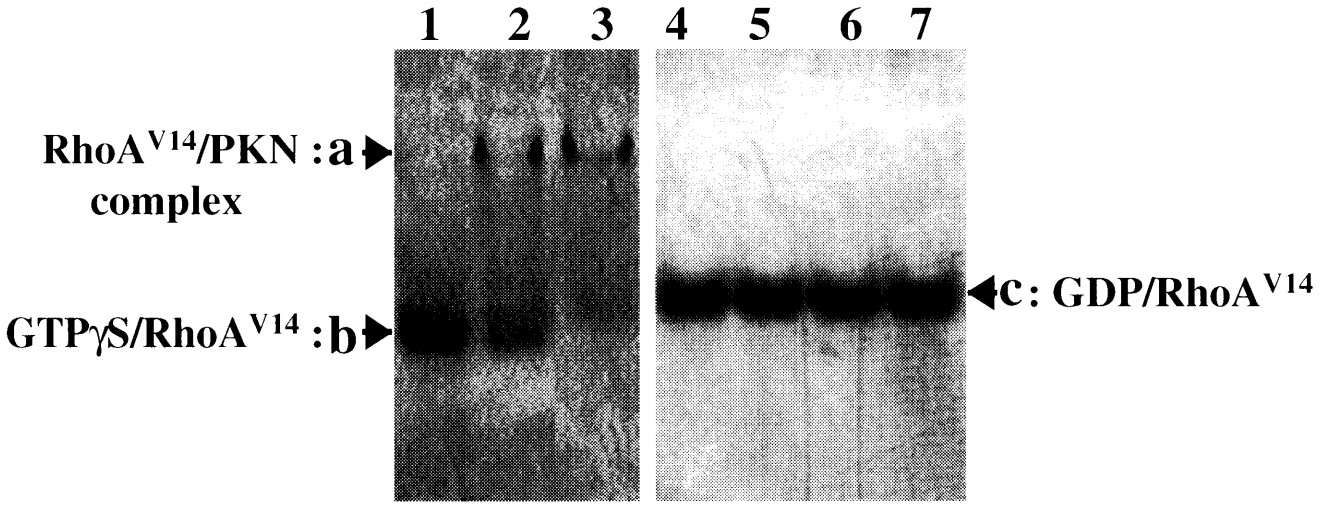

Fig.5. RhoA^{V14}/PKN(7-155) analyzed by EMSA

The GTPγS-bound form of RhoA^{V14} (lanes 1-3) and the GDP-bound form of RhoA^{V14} (lane 4-7) were analyzed by EMSA with the PKN (7-155) fragment. The shift bands marked by a correspond to the complex. The bands marked by b and c are for the GTPγS-bound forms and GDP-bound forms of RhoA^{V14}, respectively. Lanes 2 and 3 contain RhoA^{V14} and PKN(7-155) with 1:1 and 1:2 stoichiometry, respectively. Lane 5, 6, and 7 contain RhoA^{V14} and PKN(7-155) with 1:1, 1:2, and 1:3 stoichiometry, respectively.

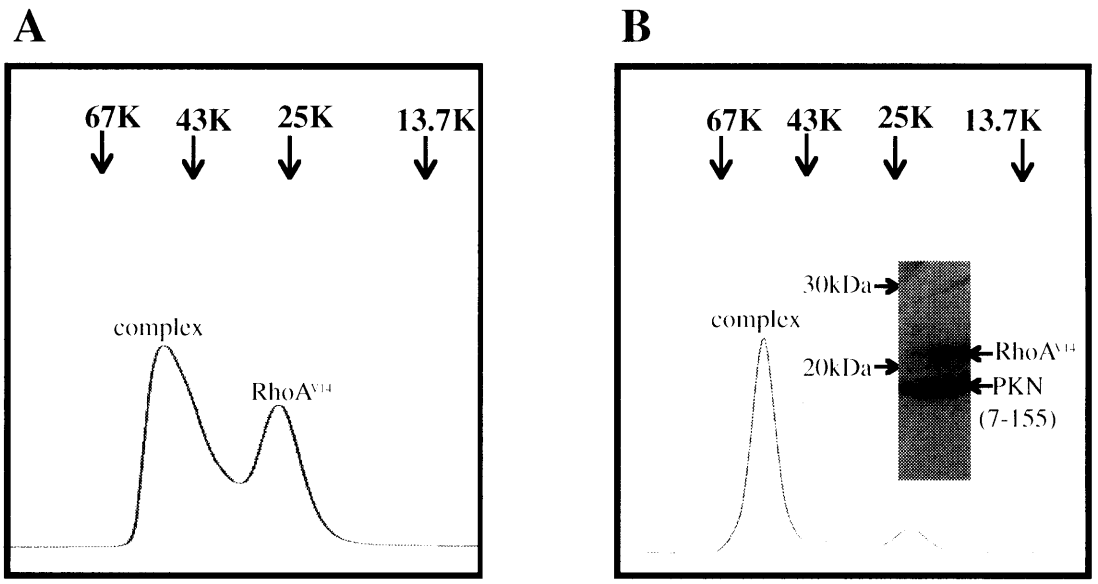

Fig.6. RhoA^{V14}/PKN(7-155) analyzed by Gel Filtration

(A) The 1:1 mixture of RhoA^{V14} -GTPγS and PKN (7-155) yielded a peak for residual RhoA^{V14} on the elution profile of gel filtration using Superose 12. Arrows indicate the positions of molecular size markers. The peaks correspond to the complex, and RhoA^{V14} -GTPγS are indicated with labels.

(B) An elution profile of gel filtration using Sephacryl S-100. The 1:2 mixture of RhoA^{V14} -GTPγS and PKN (7-155) was incubated and was loaded on the column. The purified complex was used for crystallization. The inset shows SDS-PAGE of the complex's peak.

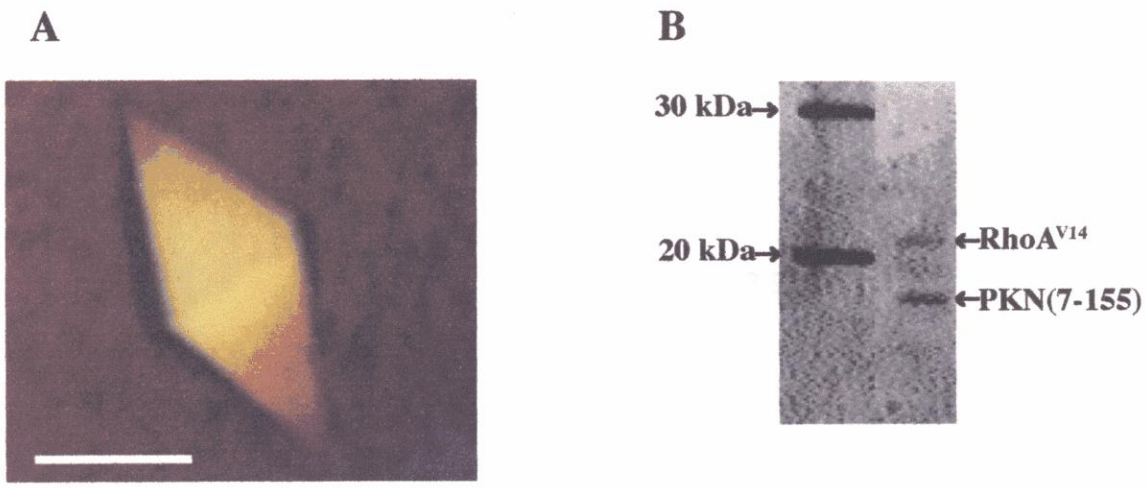

Fig.7. A Crystal of the RhoA^{V14} / PKN (7-155) Complex and SDS-PAGE of the Crystal
(A) A crystal of the RhoA^{V14} /PKN(7-155) complex. The scale bar is 100 μm-long.
(B) A SDS-PAGE of the complex crystal. The left side bands are marker, and the right side bands are RhoA^{V14} and PKN(7-155), respectively.

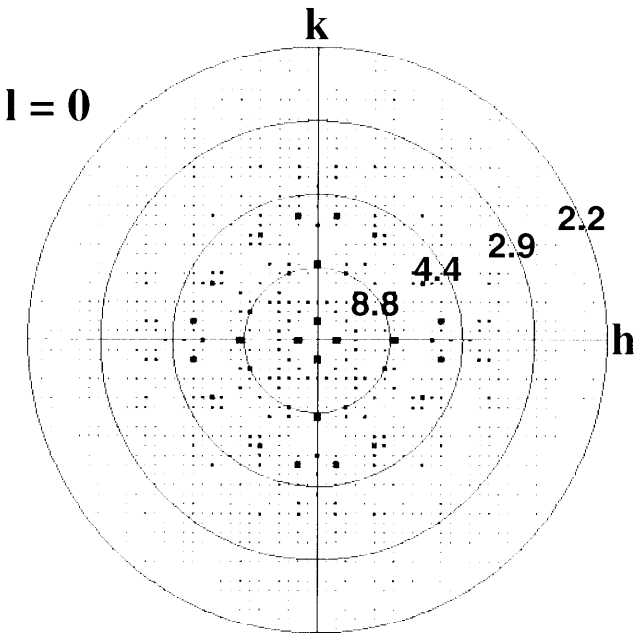

Fig.8. A Pseudo-Precession Photograph of the RhoA^{V14} / PKN (7-155) Complex

A pseudo-precession photograph of the (*hk0*) plate. Resolution shells, 2.2 A, 2.9 A, 4.4 A, and 8.8 A, are indicated with circles.

Table 1
Crystal Data of RhoA^{V14}/PKN Complex

Crystal system	**Tetragonal**
Space group	**$P4_12_12$, $P4_32_12$**
Unit cell dimensions	**$a = b = 66.90$, $c = 149.54$ A**
	$\alpha = \beta = \gamma = 90^\circ$
Unit cell volume	**6.69×10^5 A^3**
Z	**1**
V_m	**2.2 A^3/Da**
V_{solve}	**44%**

Molecular weight of RhoA^{V14} is 22,328 Da, PKN is 16,490 Da

Table 2
Intensity Data Processing

Resolution	**2.2 A**
R_{merge}*	**9.0% (31.2%)†**
Number of measurements	**696,854**
Number of independent reflections	**17,568**
Completeness	**96% (86%)†**
Mean <I/σ(I)>	**24.0 (2.8)b**

* Rmerge = 100 x Σ | I(h) - <I(h) > | / Σ I(h) , where <I(h) > is the mean intensity for reflection ***h***.
† Brackets are quantities calculated in the highest resolution bin at 2.28-2.20 A

Table 3
Molecular Replacement Statistics

Resolution range	**15.0 A - 3.0 A**
Rotation (α, β, γ)*	**12.65 °, 42.12 °, 81.49 °**
Translation (x, y, z)*	**0.0477, 0.3589, 0.2987**
Correlation coefficient†	**0.493**
R_{cryst} ¶	**51.4%**

* Eulerian angles (α, β, γ) and fractional coordinates (x, y, z) as defined in AMoRe.
† Correlation coefficient is defined as Σ ($|Fo(h)|^2 - \langle |Fo(h)|^2 \rangle$) ($|Fc(h)|^2 - \langle |Fc(h)|^2 \rangle$) / $[(\Sigma |Fo(h)|^2 - \langle |Fo(h)|^2 \rangle)^2 \Sigma (|Fc(h)|^2 - \langle |Fc(h)|^2 \rangle)^2]^{1/2}$, where Fo(h) and Fc(h) are observed and calculated structure factors and < > means averaged.
¶ Rcryst = 100 x ǂ | Fo(h) - Fc(h) | / ǂ Fo(h).

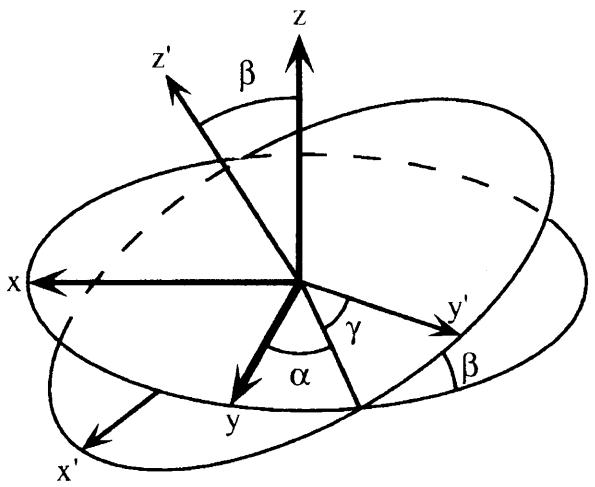

Fig.9. The definition of the Eulerian angles
A direction of a molecule is shown using three angles, the Eulerian angles (α, β, and γ).

Table 4
Solutions of Rotation function and Translation function *

	α	β	γ	x	y	z	Cc	R
$P4_122$	12.65	42.12	81.49	0.0499	0.8539	0.3085	38.1	55.8
	12.65	42.12	81.49	0.0511	0.8641	0.1726	37.8	56.0
	12.65	42.12	81.49	0.0470	0.8643	0.4218	37.2	55.7
$P4_12_12$	12.65	42.12	81.49	0.0477	0.3589	0.2987	49.3	51.4
	12.65	42.12	81.49	0.0471	0.3606	0.1567	38.2	55.5
	12.65	42.12	81.49	0.0481	0.3581	0.0481	37.6	56.0
$P4_212$	12.65	42.12	81.49	0.7942	0.4398	0.2594	31.4	57.7
	12.65	42.12	81.49	0.0128	0.4729	0.1143	29.8	59.4
	12.65	42.12	81.49	0.6435	0.3589	0.0210	29.4	60.3
$P422$	12.65	42.12	81.49	0.0321	0.0792	0.0165	30.6	58.3
	12.65	42.12	81.49	0.3130	0.6194	0.0485	30.5	59.5
	12.65	42.12	81.49	0.3054	0.5566	0.4761	30.3	59.4
$P4_22_12$	12.65	42.12	81.49	0.0570	0.8733	0.0474	30.9	58.7
	12.65	42.12	81.49	0.6452	0.3612	0.0186	30.6	59.4
	12.65	42.12	81.49	0.9996	0.9975	0.0201	30.6	59.4
$P4_222$	12.65	42.12	81.49	0.0364	0.5678	0.4747	29.7	59.4
	12.65	42.12	81.49	0.3937	0.4760	0.2289	29.6	59.8
	12.65	42.12	81.49	0.0006	0.9963	0.2695	29.5	59.6
$P4_32_12$	12.65	42.12	81.49	0.0479	0.3644	0.0492	36.4	56.3
	12.65	42.12	81.49	0.0435	0.8640	0.0486	35.9	56.2
	12.65	42.12	81.49	0.0444	0.3667	0.2982	34.5	56.9
$P4_322$	12.65	42.12	81.49	0.0469	0.3612	0.4229	37.0	55.5
	12.65	42.12	81.49	0.0517	0.8786	0.4222	31.7	58.1
	12.65	42.12	81.49	0.3090	0.6175	0.4229	31.7	58.0

* This table includes the top three solutions of the moleculer replacement sorting by the correlation cofficient (Cc), and R-factor (see text) for the repective space groups. (α, β, γ) are the Eulerian angles and (X, Y, Z) are the fractions of the unit cell axes. Space group $P4_12_12$ gave both the highest Cc and the lowest R. These calculations used the reflections between 15 - 3 A.

Table 5
Refinement Statistics

Resolution range	**2.2A**
R_{cryst} *	**20.8 % (31.4 %)†**
R_{free} §	**27.6 % (36.0 %)†**
R.m.s. bond lengths	**0.065 A**
R.m.s. bond angles	**1.246 °**
R.m.s. dihedral angles	**22.55 °**
R.m.s. Δω ¶	**1.179 °**

* R_{cryst} = 100 x Σ | Fo(h) - Fc(h) | / Σ Fo(h).

§ R_{free} is Rcryst which was calculated using 5% of the data, chosen randomly and omitted from the subsequent structure refinement.

† Brackets are quantities calculated in the highest resolution bin at 2.28-2.20 A

¶ Δω is the deviation of the peptide torsion angle from 180°

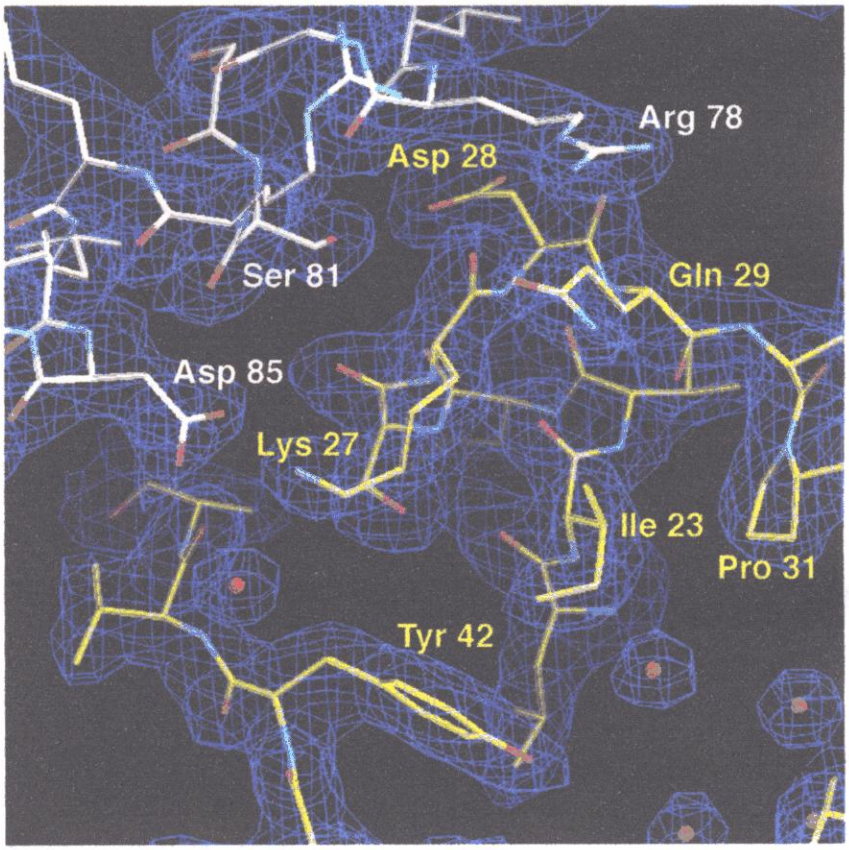

Fig.10. Electron Density of the RhoA^{V14}/PKN Complex

Representative 2 ||Fo| - |Fc|| electron density of the RhoA^{V14}/PKN complex. The map shows RhoA Lys-27 of switch I hydrogen bonded to PKN Asp-85PKN, contoured at 1.0 σ with the refined model, which is indicated by white (PKN) and yellow (RhoA) carbon traces with oxygen and nitrogen atoms in red and blue, respectively.

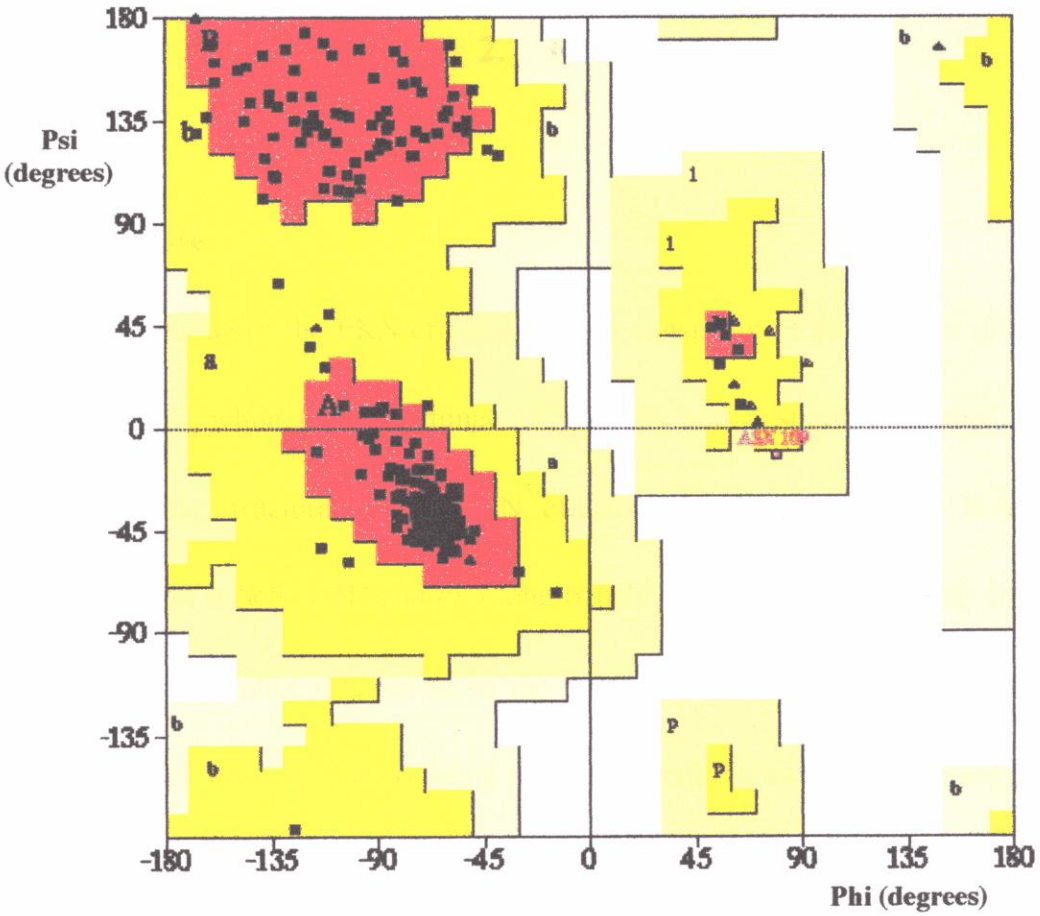

Plot statistics

Residues in most favoured regions [A,B,L]	218	92.8%
Residues in additional allowed regions [a,b,l,p]	16	6.8%
Residues in generously allowed regions [~a,~b,~l,~p]	1	0.4%
Residues in disallowed regions	0	0%
Number of non-glycine and non-plroline residues	235	
Number of end-residues (excl. Gly and Pro)	121	
Number of glycine residues (shown as triangles)	16	
Number of proline residues	13	
Total number of residues	385	

Fig.11. Ramachandran Plot of RhoA^{V14}/PKN Complex.

Main chain dihedral angles were analyzed with the program PROCHECK (Laskowski et al., 1993). The horizontal axis indicates ϕ angle around N-Cα bond and the vertical axis indicates ψ angle around Cα-C bond. Most favoured, additional allowed, generously allowed, and disallowed regions are shaded in red, yellow, light yellow, and white, respectively. Glycine residues are shown as triangles and non-glycine residues are indicated by squares. The labels A and a indicate the regions for α-helix, B and b for β-strand, and L and l for α_L-helix.

2. Results

Overall Structure

The current model of the PKN effector domain consisting of 86 residues displays a well-defined structure, while the C-terminal 57 residues and a short N-terminal segment are unstructured. The structure of the PKN effector domain features the N-terminal loop containing a short α helix (α1) and two long α-helices (α2 and α3) forming an anti-parallel coiled-coil fold, hereafter referred to as the ACC-finger domain. The ACC-finger domain binds to the Rho specificity-determining regions containing switch I, β-strands B2 and B3, and the C-terminal α-helix A5, predominantly by specific hydrogen bonds (hereafter this interaction is referred to as Contact-1) (Fig.12). RhoA in the present complex has no significant structural change if compared to that of the uncomplexed form, with a root-mean-square (rms) deviation of 0.45 A for 176 Cα-carbon atoms and 0.21 A for the GTPγS molecule and the Mg^{2+} ion (Fig.13). There are only two residues, Met-134 and Lys-135 at the extra helical subdomain, shifted greater than 1A. The structure of the PKN effector domain is described, followed by a description of the RhoA/PKN interface that involves sevelal specific interactions. We have found that the symmetry-related molecule of the PKN effector domain contacts RhoA in the crystal. We then describe this second interface (hereafter referred to as Contact-2).

Structure of the PKN Effector Domain

The structure of the PKN effector domain features ACC-finger domain (Fig.14). Two long helices encompass the basic region and the first characteristic leucine repeat region, which were previously identified as the Rho-binding domain. A segment of 20 residues followed by helix α3 contains a proline/glycine-rich region, suggesting that this region is highly flexible. The N-terminal region of the ACC-finger domain is folded back onto the bundled helices α2 and α3, and forms a hydrophobic core that contributes to the stabilization of the domain structure. The two long helices intertwine with a slight left-handed twist. The mean angle of the helical axes of helices 2 and 3 is 19 °, and the averaged interhelical distance is 10.6 A. This architecture is classified as a long α-helical hairpin fold of the two-helix bundle in the SCOP protein structure database (Murzin et al., 1995).

According to the structural comparisons with the DALI database (Holm and Sander, 1993), the ACC-finger domain has an overall structure similar to many coiled-coil segments of functionally unrelated proteins, including the coiled-coil domains of GreA transcript cleavage factor (Stebbins et al., 1995) and seryl-tRNA synthetase (Cusack et al., 1990; Biou et al., 1994). But it is distinct from those of the recently determined Cdc42-effector CRIB motifs of WASP (Abdul-Manan et al., 1999) and ACK (Mott et al., 1999), which are in largely extended conformations. The ACC-finger structure is also distinct from those of the Ras-effector domains of c-Raf1 (Nassar et al., 1995; Emerson et al., 1995) and RalGDS (Huang et al., 1997; Geyer et al., 1997), the Ran-effector domain of karyopherin-b2/importin b (Chook and Blobel, 1999; Vetter et al., 1999), and the catalytic domains of adenylyl cyclase, which

bind to heterotrimeric G proteins (Tesmer et al., 1997) (Fig.26). In contrast, the α-helical structure of the ACC-finger domain is reminiscent of the Rab-effector domain of rabphilin-3A (Ostermeier and Brunger, 1999) and Rac-effector protein Arfaptin (118-341) (Tarricone et al., 2001) (Fig.25).

There is no bulged out area or apparent kink in the bundled helices. The mean main chain dihedral angles are -66.6 ° for ϕ and -38.3 ° for ψ, as in globular proteins (Blundell et al., 1983), yet the hydrophobic interactions between the two helices are somewhat irregular (Fig.14). Notably, the characteristic heptad repeat, (abcdefg)n, with hydrophobic residues at the a and d positions, is broken at the middle of each helices α2 and α3. Instead, hydrophilic residues (Glu-45, Glu-49 and Lys-53 of helix α2 and Ser-80, Ser81, Arg-83 of helix α3) form interhelical hydrogen salt bridges / hydrogen bonds on the molecular surface (Fig.14). Interestingly, one of the apparent leucine repeats (at positions 52, 59, and 66) located on helix α2 is away from the interhelical interface, while another leucine repeat of helix α3 participates in the interhelical interactions (Fig.14). The projected leucines form a hydrophobic patch with other hydrophobic residues (Ala-62PKN from helix α2 and Pro-72PKN and Leu-76PKN from helix α3) on the molecular surface. This hydrophobic patch is the main region for Contact-2 (Fig.15).

The Interface between RhoA and the PKN ACC-finger Domain (Contact-1)

At the interface of the RhoA/PKN complex, the interacting PKN residues are clustered into two regions: box A at helix α2 and box B at helix α3 as shown in Fig.16 (PKN(ACC-1)).

The interacting PKN residues are located on the molecular surface opposite that for the hydrophobic patch as described (Fig.15). The ACC-finger domain binds to RhoA at four-contact sites (RhoA/PKN Contact-1 shown in Fig.17). The regions of RhoA that interact most closely with the ACC-finger domain include the N-terminal region of Switch I, the antiparallel β sheet formed by strands B2/B3 and the N-terminal half of helix A5 located at the C-terminus of the protein. The interface between RhoA and the ACC-finger domain is predominantly hydrophilic, and the complex buries 2080 A^2 of the accessible surface areas in the two proteins (Fig.12).

The major interaction between RhoA and the ACC-finger domain occurs primarily at the side chain level but also includes the backbone level. An extensive hydrogen bond and salt bridge network contains 17 direct hydrogen bonds and 9 water-mediated hydrogen bonds. At the interface, 17 residues from RhoA and 15 residues from the ACC-finger domain play roles in the intermolecular interactions. Among them, the side chains of 9 residues from RhoA participate in the direct hydrogen bonding interactions. The main chains of two residues (Phe-25 and Ser-26) at the Switch I N-terminus are directly hydrogen bonded to the ACC-finger domain (Fig.18). Moreover, complementary electrostatic potential distribution exists at the interface, where the positively charged ACC-finger domain contacts RhoA in the negatively charged region. At the heart of the interface, the ACC-finger domain sticks Lys-53PKN into the shallow groove of RhoA to form hydrogen bonds with Asp-28 and the main chain of Phe-25 (Fig.19). These interactions are surrounded by three hydrophobic side chains (Leu-50, Leu-77 and Leu-84) from the ACC-finger domain, which covers a small hydrophobic patch

(Val-43, Ile-46, Phe-25 and Val-167) of RhoA located at the base of the interface. There are van der Waals contact involving Val-43 and Ile 46 of RhoA, the side chain of Phe-25 has no contact with the ACC-finger domain and faces to the hole covered by the ACC-finger domain. In contrast, Leu-50 of the ACC-finger domain projects the hydrophobic side chain toward RhoA and extensively contacts with Ile-46, Asp-45 and Glu-52 of RhoA. Ile-46, Ile-84 and His-88 of the PKN ACC-finger domain also participate in contacting with RhoA (Fig.18).

These interactions are unlike those seen in Cdc42 (Abdul-Manan et al., 1999; Mott et al., 1999), where the CRIB motifs wrap around the G protein, and in other families of small G proteins including Rab (Ostermeier and Brunger, 1999) and Ran (Vetter et al., 1999) (Vetter and Wittinghofer, 2000). There is no interaction between the ACC-finger domain and the RhoA extra-helical domain (Fig.22) which defines the Rho-family members. Similarly, no such interaction has been observed between the Cdc42 extra-helical domain and the CRIB domains of WASP and ACK.

The Determinants of Rho for the Effector Specificity on Contact-1

The present structure reveals how RhoA recognizes its effector protein. The interface contains several contacts involving RhoA residues that have no homologous replacements in Rac/Cdc42, nor other small G proteins (Fig.27). These Rho-characteristic residues, which are strongly conserved in the three Rho isoforms, are Lys-27 and Gln-29 of Switch I and Glu-47, Gln-52 and Glu-54 of the antiparallel β-sheet B2/B3, and Glu-169 of helix A5 (Fig.17). Especially, Gln-29, which interacts with the positively charged Arg-78 of the ACC-finger

domain, is replaced with negatively charged glutamic acid in RhoB but this change may enhance the binding by ionic interactions rather than impair it. These residues are the first candidates for the Rho determinants of the effector specificity.

In addition, some other residues whose corresponding residues in other G proteins are nearly homologous with RhoA may also contribute to the specificity. It is remarkable that these residues are different from those of specificity determinant residues of Cdc42 (Asp-38, Val-42, Gly-47 and Leu-174), whose residues in RhoA are Glu-40, Ala-44, Asp-49 and Arg-176. Moreover, the negatively charged Asp-28 of the Switch I, which interacts with the positively charged Lys-53 of the ACC-finger domain in the present structure, is replaced with asparagine in Rac and Cdc42, suggesting discrimination of these G proteins by loosing the ionic interaction (Fig.17).

In addition to the side chains, the binding affinity is presumably conferred from contacts mediated by the main chains of Switch I (Phe-25 and Ser-26), the β-sheet B2/B3 (Glu-47 and Val-53) and helix A5 (Thr-163, Lys-164, and Arg-168). Thus, all these Rho-specificity determinant regions, RhoDRs, including the canonical Switch region both enhance the binding affinity and establish the specificity. Interestingly, the discrimination of Cdc42 from the other Rho family members by the CRIB motifs of WASP and ACK was also governed in part by contacts to helix A5. Moreover, Rab3A serves the C-terminal half of helix A5 as one of the Rab complementary determining regions, which contacts rabphilin-3A. Thus, the regions around helix A5 are important in allowing a subset of small G proteins to establish the specificity (Fig.27).

Switching Mechanism for Effector Recognition at Contact-1

As in H-Ras, Switch-I and Switch-II of RhoA are the regions in which extensive structural changes involving main-chain conformations are directly induced by GTP/GDP exchange (Fig.20). The structurally changes of the Switch regions by binding of GTP are served for the binding to the downstream effector proteins. According to the structural comparison of the GTPγS- bound form with GDP-bound form (Ihara et al., 1998; Wei et al., 1997), Switch I of RhoA consists of residues 28-44 including the N-terminal part of β-strand B2. While the Switch II region is somewhat limited at residues 62-69, as compared with that of H-Ras (residues 60-72) (Milburn et al., 1990). The interactions of the ACC-finger domain with Switch I are localized to the N- and C-terminal regions, where the main chain displacements induced by GTP/GDP exchange are relatively small (less than 1.5 A) but significant. In addition, the nucleotide exchange induces drastic rearrangements of the side-chain packing at the molecular surface of Switch I, which strongly affect RhoA-PKN interactions. In particular, one of such effect is obvious for Tyr-42. In the GDP-bound form, this residue is projected toward the solvent region and may sterically inhibit the hydrogen bond between Lys-27 of the Switch I and Asp-85 of the ACC-finger domain. In the GTP-bound form of the complex, Tyr-42 is buried inside the hydrophobic core of the Switch I loop and pushes out the side chain of Lys-27 from the inside of the loop leading to formation of the hydrogen bond with Asp-85 of the ACC-finger domain (Fig.20). Moreover, Val-43 of the GDP-bound form interferes with Glu-54 of strand B3 to form a hydrogen bond with His-88 of the ACC-finger domain.

Stabilization of the Switch Regions

It is notable that extensive stabilization of the entire Switch I and Switch II structure are revealed by comparison of the temperature factor distributions in the present complexed and the uncomplexed GTP-bound RhoA molecules (Fig.21). This stabilization should be attributable to Contact-1 interactions at the N-terminal and the C-terminal regions of Switch I and Contact-2 interactions at Switch II. These results suggest that the enthalpic contribution of the binding energy is sufficient for the drastic changes in conformational properties of the Switch I and Switch II that is descrived follow. Similarly, significant stabilization is observed at the antiparallel β-sheet B2/B3, which is also flexible in the uncomplexed form.

Hydrophobic Contacts between RhoA and the PKN ACC-finger Domain

In the present crystal, RhoA contacts the symmetry related ACC-finger domain (Fig.22). The contact regions of RhoA include the C-terminal half and flanking region of Switch II (residues 66 - 76) and adjacent parts from the strand B3 and switch I (Hydrophobic contacts in Fig.17). This contact 2 interface is predominantly hydrophobic and buries accessible surface areas of 1640 A^2, which is unexpectedly large for a nonspecific interface produced by crystal packing.

At the center of the interface, Leu-69 of Switch II is located. And surrounded that Leu-72 and Tyr-66 from Switch II and Phe-39 and Trp-58 from the antiparallel β-sheet B2/B3 are located to form a cluster of hydrophobic side chains which associate with the hydrophobic patch of the ACC-finger domain around the tip of the finger. At the edge of the interface, Val-

38 and The-39 from Switch I associate with the hydrophobic interface and two charged residues, Arg-68 and Asp-76 of Switch II, form direct ionic hydrogen bonds with Glu-49 and Arg-68 of the ACC-finger motif, respectively. The main-chain carbonyl group of Phe-39 is hydrogen bonded to the side-chain amid group of the PKN Asn-58 residue which also form a hydrogen bond to one of water molecules hydrated to Glu-40 and Asn-41 of RhoA (Fig.23).

The Possibility of the Contact-2 Interaction

Following three of evidence imply that this interaction may be relevant to the PKN recognition by RhoA. First, we found that RhoA binds to the PKN effector fragment to form a stable complex with 1 : 2 stoichiometry as determined by gel filtration and EMSA (Fig.5). Second, the PKN effector domain interferes with the RhoA GTPase activated protein (GAP) (Shibata et al., 1996), which is often referred as GAP-inhibiting protein activity (GIP activity) (Kishida et al,. 1993). The most straightforward explanation of the observed GIP activity of the PKN effector domain is that PKN effector domain and Rho-GAP compete to bind to the overlapped site on the molecular surface of Rho around the Switch II region. This explanation would be explained by superposition of the present complex on that of RhoA bound to the catalytic domain of the Rho-specific GTPase activation protein p120 Rho-GAP (Rittinger et al., 1997). Contrary, the binding of the ACC-finger motif at the Contact-1 site causes no structural interference with the binding of p120 Rho-GAP (Fig.24). Because of the small structural changes of RhoA as described, it is unlikely that the conformational changes of RhoA induced by the binding to the ACC-finger domain at Contact-1 site. The GIP activities

of effector proteins were also reported for c-Raf-1 with H-Ras (Zhang et al., 1993; Warne et al., 1993), Rabphilin-3A with Rab3A (Kishida et al., 1993), and RalGDS with H-Ras (Kikuchi et al., 1994) and RalGDS with Rap1A (Hermann et al., 1996). In all the cases, their effector and GAP binding regions are overlapped, these results support the present interpletation of the GIP activity of PKN against RhoA by Contact-2. Third, PKN and all its homologs have two additional region (residues 115-203 as ACC-2 and residues 220-283 as ACC-3 in Fig.3), these homologous to the present effector domain (ACC-1 in Fig.3) are about 25% identities. Recent in vitro experiments indicates that PRK1 binds to RhoA via the ACC-1 and ACC-2 regions, suggesting independent contact regions on RhoA (Flynn et al., 1998).

The Contact-2 like Interactions in Other Effector Proteins

The Contact-2 interactions are reminiscent of the rabphilin 3A effector domain interacting with Switch II of Rab3A (Ostermeier and Brunger., 1999) and Arfaptin(118-341) interacting with Switch II of Rac1 (Tarricone et al., 2001) (Fig.25). The Structures of Rabphilin-3A effector domain bound to Rab3A and Arfaptin(118-341) bound to Rac display a long α-helix that contacts with Switch II and surrounding segments mainly by hydrophobic interactions. Superposition of these complexes using RhoA and Rab3A or RhoA and Rac displays unexpected overlap of the PKN ACC-finger domain and rabphilin-3A or PKN ACC-finger domain and Arfaptin. These complexe form several hydrophobic contacts with a similar region involving Switch II. Moreover these helices also have the same helix polarity relative to the G protein. Some hydrophobic residues conserved in the Switch II regions of RhoA,

Rab3A and Rac participate in the contacts, while there are no detectable similarity of the amino acid sequences of the contact regions of PKN, rabphilin-3A and Arfaptin.

Notably, the C-terminal helix of the WASP CRIB motif also makes hydrophobic contact with Switch II of Cdc42, with similar interactions having also been observed in the ACK/Cdc42 complex. This similarity may argue that Contact-2 of the present structure may not be a result of crystal packing effects but may reflect the interactions between the ACC-finger domain and RhoA in solution.

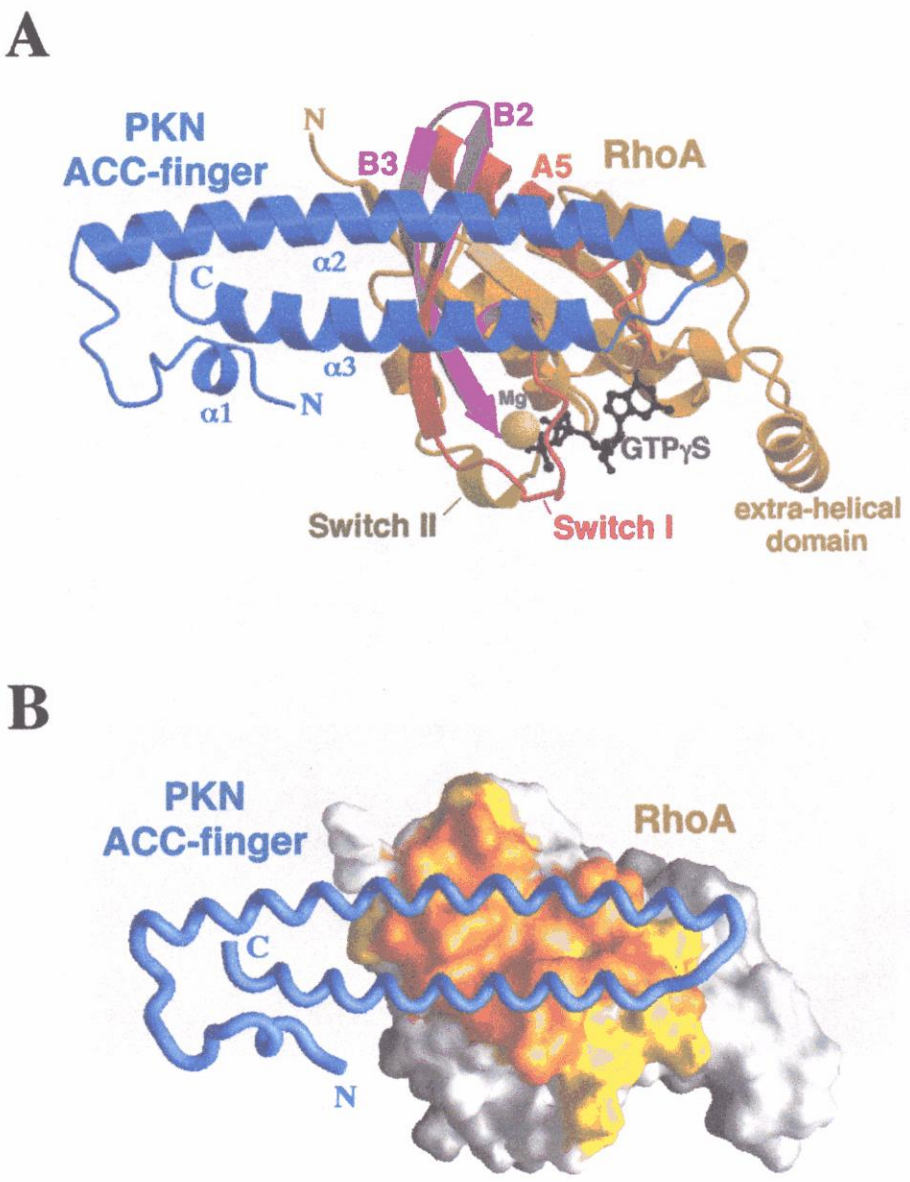

Fig.12. RhoA/PKN Complex Structure

(A) A ribbon representation of the PKN effector domain (blue) bound to RhoA (brown). The bound GTPγS molecule (black) and the magnesium ion (yellow) are shown in ball-and -stick models. The RhoDRs are labeled and highlighted with each color; switch I in red, strands B2 and B3 in purple, and helix A5 in orange. Switch II is colored in light green.

(B) The complex is shown with RhoA depicted as a molecular surface that is colored using a gradient; bright orange indicates atom < 4 Å, and white atoms 7 Å > from the bound PKN effector domain (shown as a blue tube), white lighter shades of orange indicate intermediate distances.

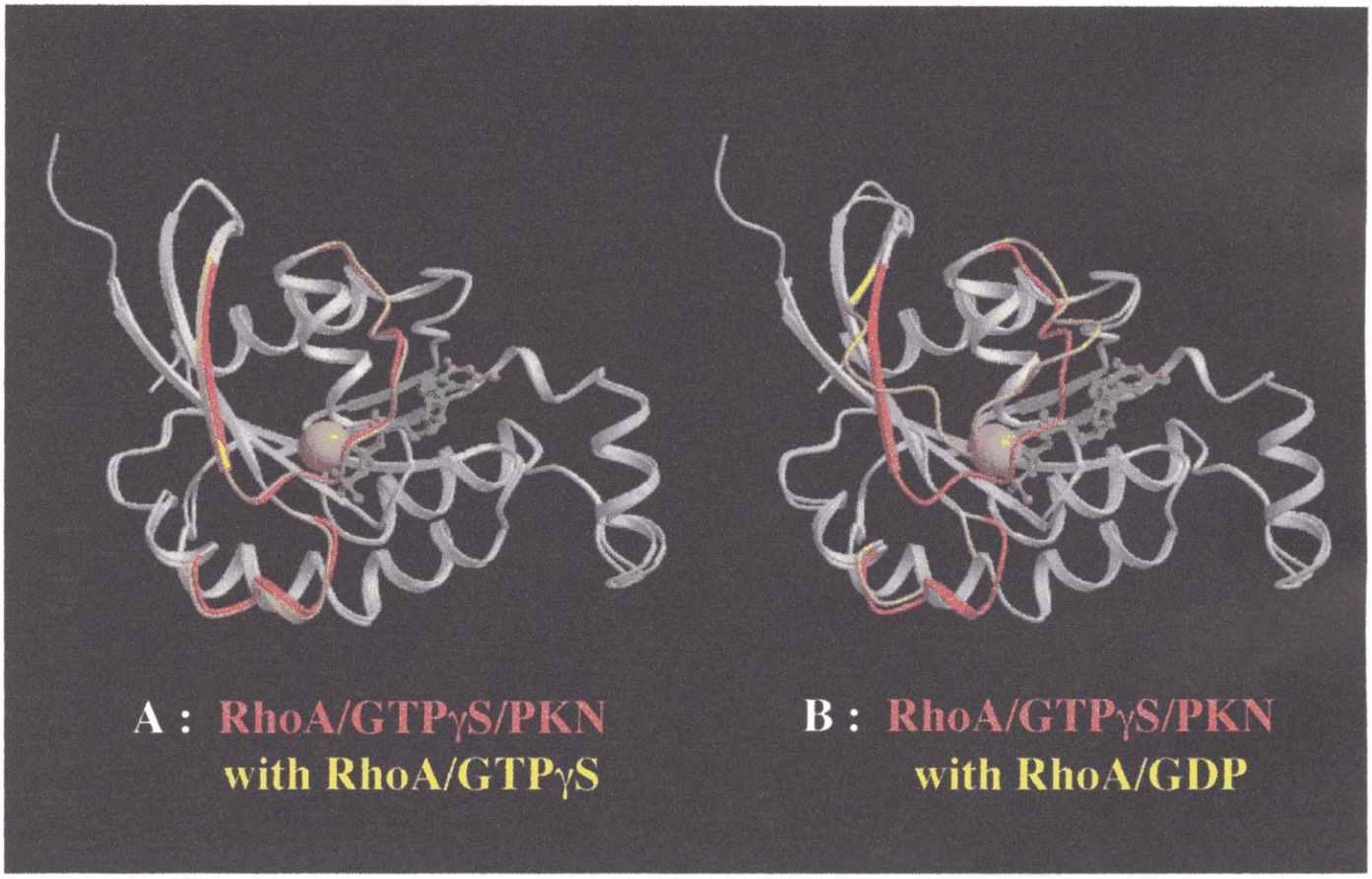

Fig.13. RhoA Structures in Different State

(A) Structural comparison of Cα-carbon atom tracings of RhoA/GTPγS/PKN with RhoA/GTPγS

(B) Structural comparison of Cα-carbon atom tracings of RhoA/GTPγS/PKN with RhoA/GDP

The GTPγS in the RhoA/PKN complex is colored in magenta, the GTPγS and GDP at free RhoA is colored in green. The switch regions are highlighted with each colors ; RhoA/PKN complex in red, free RhoA in yellow.

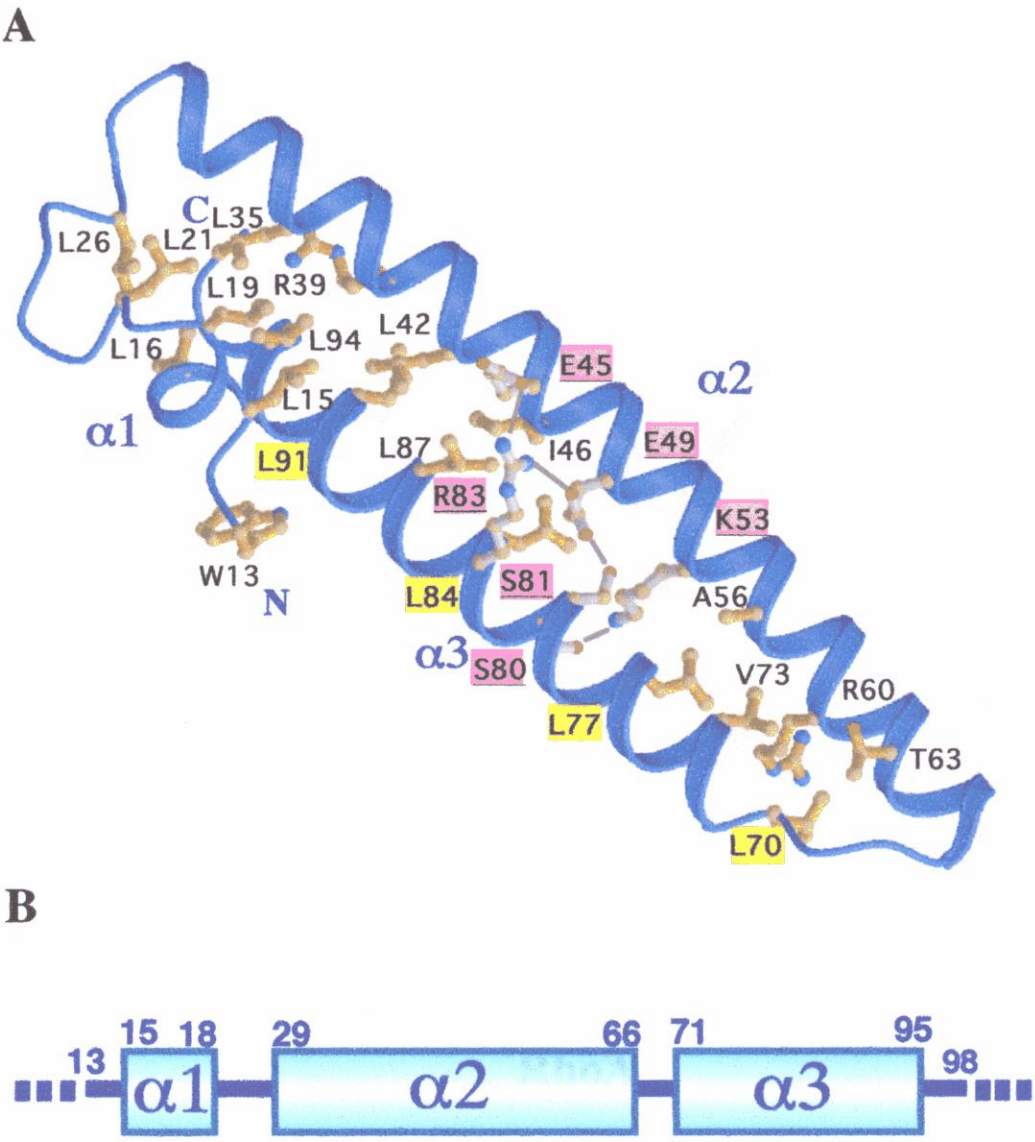

Fig.14. Structure of the PKN ACC-finger Domain

(A) The interhelical interactions between the two long α helices of the PKN ACC-finger. Residues forming the interhelical hydrophobic core (bonds indicated in brown) and interhelical hydrogen bonds (black solid lines) are shown in ball-and-stick models (gray with labels in pink). Leucine repeat that participates in the interhelical interactions are highlighted in yellow. The hydrophobic interactions involving the N-terminal loop are also shown.

(B) The secondary structure elements of the PKN ACC-finger domain.

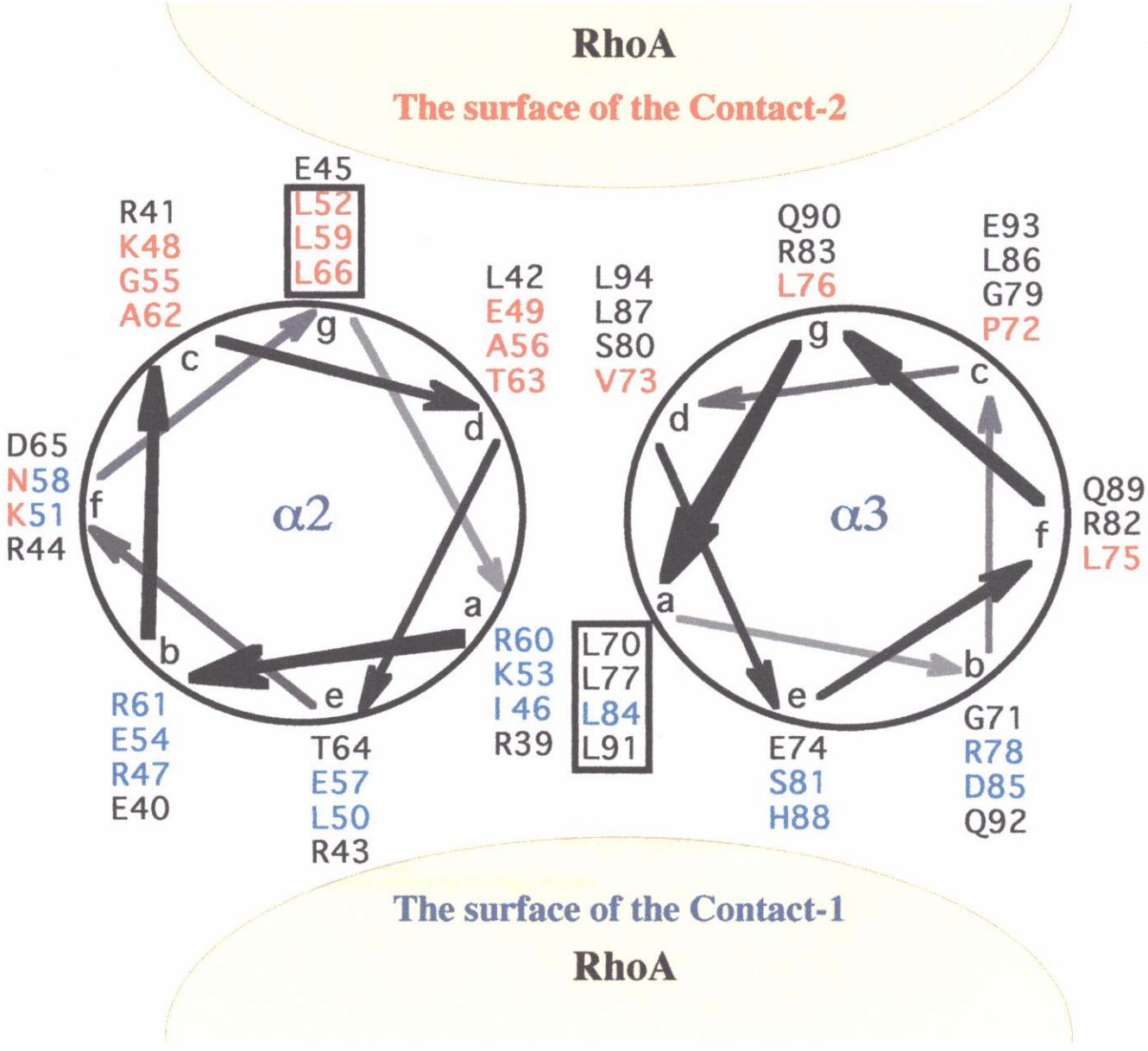

Fig.15. An Axial Helical Projection of the PKN (7-155) Helix Bundle

Axial helical projections looking down the helix bundle from the N and C termini of helices α2 and α3, respectively. The residues shown in blue participate in the interactions with RhoA at the RhoA/PKN complex shown Fig.9 (contact-1). The residues participating in the second contact site (contact-2, shown Fig.22) are colored in red. Two residues, Asn-58 and Lys-51, participate in both contacts. The leucine repeats are boxed.

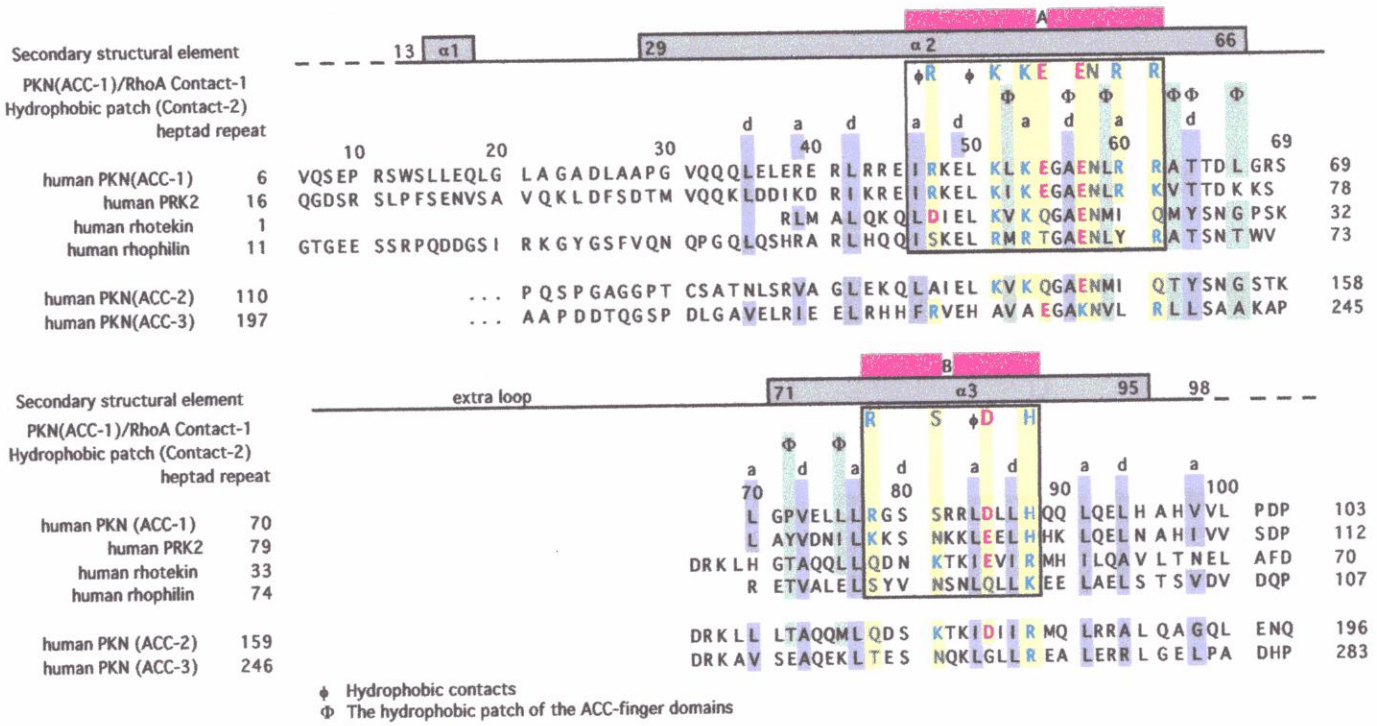

Fig.16. Sequence Alignment of the PKN ACC-finger Domain with the Related Rho Effector Domains

The secondary structural elements (α1-α3) of the PKN ACC-finger domain are indicated at the top. The residues that participate in interactions with RhoA at the interface of the RhoA/PKN complex shown in Fig.9 (contact-1) are indicated and are highlighted in yellow. These residues are clustered into box A and box B. The one-letter codes for these residues are colored in red (for acidic), blue (basic), and green (other hydrophilic residues). The a-g heptad repeats of helices α2 and α3 are displayed above the sequence in the coiled-coil domain. Hydrophobic residues at a and d positions are highlighted in purple. Residues that form the hydrophobic patch participating in the second contact site (contact-2, shown in Fig.22) are also indicated and are highlighted in light blue.

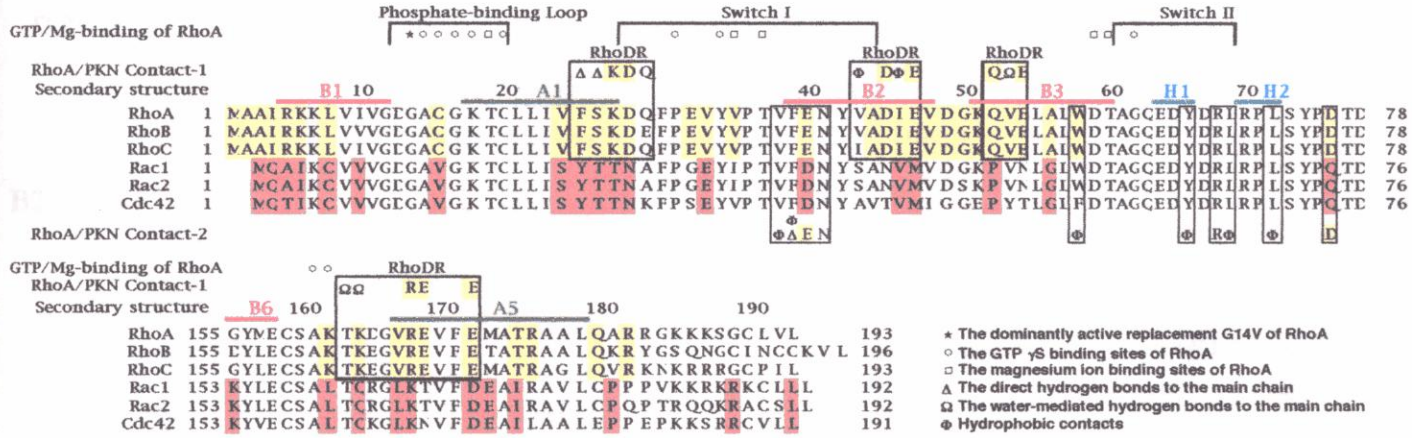

Fig.17. Sequence Alignment of RhoA with the Related Small G Proteins

Residues that participate in GTP/Mg^{2+} binding are indicated at the top. The residues that participate in interactions with RhoA at the interface of the RhoA/PKN complex shown in Fig.9 (cantact-1) are boxed by heavy lines with RhoDR labels. The secondary structural elements of RhoA are indicated at the top of the aligned sequences; the α helices (A1-A5) in green, extended β strands (B1-B6) in red, and 3_{10} helices (H1, H2) in blue. Conserved residues are highlighted in yellow for the RhoA subfamily (RhoA, RhoB, and RhoC) and in red for the Rac/Cdc42 subfamily (Rac1, Rac2, and Cdc42). The residues that participate in interactions with RhoA at the second contact site (contact-2, shown in Fig.22) are boxed by thin lines and are indicated at the bottom of the alignment. Only segments around the contact regions are shown.

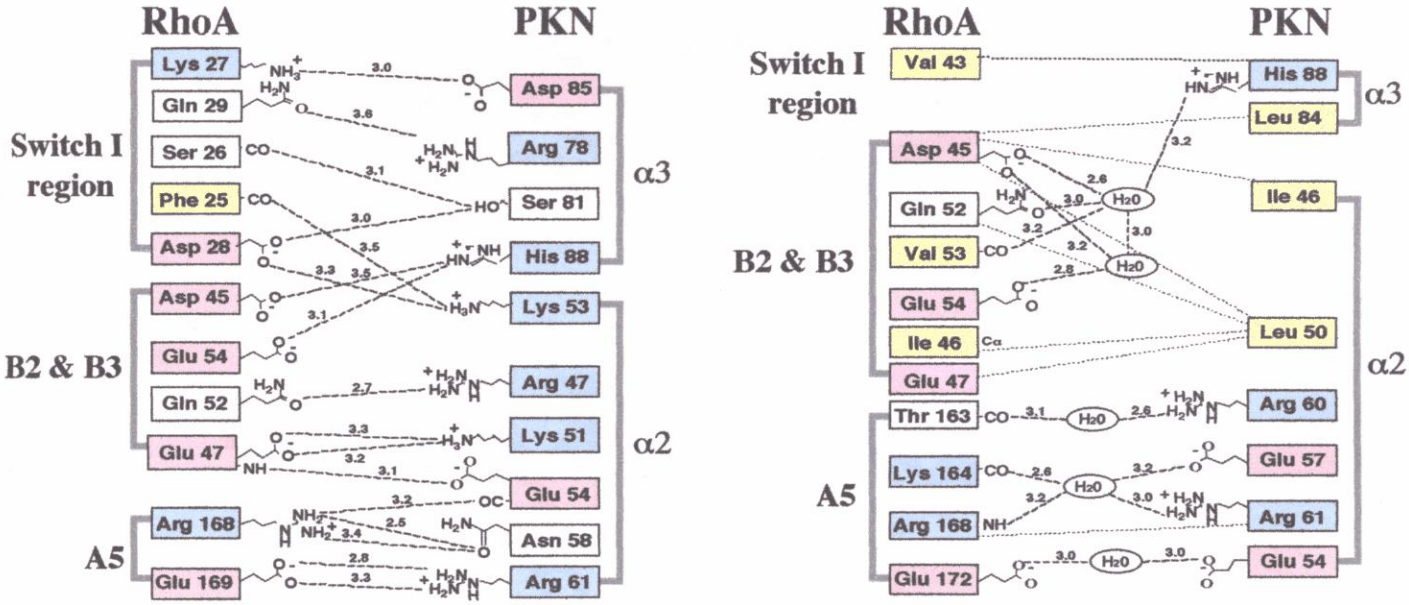

Fig.18. Interactions between the PKN ACC-finger Domain (contact 1) and RhoA

A schematic representation of the direct hydrogen bonding (left) and water-mediated hydrogen bonding or van der Waals (right) interactions of RhoA/GTPγS/Mg^{2+} with the PKN ACC-finger domain at the interface of the RhoA/PKN complex shown Fig.9 (contact-1); acidic residues are shown in red, basic residues in blue, and hydrophobic residues in yellow.

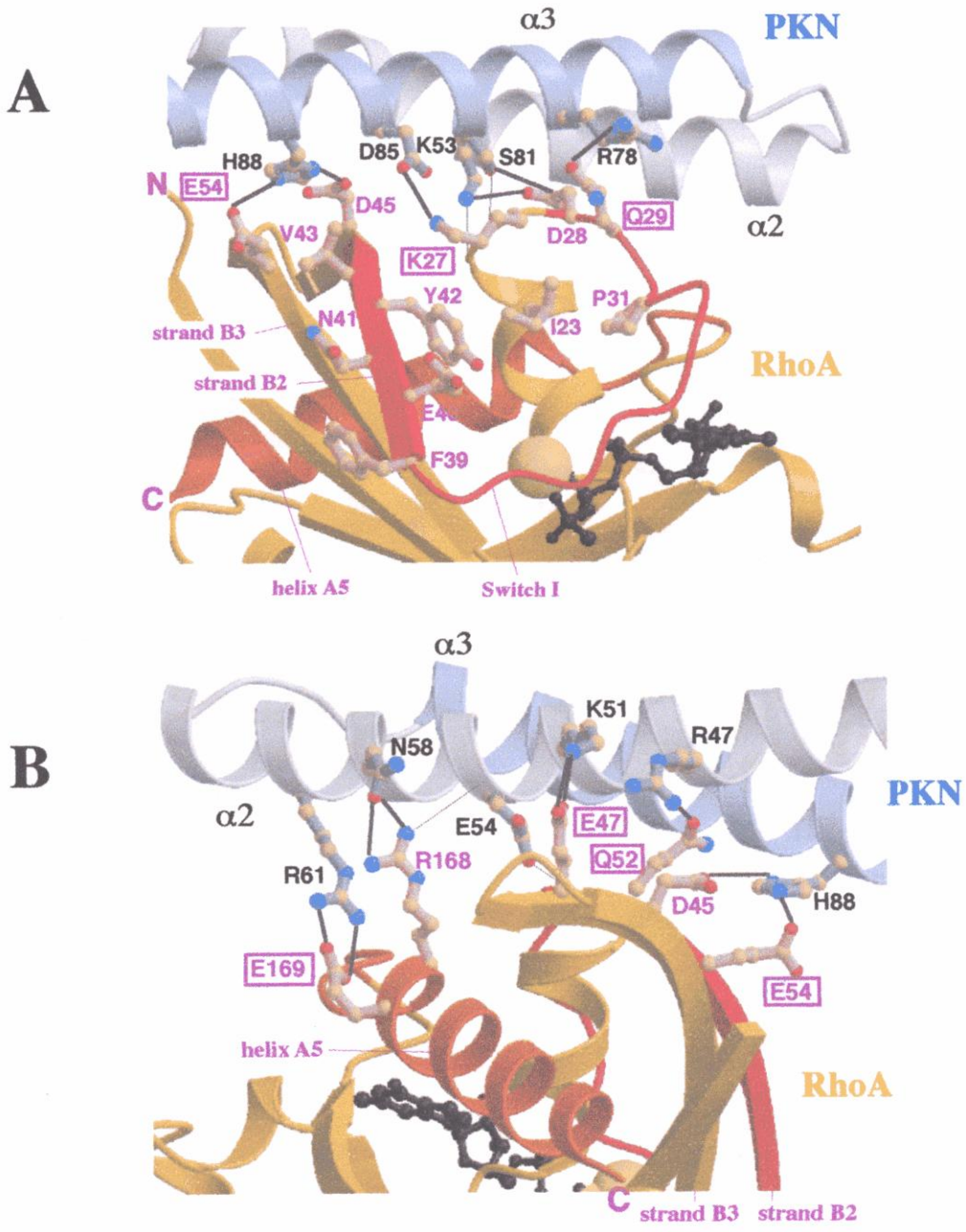

Fig.19. Interactions between the PKN ACC-finger (contact 1) and RhoA

(A) The direct hydrogen bonds (black solid lines) between the PKN ACC-finger domain and RhoA switch I and β sheet B2/B3. Thin lines indicate the hydrogen bonds involving main chain atoms. The ACC-finger domain is shown in gray (α2) and light blue (α3), and RhoA in brown, with switch I in red and helix A5 in orange. The side chains forming the hydrogen bonds are shown in ball-and-stick models with labels in black (PKN) and in purple (RhoA). The bound GTPγS molecule (black) and the magnesium ion (yellow) are also shown in ball-and-stick models. The side chains of Tyr-42, Ile-23, and Pro-31, which form a hydrophobic core inside the switch I loop, and the side chains of switch I residues (39-42) are also shown. (B) The direct hydrogen bonds between the PKN ACC-finger domain and RhoA helix A5 (orange) and β sheet B2/B3. The 180° rotation of the complex from that shown in (A) is indicated to clarify the interactions between PKN helix α2 and RhoA helix A5

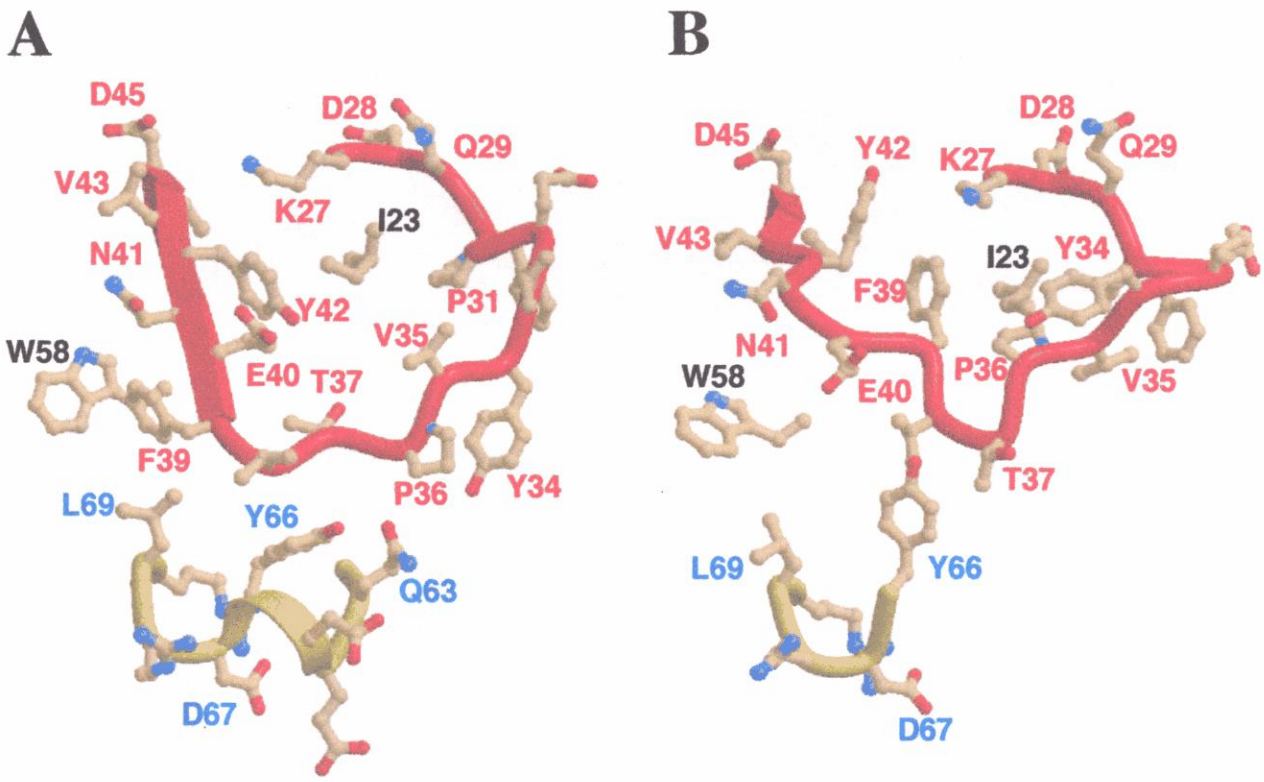

Fig.20. Structural Differences of the Switch Regions between RhoA/GTPγS and RhoA/GDP

(A) Switch regions of RhoA bound to GTPγS. Switch I and Switch II are colored in red and yellow respectively.

(B) Switch regions of RhoA bound to GDP are colored in the same as (A)

The GTP-dependent PKN binding is due to changes in the side chain packing of RhoA switch I involving Tyr-42 together with Lys-27, which is hydrogen bonded to PKN (Asp-85).

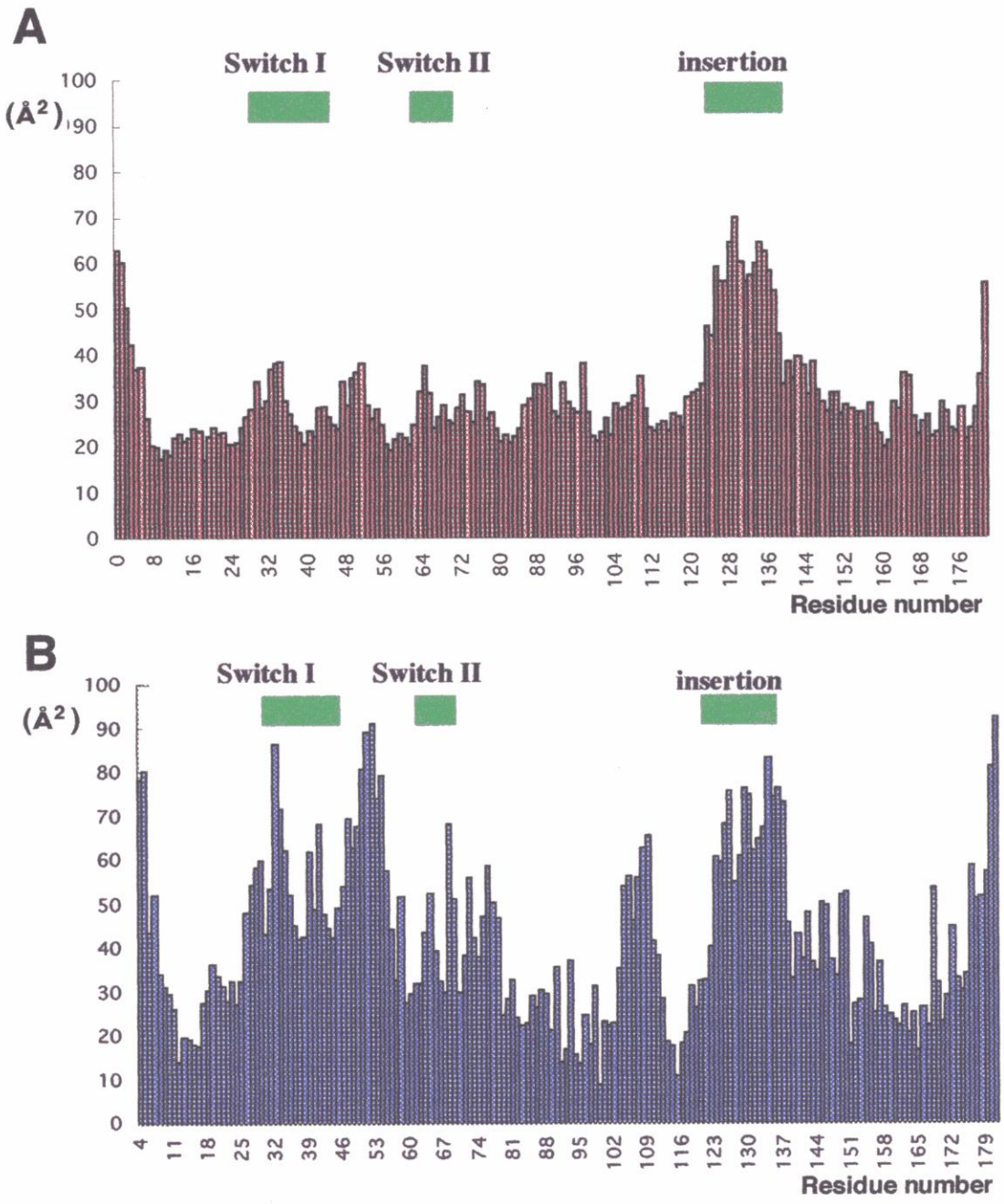

Fig.21. Residual averaged B-factors of RhoA in different state

A histogram shows B-factor values of the RhoA residues with the green bars of switches and insertion regions.

(A) B-factor plot of RhoA in the RhoA/GTPγS/PKN complex crystal

(B) B-factor plot of RhoA in the free RhoA/GTPγS crystal

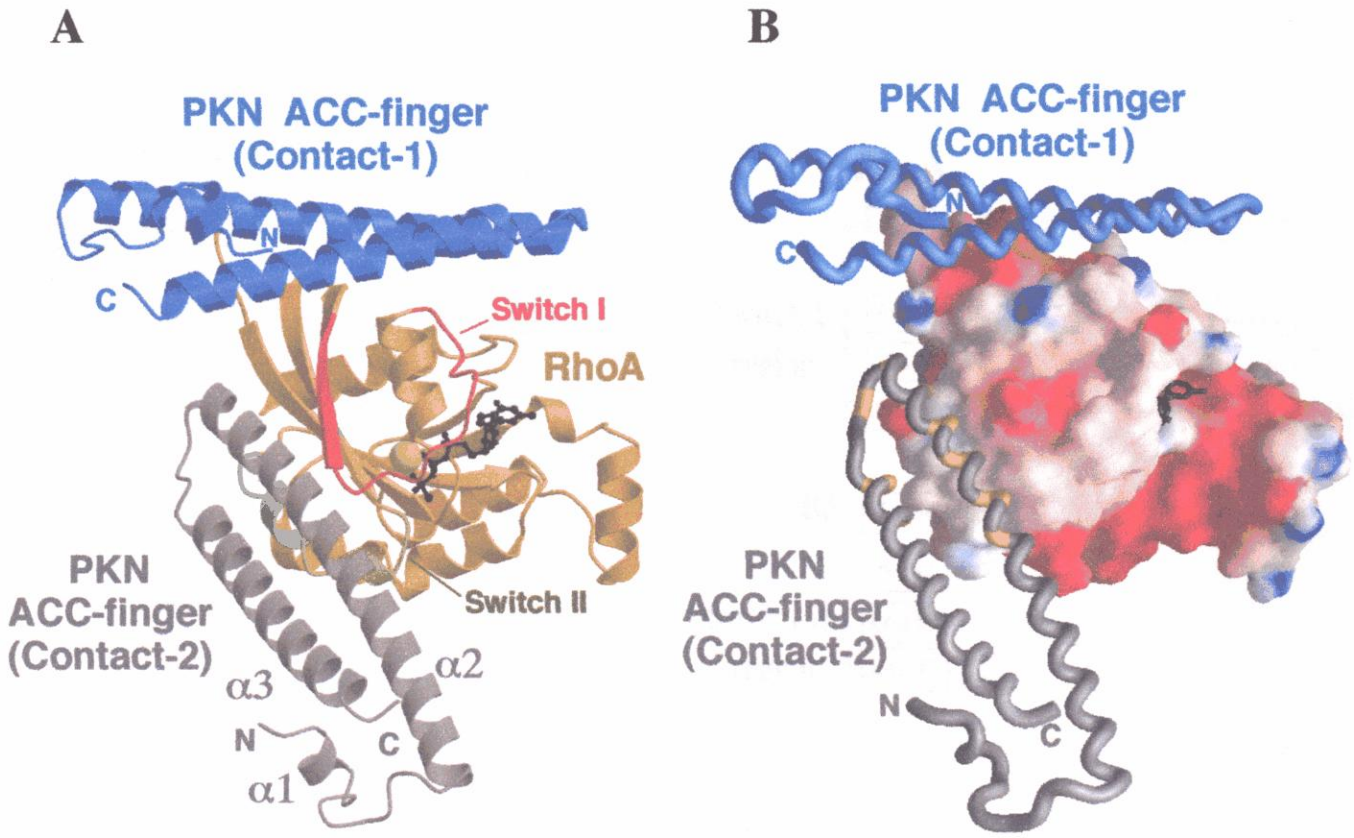

Fig.22. The Second Contact Site in the RhoA/PKN Complex

(A) A ribbon representation of the symmetry-related PKN ACC-finger domain (gray) at the second contact (contact 2) site of RhoA with the PKN ACC-finger domain (blue) at contact-1 shown in Fig.9. Switch II and other regions for contact-2 are in dark green and green, respectively.

(B) Electrostatic surface potential of RhoA/GTPγS/Mg^{2+} viewed from the same direction as in (A) with two bound PKN ACC-finger domains. Negative potential is red, uncharged surface is white and positive potential is blue. The contact-1 surface of the RhoA have mainly negatively charge, on the other hand, contact-2 surface of the RhoA is covered with the hydrophobic patch. The residues colored in yellow at ACC-finger (contact-2) participate in the hydrophobic interactions with RhoA.

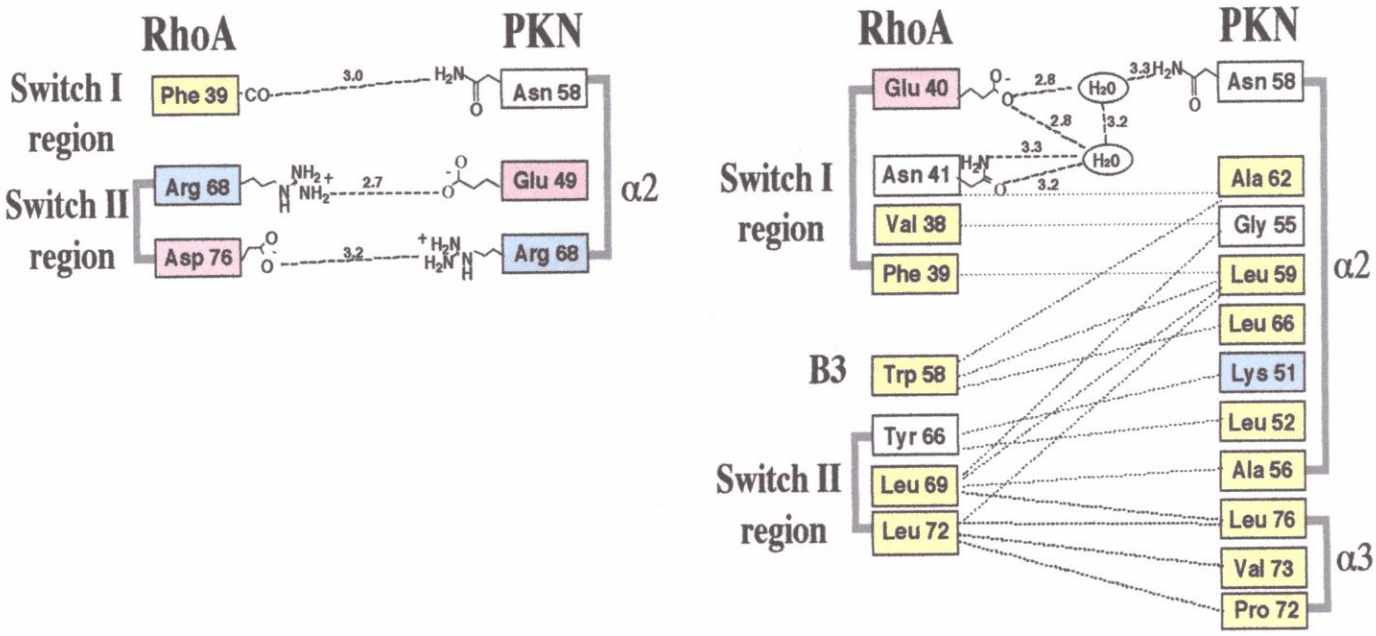

Fig.23. Interactions between the PKN ACC-finger Domain (contact 2) and RhoA

A schematic representation of the direct hydrogen bonding (left) and water-mediated hydrogen bonding or van der Waals (right) interactions between RhoA and the PKN ACC-finger domain in the RhoA/PKN complex (contact-2); acidic residues are shown in red, basic residues in blue, and hydrophobic residues in yellow.

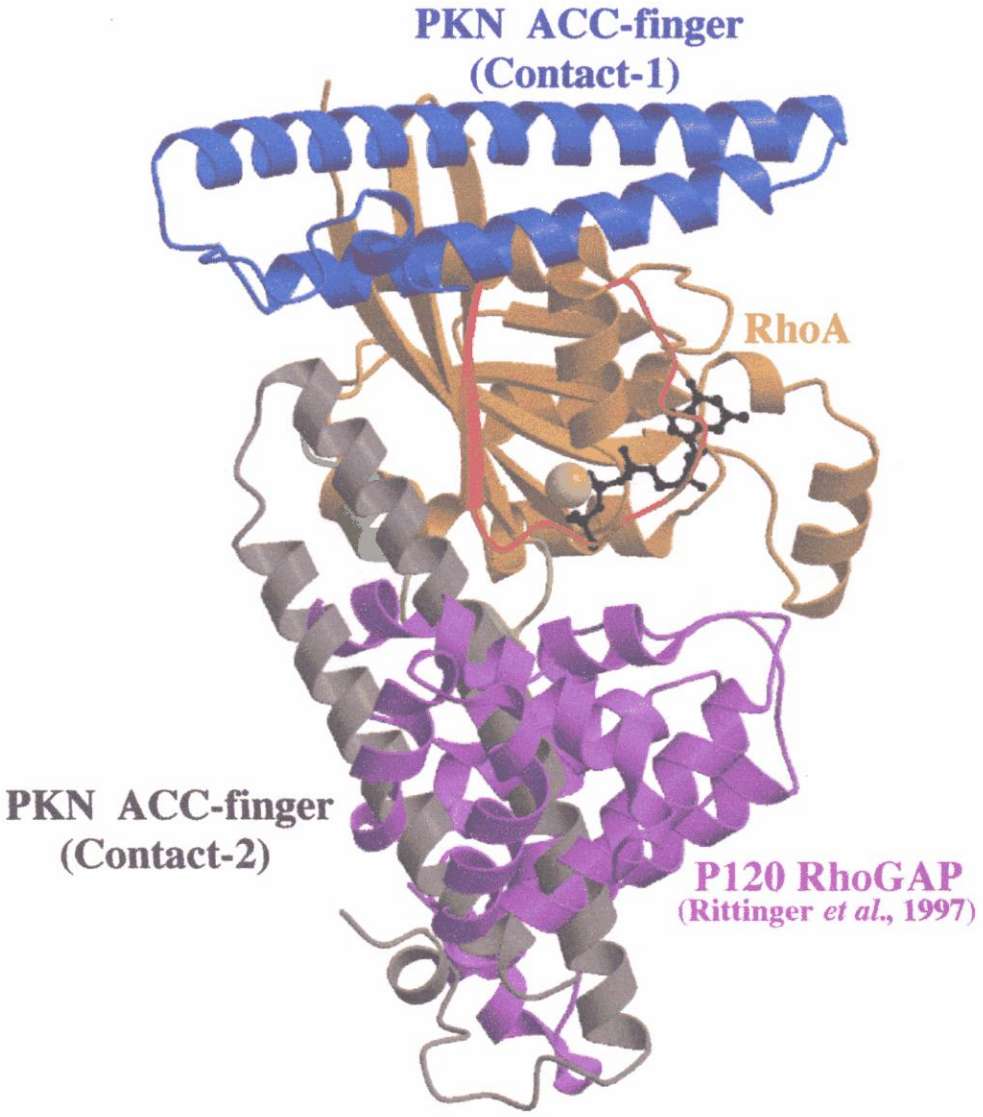

Fig.24. Structure of the RhoA/PKN Complex and RhoGAP

A ribbon representation of the RhoGAP (colored in purple) molecular overlaid onto the RhoA/PKN complex (RhoA, PKN contact-1 and PKN contact-2 are colored in brown, blue and gray respectively). The PKN contact-2 interaction overlaps with the binding site of p120 Rho-GAP.

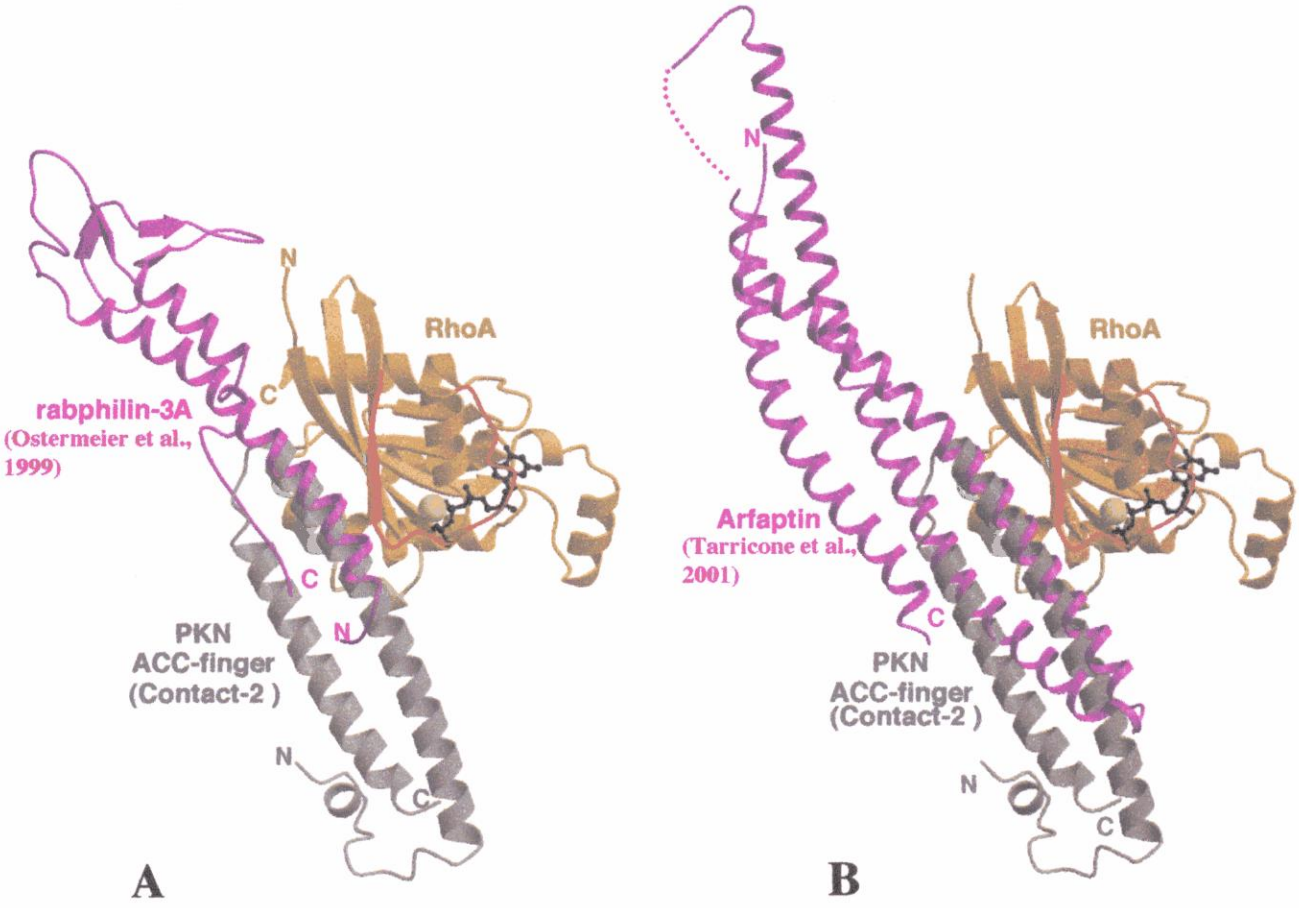

Fig.25. Structural Comparison of the RhoA/PKN Complex, rabphilin-3A and Arfaptin

A ribbon representation of rabphilin-3A (A:colored in magenta) and Arfaptin (B:colored in magenta) overlaid onto the current RhoA/PKN complex (Contact-2).

(A) Superposition of two complexes using RhoA (colored in brown) and Rab3A (with an rms deviation of 1.35 Å for 156 Cα-carbon atoms) displays unexpected overlap of the C-terminal half of the PKN (colored in gray) helix α2 and N-terminal half of the rabphilin-3A helix α1, which forms several hydrophobic contacts with a similar region involving Switch II (colored in green).

(B) Superposition of two complexes using RhoA (colored in brown) and Rac1 (with rms deviation of 0.677 for 50 Cα-carbon atoms) displays unexpected overlap of the PKN helix α2 and α3 (colored in gray) with Arfaptin helix α1 and α2, which forms several hydrophobic contacts with a similar region involving Switch II (colored in green).

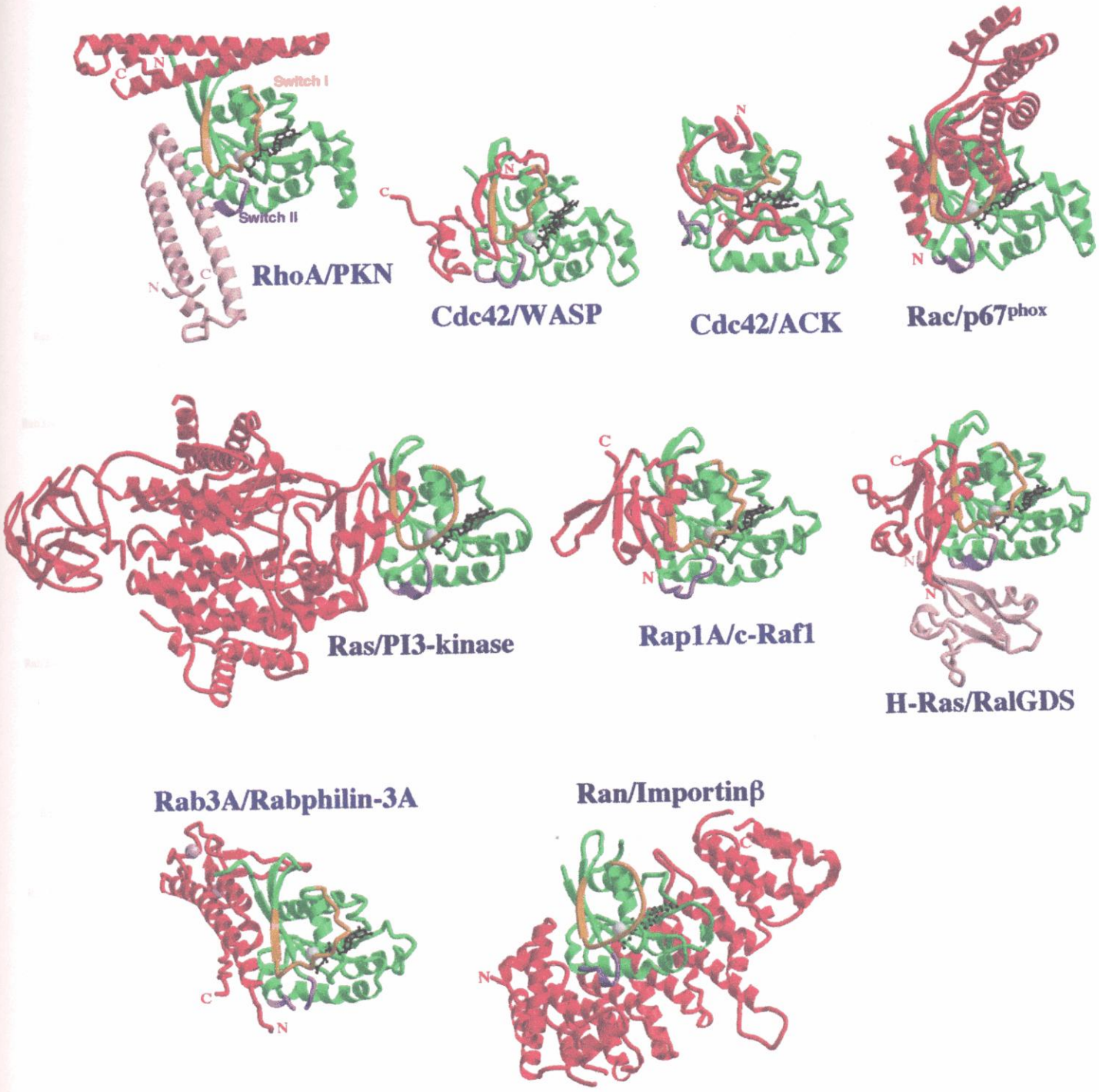

Fig.26. Structural Comparison of the Small G Protein and Effector Complexes

Ribbon representations of small G protein /effector complexes. Small G proteins are colored in green and their effector proteins in rose. Switch I and Switch II regions are colored in yellow and purple, respectively.

Fig.27. Sequence Alignment of the Small G Proteins

Sequence alignment of the Small G proteins whose structures complexed with their effector proteins have already determined. The secondary structural elements α-helix (A1 - A6) and β-strand (B1 - B6) are indicated above the each sequences with red and blue bars, respectively. The residues that participate in interactions with effector proteins are highlighted in yellow. The one-letter codes for these residues are colored in rose (for residues conserved in all small G proteins), blue (conserved in H-Ras and Pap1A), and purple (conserved in RhoA and Cdc42).

3. Discussion

Multiple ACC-finger Domains of the PKN N-terminal Region

In addition to the first repeat of leucine zipper-like sequences forming the present PKN ACC-finger structure (Fig.3), the following second and third repeats of leucine zipper-like sequences may form similar helix bundle structures, where the key residues for the ACC-finger structure formation are largely conserved. In vitro experiments have shown that a fragment containing the ACC-2 region weakly binds to RhoA, while a fragment containing the ACC-3 region has no detectable binding activity to RhoA (Flynn et al., 1998). These differences in Rho binding of three PKN ACC-finger domains may be explained in terms of the lack of the determinant residues for Rho binding. The ACC-3 region has alanine, leucine, or glycine at positions corresponding to the determinant residues, Lys-51, Lys-53, Arg-60, and Asp-85, of the present ACC-finger (ACC-1) domain. Moreover, PKN ACC-3 has charged residues at the positions corresponding to Pro-72 and Leu-76 of the PKN ACC-1 finger domain that form a hydrophobic patch to interact with the Contact-2 region of RhoA. In contrast, the corresponding hydrophobic residues of the PKN ACC-2 region are largely conserved, whereas two determinant residues, Arg-47 and Arg-60, are replaced with alanine and isoleucine, respectively (Fig.16). These variational differences may endow ACC-2, but not ACC-3, with the tendency to bind weakly to RhoA.

PKN may bind RhoA through both the ACC-1 and ACC-2 motifs. Unfortunately, no quantitative data for the cooperativity or interference between these two Rho-effector motifs

is available at present. In the crystal, the buried surface area of the interface between two ACC-finger motifs is small 140 A^2 but Gln-92 of one molecule forms a hydrogen bond to Asp-65 of the symmetry related molecule. This Asp-65 residue is replaced by asparagine in the ACC-2, indicating the observed hydrogen bond could occur between ACC-1 and ACC-2 bound to Contact-1 and Contact-2, respectively. The hypothesis must be verified by further experimental tests. As pointed out previously (Flynn et al., 1998), the evolution to a high affinity effector domain has been permitted by duplication of the ACC-finger domains. In this case, the interaction of PKN ACC-2 binds to both RhoA/GTP and RhoA/GDP weakly (Flynn et al., 1998) could be similar to that of Arfaptin binds to both Rac/GTP and Rac/GDP (Fig.25).

It is of interest that two distinct coiled-coil regions of kinectin (residues 630-935 and residues 1053-1327) have been reported to bind to RhoA in a GTP-dependent manner, as identified by the binding assay using two-hybrid and affinity chromatographic approaches (Hotta et al., 1996; Alberts et al., 1998). However in this case, two domains are separated for a longer stretch of peptides (176 residues) and there is no available data indicating that these domains bind to the same molecule of RhoA or not. Recently, multidomain interactions in effector recognition has also been suggested for the Raf-1/H-Ras complex, in which two distinct and nonhomologous domains, an ubiquitin-fold domain and an adjacent zinc finger-like domain, of Raf-1 bind to Switch I and II regions of H-Ras, respectively (Drugan et al., 1996).

PKN Activation Mechanism

The PKN N-terminal half fragment binds to the C-terminal half fragment containing the catalytic domain and inhibits the protein kinase activity, suggesting a masking mechanism by a possible autoinhibitory effect of the N-terminal region (Kitagawa et al., 1996). RhoA binding to the ACC-finger domains at the PKN N-terminal region could produce unmasked and, therefore, active catalytic domain (Fig.28). The N-terminal basic region spanning residues 39-53, which displays similarity to a consensus phosphorylation sequence for PKN, has been reported as a pseudo substrate region that inhibits the protein kinase activity of PKN. However, this region overlaps with the ACC-finger domain (ACC-1) and is folded into an α-helix(α2), which may inhibit its binding to the catalytic center as a pseudosubstrate. Therefore, the binding mode between the N- and C-terminal halves of PKN and the unmasking await further analyses.

PKN binds to its substrate proteins, α-actinin (Mukai et al., 1997) and PCD17 (Takanaga et al., 1998), through the N-terminal region (residues 136-189) that overlaps with ACC-2 finger domain. The binding site on actinin has been mapped at a spectrin-like repeat SR III. Interestingly, crystal structure of the repetitive segment of spectrin has shown its three-helix bundle structure (Yan et al., 1993), which may interact with the PKN ACC-2 finger motif by forming further helix bundle structure. Another interesting issue about these substrate binding is that this PKN ACC-2 finger region is multifunctional; participating in both binding to RhoA and to these substrate protein. Since PKN is also activated by unsaturated fatty acids (Mukai et al., 1994; Kitagawa et al., 1995) such as arachidonic acid and phospholipids such as

phosphatidylinositol (Palmer et al., 1995b) and cardiolipin (Peng et al., 1996), the dual binding of the ACC-2 finger domain is not necessarily contradictory. Alternatively, this dual binding of the ACC-2 finger domain may play a role of the molecular switch for substrate selection, where fatty acids-activated PKN phosphorylate the proteins that could bind to the ACC-2 finger region but RhoA-activated PKN phosphorylates other substrate protein. However, these possible mechanisms should be verified by experimental tests.

The ACC-finger Domains in Other Effector Proteins

The present structure of the PKN ACC-finger domain provides a clue for understanding the general architecture of the related Rho effector domains. As well as the PKN homologs, the effector regions of rhotekin and rhophilin preserve both the hydrophobic residues. These residues are essential for the formation of the coiled-coil structure and the determinant residues for the specificity indicating their formation of an ACC-finger structure like that of PKN as expected from their relatively high homology (43% and 26% identities, respectively) with that of the PKN ACC-finger domain (Fig.16). They also preserve residues forming the hydrophobic patch that participates in Contact-2 interactions. This observation implies that these effector proteins could bind to RhoA at Contact-2 site, these prospects are consistent with the fact that a fragment containing the rhotekin effector domain exhibits the GIP activity against RhoA (Reid et al., 1996). It should be noted that some of the determinant residues are variance with homologous or non-homologous but preserve charged residues. Especially, Ser-81 and Asp-85 of PKN is mostly replaced by asparagine and glutamic acid, respectively, and

Arg-47, Arg-61, Arg-78 and His-88 are rather variance. These variations have been inspected on the present structure and shown that these variant residues are also relevant for the RhoA binding. In these cases, asparagine at PKN Ser-81 may form alternative interactions with Ser-27 and /or Lys-27 rather than Glu-29, because of steric effects. The N-terminal region including the loop, helix α1 and the N-terminal one third of helix α2 is poorly conserved in the related proteins, implying that these regions may adopt in different conformations from that of the PKN ACC-finger domain. These regions are not essential for formation of the recognition surfaces and the structures, while our data and other's data indicate these regions contribute to the structural stability of the motifs.

Differentiation of Effector Selection

Recently, a new approach for the functional dissection of Rho family G proteins has been carried out using point mutations of a limited region (residues 39-42) of Switch I (Joneson et al., 1996; Lamarche et al., 1996; Sahai et al., 1998). These residues do not participate in the direct interactions with the PKN ACC-finger domain, but some of these mutated G proteins have been reported to select the effector proteins of specific signalling pathways. Interestingly, replacement of Tyr-42 of RhoA with cysteine abolishes the PKN binding. This effect on PKN binding is probably due to changes in the side-chain packing of RhoA Switch I involving Tyr-42 together with Lys-27, which is hydrogen bonded to Asp-85PKN, as described above. On the other hand, this mutation exhibits no effect on the binding to ROCK-I, indicating the different natures of their interfaces in the RhoA/PKN and RhoA/ROCK-I

complexes. Some Rho-effector proteins such as p140mDia have effector domains which exhibit no sequence homology with the ACC-finger domains. For these proteins' mutations may possibly play a great role in differentiating the effector selection.

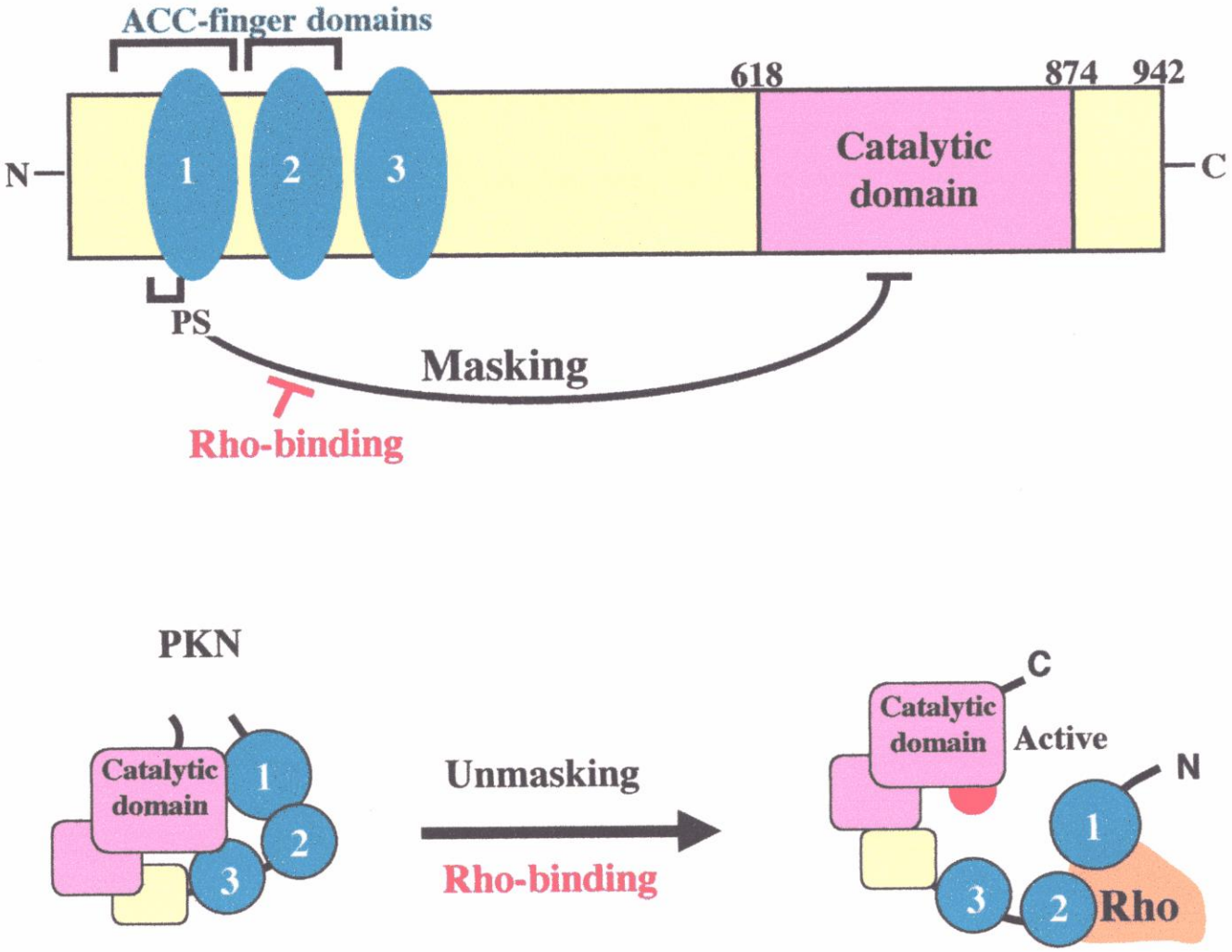

Fig.28. A Model of the PKN Activation Mechanism by RhoA/GTP

The autoinhibition of the PKN catalytic activity. PKN ACC-1, ACC-2, and ACC-3 domains are colored in green, and catalytic domain is colored in rose. The PKN N-terminal half fragment binds to the C-terminal half fragment containing the catalytic domain and inhibits the protein kinase activity, suggesting a masking mechanism by the N-terminal region (Kitagawa et al., 1996). RhoA binding to the ACC-finger domain at the PKN N-terminal region could produce the activation by unmasking.

III. Crystal Structure of RhoBD(69)

1. Materials and Methods

Expression and Purification

RhoBD (69), the minimum Rho-binding domain (RhoBD; residues 979-1047) of bovine Rho-kinase (Leung *et al.*, 1995; Fujisawa *et al.*, 1996), was subcloned into pGEX-2T, and the GST-fused proteins were expressed in *E.coli* DH5α cells. For the expression of Se-Met substituted protein, this construct was also transformed into the methionine auxotrophic *E.coli* strain B834(DE3)pLysS (Novagen). The GST-fused protein was purified using glutathione Sepharose 4B. Removal of GST from GST-RhoBD was achieved within the column using by human thrombin (Sigma) with 2 units/ml for 24 hours at 4℃. RhoBD was eluted with a buffer containing 20 mM HEPES pH 7.0 and 50 mM KCl. This eluate was applied to HiTrap S and HiTrap Q (Amersham Pharmacia Biotech) and the eluates from each column were collected and concentrated to 6 mg/ml using Centricon-3 (Millipore). The purified samples used in this study were verified with MALDI-TOF MS and N-terminal analysis. The N-terminal analysis of the resulting sample showed that the additional glycine and serine residues at the N-terminus originated from the site of cleavage by thrombin. The molecular weight of the purified RhoBD(69) observed by MALDI-TOF MS was 7,996 Da, which is virtually the same as its calculated value (7,997 Da).

Overlay assay

The Rho-binding activity was confirmed by an overlay assay using ^{35}S-labeled RhoA

complexed with GTPγS. Purified GST-RhoBD(69) were separated on an SDS-PAGE, transferred to nitrocellulose membrane, and probed with [^{35}S]GTPγS-GST-RhoA. The labeled bands were visualized by an image analyzer (Fuji) (Fig.29).

Dynamic Light Scattering

Dynamic light scattering studies were carried out using a DynaPro-801 instrument (Protein Solutions, Inc.). It was attempted for each solutions, RhoBD(69), PKN(7-155), RhoA/GTPγS, mixture of RhoBD(69) and RhoA/GTPγS, and mixture of PKN(7-155) and RhoA/GTPγS. All solutions were filtered through 0.22-μm filters (Millipore) to remove particulates. Scattering of these protein solutions were analyzed at concentrations of 2.5 ~ 10 mg/ml in its storage buffer (20 mM HEPES pH 7.5, 100 mM KCl, 5 mM $MgCl_2$ and 10 mM β-mercaptoethanol).

The principle of dynamic light scattering is based on the Brownian motion of molecules in solution, which causes scattered light intensity to fluctuate (Schurr J. M., 1977). These fluctuations are measured by the DynaPro instrument. The DYNAMICS software was used to calculate the hydrodynamic radii of solution particles and to estimate particle molecular weight and regularize scattering data (table 6).

Crystallization

Crystals were obtained at 4℃ using hanging-drop vapour-diffusion by mixing 2.7 mg/ml RhoBD(69), 55 mM HEPES pH 7.0, 23 mM KCl, 11% PEG 1000, 14% ethylene glycol and 22 mM *n*-octanoylsucrose (Hampton Research) over a 500 μl reservoir of 100 mM HEPES

pH 7.0 containing 25% PEG 1000 and 30% ethylene glycol. Clusters of crystals appeared in a few days and were successively micro-seeded and macro-seeded, which gave single crystals suitable for diffraction analysis. Typically, crystals grew to dimensions of $0.7 \times 0.2 \times 0.05$ mm^3 in a week (Fig.30).

Data Collection and Processing.

Crystals were flash frozen in liquid nitrogen for data collection. X-ray diffraction data were collected at 2.0 A resolution using a Rigaku R-Axis IV on a rotating anode generator (Rigaku FR-C) operating at 50 kV and 60 mA with Cu-K_α radiation (λ = 1.54178 A) at 100K using a Rigaku Cryosystem. The focus size of the X-ray beam was 100 μm, and the beam was focused using a Supper double-focusing mirror. The diffraction data were processed using the programs DENZO and SCALEPACK. Each intensity, *I(h k l)*, was evaluated from the imaging plates and transformed to the amplitude of structure factor, *F(h k l)*, where *h*, *k*, and *l* are the reciprocal lattice points. The crystals belong to the Monoclinic space group *C*2, with unit cell dimensions *a* = 148.1 A *b* = 25.9 A, *c* = 39.4 A. A total of 64,203 independent measurements were merged to obtain 9,933 unique reflections. The R_{merge} value based on intensity data (1.0 σ cutoff) was 5.8% with a completeness of 94.7% (in the highest-resolution shell of 2.07 - 2.00 A with a completeness of 81.7% and an R_{merge} of 22.6%). The I/σ(I) ratio is 3.5 for all data and 2.2 in the highest shell.

As attempts to find heavy-atom derivatives had failed because of their high-order non-isomorphism, we used selenomethionyl RhoBD(69) and its crystals, which were obtained as

outlined above. The number of methionines per monomer is one. X-ray intensity data were collected with FUJI large X-ray image-plates (400×800 mm^2) using synchrotron radiation at the beamline BL-18B of the Photon Factory (PF; Tsukuba, Japan). X-ray diffraction data were collected at 1.5 A resolution using synchrotron radiation. The best crystals belong to the Monoclinic space group *C*2, with unit cell dimensions a = 148.0 A, b = 26.1 A, c = 39.6 A (Table 7). The details of the intensity data processing are indicated in Table 8.

Selenium positions were identified using the SnB program (Weeks and Miller, 1999), showing three prominent peaks. Since each chain of RhoBD(69) contains one Met, this result suggests one Met residue has two conformers. Phase calculation and heavy atom refinement using the program SHARP (de La Fortelle and Bricogne, 1997) resulted in a final overall figure of merit of 0.35 from 30 to 1.8 A. Solvent flattening using the program Solomon (Abrahams and Leslie, 1996) resulted in an electron density map of good quality, into which a nearly complete model was built. The model was built and refined through alternating cycles using the program O (Jones et al., 1991) and the program CNS (Brunger et al., 1998), respectively. The current model, which was refined with crystallographic R_{value} 21.8 % (free R_{value} of 24.5 %) for all intensity data at 1.8 A resolution, includes residues 979-1045 and 979-1044 for each chain and 137 water molecules. A summary of the refinement statistics is given in Table 9. There is no residue in disallowed regions of the Ramachandran plots as defined in the program PROCHECK (Fig.31). Due to weak electron density, the 21 residues are modeled as Ala. Identification of knobs-into-holes packing is analyzed by the program SOCKET (Walshaw and Woolfson, 2001). Accessible surface areas were calculated using the program

NACCESS (Hubbard et al., 1993). The figures are displayed by the programs GRASP, MolScript and raster3d.

The coordinates and structure factors will be deposited in the RCSB Protein Data Bank.

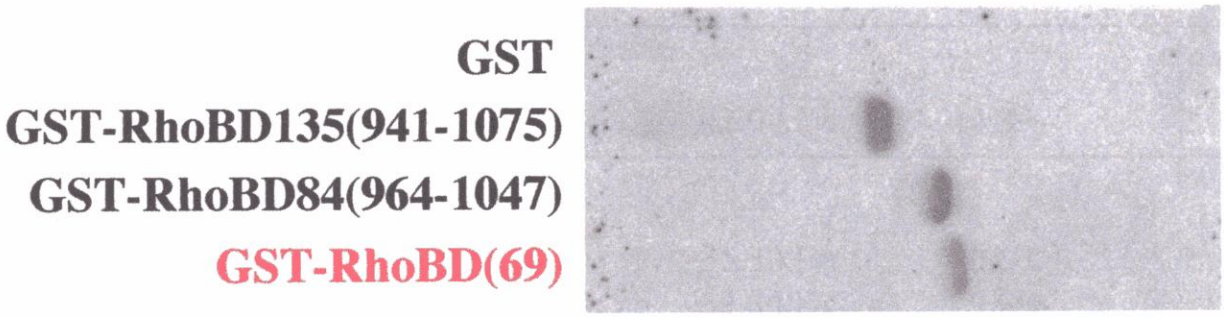

Fig.29. Ligand overlay assay

Interactions of RhoBD(69) with RhoA revealed by an autoradiogram. For comparison, GST, GST-RhoBD (941 - 1075), and truncated form of RhoBD (964 - 1047) are also shown,

Table 6
Dynamic Light Scattering Results

Protein	Molecular weight	Estimated M.W.	Polyd./ Radius*	SOS Error §
RhoBD(69)	8.0 kDa			
5 mg/ml		28,8 kDa	9.4%	2.921
2.5 mg/ml		23.8 kDa	20.7%	3.939
PKN (7-155)	16.5 kDa			
5 mg/ml		42.0 kDa	14.3%	2.015
RhoA^{V14}/GTPγS	22.3 kDa			
10 mg/ml		35.3 kDa	10.6%	0.964
5 mg/ml		32.8 kDa	9.8%	0.983
RhoBD(69) + RhoA^{V14}/GTPγS				
5 mg/ml (2 : 1)‡	38.3 kDa	-	-	-
5 mg/ml (1 : 1)‡	30.3 kDa	62.1 kDa	8.5%	2.024
PKN (7-155) + RhoA^{V14}/GTPγS				
5 mg/ml (2 : 1)‡	55.3 kDa	67.3 kDa	17.6%	3.025
5 mg/ml (1 : 1)‡	38.8 kDa	-	-	-

* Polydispersity as a % of the average radius. < 15 % ; a monodisperse solution, > 15 % ; a polydisperse solution.

§ The SOS parameter represents the amount of residual noise or error associated with the autocorrelation function. < 5.0 ; Negligible, 5.0 - 20.0 ; Significant background errors, which may be due to noise caused by solvent at low protein concentrations, or a small amount of polydispersity.

‡ sample was mixed 2 : 1 or 1 : 1 stoichiometry.

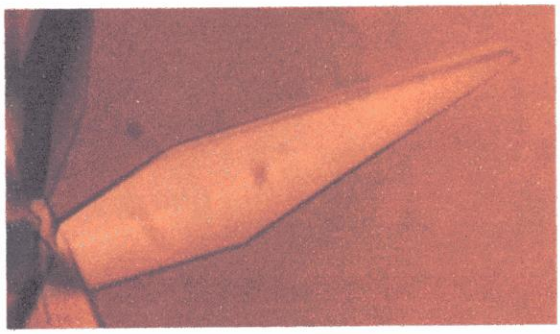

A

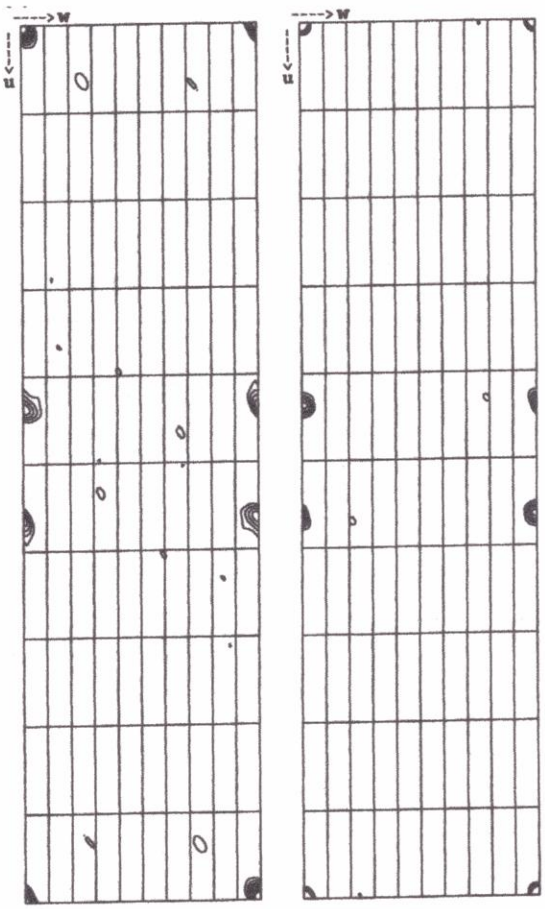

B (a) (b)

Fig.30. A crystal of the RhoBD(69) and Haeker sections

(A) A native crystal of the Rho-binding domain of bovine Rho-kinase. The approximate dimensions of this crystal are 0.7 × 0.2 × 0.05 mm.

(B) The v = 0 Harker sections of the (a) Bijvoet (λ_2) and (b) dispersive (λ_1 - λ_3) difference Patterson functions. The resolution range is 10 - 2.5 Å and the contour level is 3 - 20σ with 2σ intervals.

Table 7
Crystal data of RhoBD(69)

Crystal system	**Monoclinic**
Space group	***C*2**
Unit cell dimensions	**a = 148.0, b = 26.1, c = 39.6 A**
	$\alpha = \gamma = 90^\circ$ $\beta = 90.3^\circ$
Unit cell volume	**1.53 x 10^5 A^3**
Z	**2**
V_m	**2.36 A^3/Da**
V_{solve}	**48%**

The molecular weight of RhoBD(69) is 7,997 Da.

Table 8
Intensity data processing

	Native (λ=1.000)	edge (λ_1=0.9784)	peak (λ_2=0.9778)	high remote (λ_3=0.9600)	low remote (λ_4=1.000)
Resolution	1.8	1.9	1.9	1.9	1.9
R_{merge}* †	4.5 / 8.2	3.5 / 10.3	5.6 / 12.1	4.5 / 12.1	2.2 / 4.2
Number of Measurements	139,215	26,293	53,024	28,161	44,959
Number of Independent reflections	12,896	10,783	10,924	10,909	11,434
Completeness †	89.0 / 68.4	87.7 / 86.1	89.3 / 88.4	88.5 / 86.4	93.2 / 80.2
Mosaicity	0.301	0.273	0.420	0.284	0.290
Mean <I/σ(I)> †	18.2 / 14.8	15.2 / 9.8	15.2 / 10.9	13.9 / 8.8	17.8 / 14.1

* R_{merge} = 100 x Σ | I(h) - <I(h) > | / Σ I(h) , where <I(h) > is the mean intensity for reflection ***h***.
† Each pair of values are for overall / outer shell. The resolution ranges of their outer shells are 1.86-1.80 A for native, 1.97-1.90 A for Se-Met proteins

Table 9
Refinement statistics

Resolution range	**1.8 A**
R_{cryst}*	**21.8 % (31.4 %)†**
R_{free} §	**24.5 % (36.0 %)†**
R.m.s. bond lengths	**0.006 A**
R.m.s. bond angles	**0.934°**
R.m.s. dihedral angles	**1.053°**
Number of residues	**137**
Atoms included	**11,002 for protein (174 for water molecules)**

* $R_{cryst} = 100 \times \Sigma \mid Fo(h) - Fc(h) \mid / \Sigma Fo(h)$.

§ R_{free} is R_{cryst} which was calculated using 5% of the data, chosen randomly and omitted from the subsequent structure refinement.

† Brackets are quantities calculated in the highest resolution bin at 1.86-1.80 A

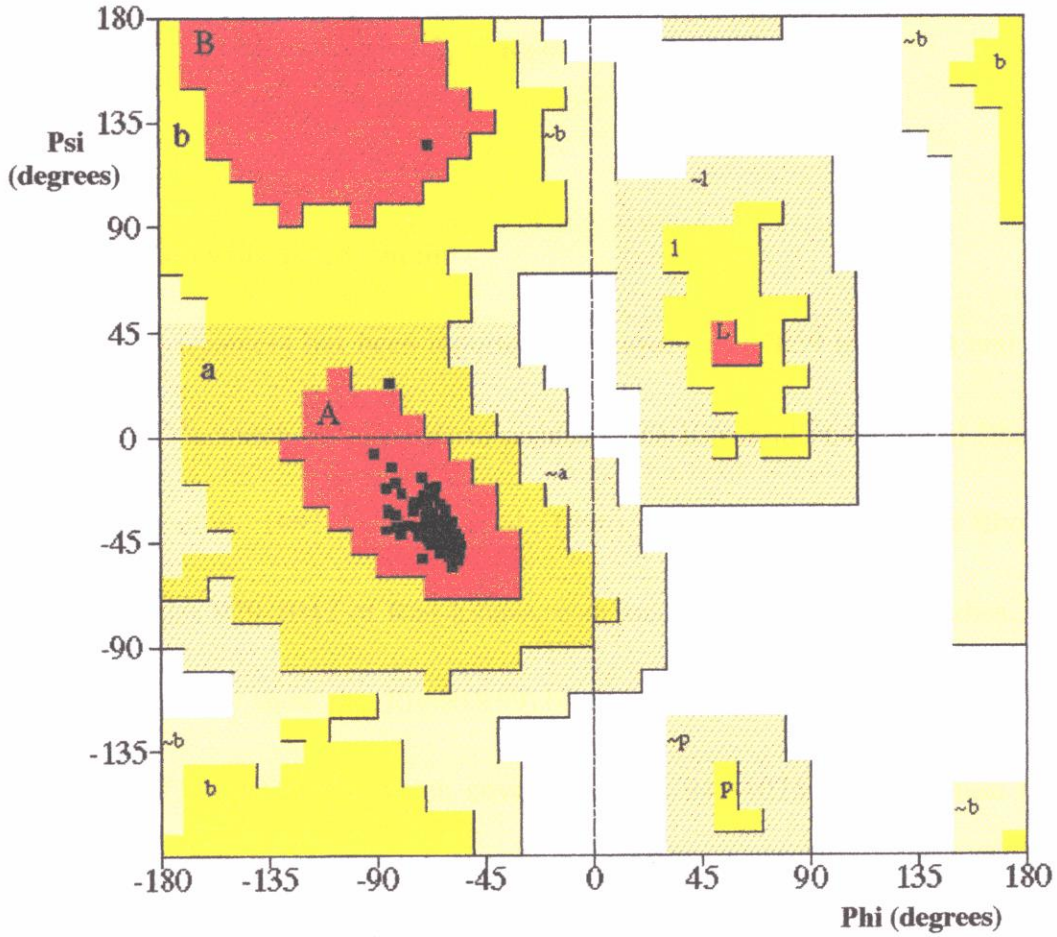

Plot statistics

Residues in most favoured regions [A,B,L]	132	99.2%
Residues in additional allowed regions [a,b,l,p]	1	0.8%
Residues in generously allowed regions [~a,~b,~l,~p]	0	0%
Residues in disallowed regions	0	0%
Number of non-glycine and non-plroline residues	133	
Number of end-residues (excl. Gly and Pro)	3	
Number of glycine residues (shown as triangles)	2	
Number of proline residues	0	
Total number of residues	138	

Fig.31. Ramachandran plot of RhoBD(69).

Main chain dihedral angles were analyzed with the program PROCHECK. The horizontal axis indicates ϕ angle around N-Cα bond and the vertical axis indicates ψ angle around Cα-C bond. Most favoured, additional allowed, generously allowed, and disallowed regions are shaded in red, yellow, light yellow, and white, respectively. Glycine residues are shown as triangles and non-glycene residues are indicated by squares. The labels A and a indicate the regions for α-helix, B and b for β-strand, and L and l for α_L-helix.

2. Results

Identification of RhoA binding Domain

The Rho-binding fragment has been reported as residues 970-1059 in ROKα and residues 934-1015 in $p160^{ROCK}$, which corresponds to residues 979-1068 and 964-1045 of Rho-kinase, respectively (Leung et al., 1995; Fujisawa et al., 1996). In this study, a fragment RhoBD(69), which covers residues 979-1047 of Rho-kinase, was used for the structural studies. Overlay assay experiments clearly show that RhoBD(69) binds to RhoA. The affinity of RhoBD(69) is weaker than that of RhoBD(135), which covers residues 941-1075 of Rho-kinase (Fig.29). This difference in the affinity may be due to the lack of the N-terminal segment (934-945 in $p160^{ROCK}$, 964-975) that contributes to Rho-binding (Fujisawa et al., 1996).

Overall Structure

The current model of RhoBD(69) solved at high resolution (1.8 A) displays a well-defined structure, while three C-terminal residues are unstructured. RhoBD(69) forms a ~97 A-long parallel coiled-coil structure with two long consecutive helices (Fig.32A), while the MULTICOIL program (Wolf, E. et al., 1997) predicts the low probability to form coiled-coil structure in the C-terminal region (1024-1047). The total buried accessible surface area is ~2900 A^2, which seems enough to form a stable dimer. This parallel coiled-coil structure is similar to the parallel coiled-coil structure of tropomyosin (Whitby, F.G. et al., 2000) rather than the anti-parallel coiled-coil structure of PKN and three-helix coiled-coils structure of

arfaptin that is an effector of Rac and Arf (Tarricone et al., 2001) (Fig.32). A root-mean-square deviation for the 100 Cα-carbon atoms of the RhoBD(69) and tropomyosin is 2.0 A. On the other hand, superposition of RhoBD(69) and PKN ACC-finger domain shows that individual helices have similar main-chain conformations, although the C-terminal regions are poorly superimposed.

Coiled-coil Formation

Interactions in the coiled-coil of RhoBD(69) at the N-terminal (979-1002) and C-terminal (1024-1044) regions are similar to those in previously determined structures of leucine zipper and dimeric coiled-coil proteins encoded by a characteristic seven-residue repeat $(abcdefg)_n$ (Fig. 33). The helices generally display canonical knobs-into-holes packing, in which the side chains at *a* and *d* positions form successive layers and contacts are made with four residues from the opposing helix. In contrast, the coiled-coil packing around the middle region (1003-1023) is loose. Knobs-into-holes packing is not identified by the SOCKET program (Walshaw and Woolfson, 2001) in this region excluding two positions (residues 1003 and 1020). Moreover, the buried accessible surface area of the middle region is two fold lower than those of the N- and C-terminal region. Generally, hydrophobic residues tend to be present at *a* and *d* positions with low accessibility (<30%). However, the accessibility of the residues at these positions is high (> 30-40%) in the middle region because of the loose packing.

The interhelix distance between two helices shows the helices diverge around the middle region. Correspondingly, the averaged B-factor (40.3 A^2) in this region is ~2 fold higher than

overall B-factor (22.9 A^2) (Fig.34). Interestingly, sequence alignment among Rho-kinase and its homologs shows an insertion/deletion in the middle region (Fig.33).

In the typical parallel coiled-coil structures, hydrogen bonded ion pairs occur between oppositely charged residues at *g* and succeeding *e* positions (where prime denotes the other chain). Only one possible *g*-to-*e* pair is apparent in the RhoBD(69) coiled-coil segment. Notably, Glu-1027 at the d position makes salt bridge with Lys-1031 at a position. Ordered solvent molecules are not observed between helices, where Ala residue that fails to fill the space occupies the *d* position, while several solvent molecules in the coiled-coil region of APC are identified between the helices (Day and Alber., 2000).

Mapping of Mutation Analysis

Mutation analysis reveals that several residues are critical for Rho binding (Fujisawa et al., 1996, Leung et al., 1996). Lys-964 and Leu-971 mutations ($p160^{ROCK}$) were reported to weaken Rho binding significantly, but these residues are not included in the current model (Numbering scheme corresponds to Rho-kinase (Fig.35)). Glu 1040 mutation also significantly weakens and Ile-1041 mutation completely abolishes Rho binding ($p160^{ROCK}$). Double mutations of Glu-1027 + Arg-1028, Lys-1031 + Gln-1033, and Asn-1036 + Lys-1037 (ROKα) showed loss of RhoA binding. These residues are spread in a limited region around the C-terminus (Fig.35, 36A).

Electrostatic potentials of RhoBD(69) show that the negatively and positively charged region is separated in the N-terminal and C-terminal region, respectively (Fig.36B). In the

PKN/RhoA complex, complementary electrostatic potential exists at the interface, where the positively charged ACC finger domain contacts RhoA in the negatively charged region (Fig.22B). The distribution of the residues critical for Rho binding is consistent with that of the positively charged region.

Oligomeric State of RhoBD (69)

To determine the oligomeric state of RhoBD(69), we carried out dynamic light scattering and gel-filtration studies. The results of the dynamic light scattering experiments are given in Table 6. The estimated molecular weight of RhoBD(69) by the dynamic light scattering measurements were 23.8 kDa ~ 28.8 kDa with relatively small dispersity indicating that the particles in solution are the same size. This result is coincident with the fact that RhoBD(69) is eluted at 23 kDa by a gel-filtration. These results indicate that RhoBD(69) exists as a dimer or a tetramer states in solution.

Moreover, we carried out dynamic light scattering mesurements with a mixture of RhoA and RhoBD(69), PKN(7-155) and a mixture of RhoA and PKN(7-155) (Table 6). The estemated molecular weight of the 1 : 1 stoichiometry mixture of RhoA and RhoBD(69) was 62.1 kDa, which is almost twice as the calculated one. These results suggest that RhoA and RhoBD(69) may form a 2 : 2 complex in solution.

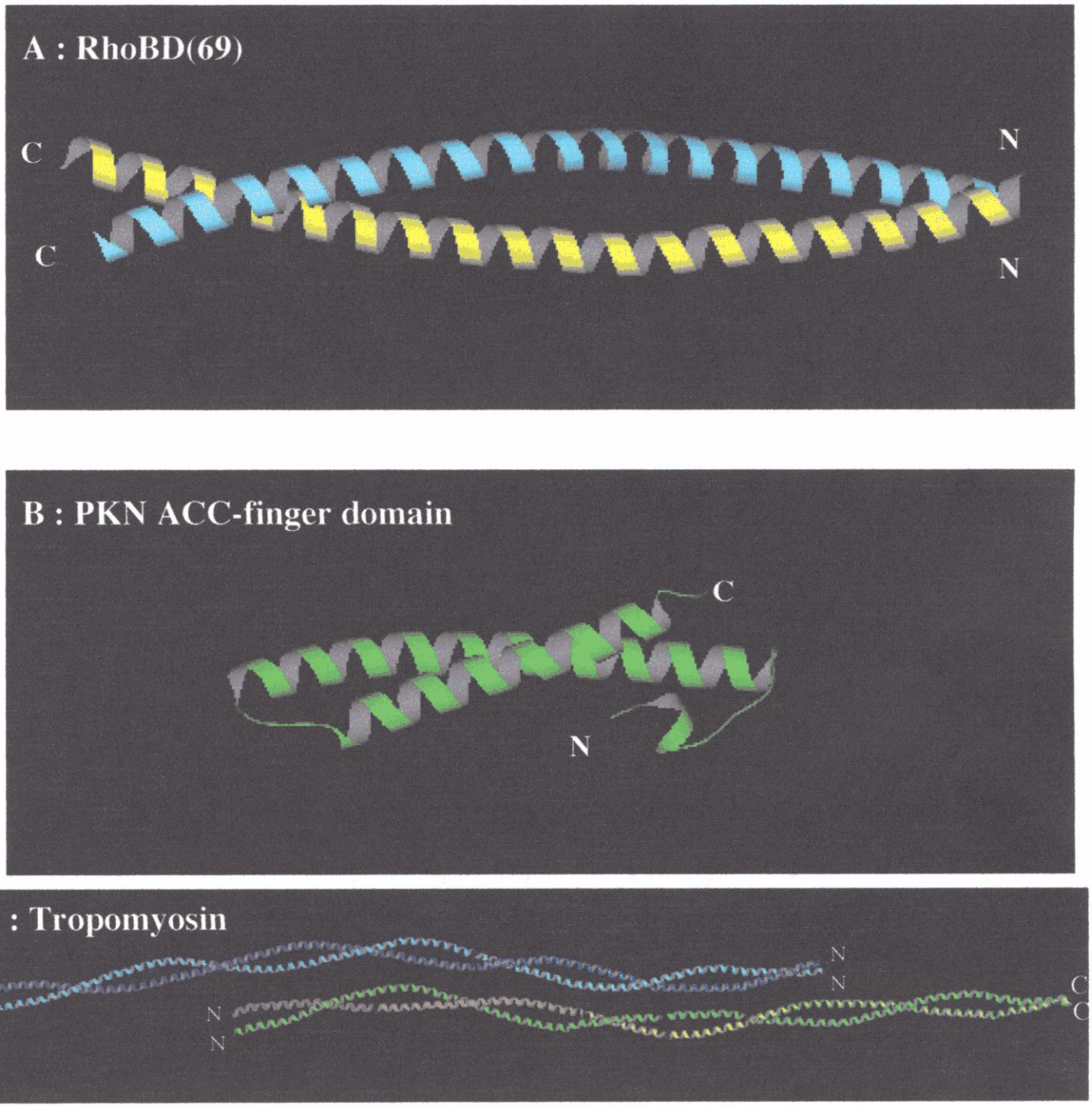

Fig.32. Coiled-coil Structural of RhoBD(69), the PKN ACC-finger domain and Tropomyosin

(A) Overall structure of RhoBD(69)

(B) The antiparallel coiled-coil structure of PKN is different from the parallel coiled-coil structure of RhoBD(69).

(C) The coiled-coil structure of RhoBD(69) is similar to tropomyosin rather than the PKN ACC-finger domain.

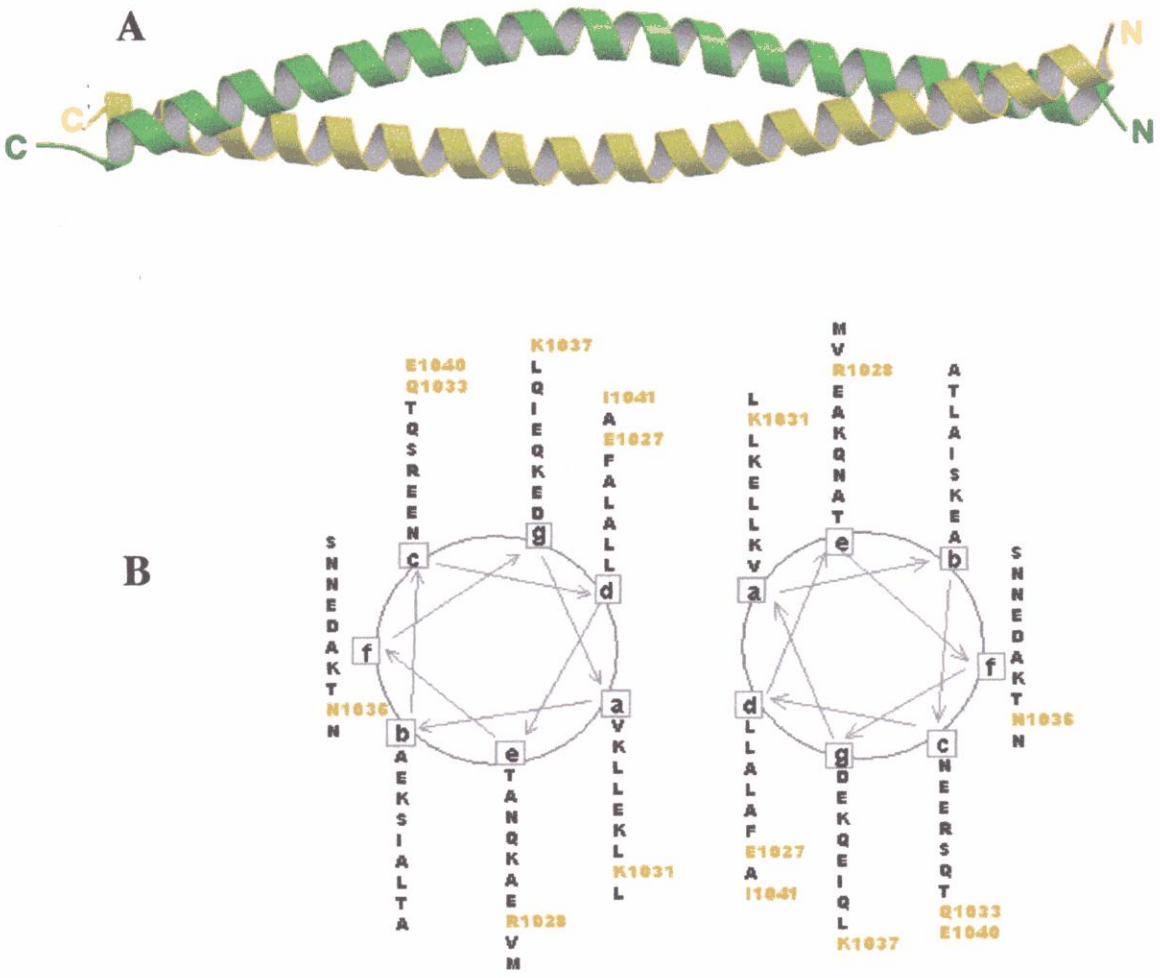

Fig.33. Structure of the RhoBD(69)

(A) A ribbon representation of RhoBD(69). Each chain is colored green and yellow, respectively.

(B) Helical wheel diagrams of the sequence and structure of RhoBD(69) from the amino terminus of the dimer. Residues that affects the binding to RhoA are colored yellow.

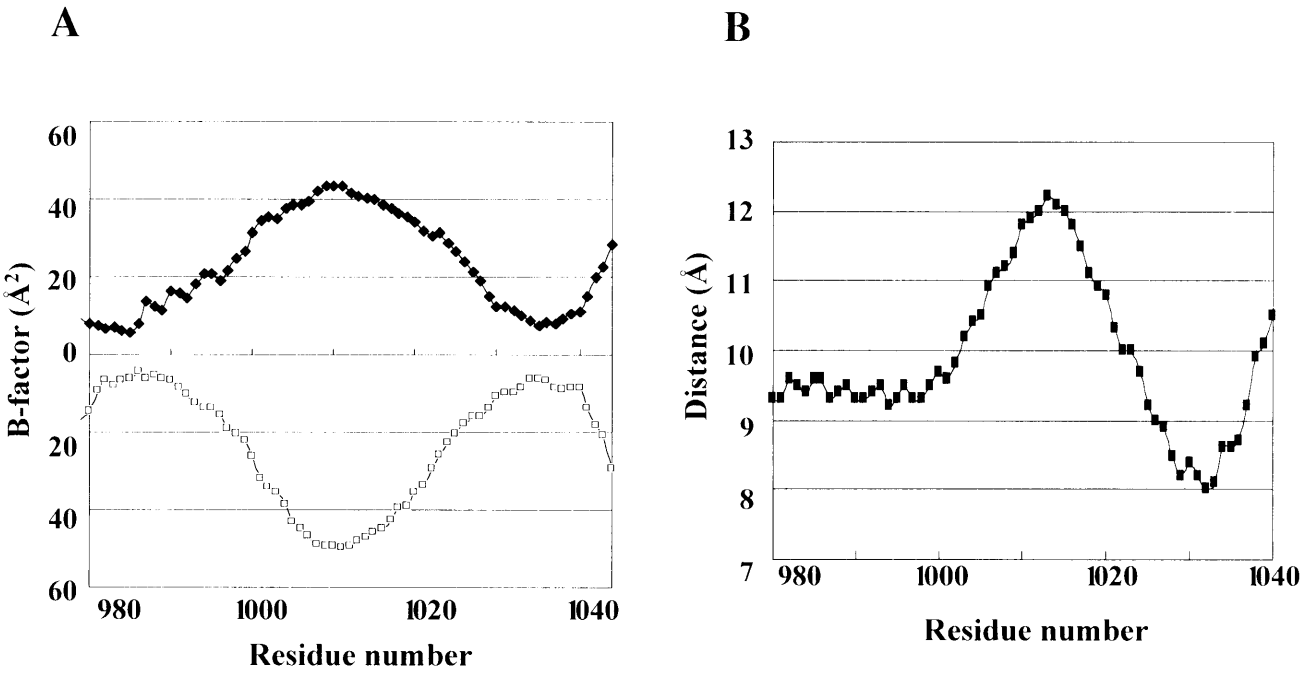

Fig.34. Helix separation and averaged B-factor plot

Averaged B-factor plot (A) and helix separation (B) of the main chain atoms in the RhoBD(69) crystal structure. Interhelix distances between Cα-carbonatoms are plotted as a function of residue number.

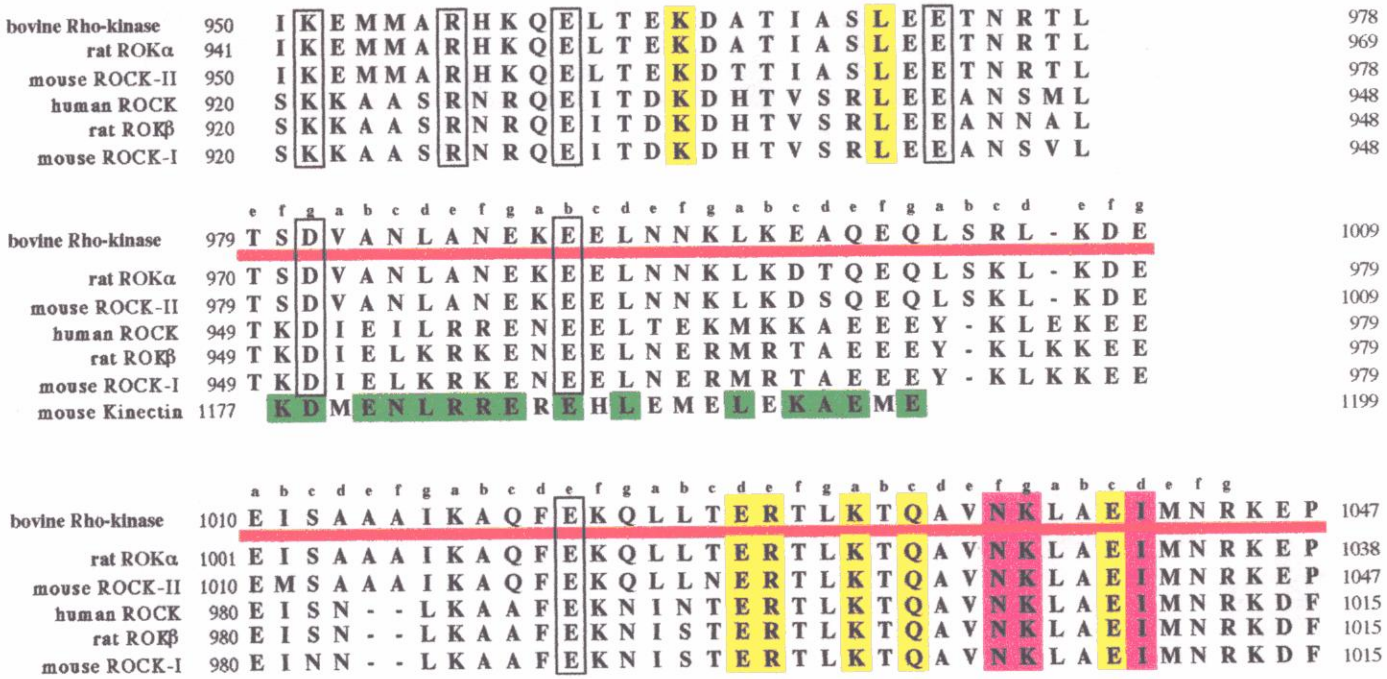

Fig.35. Sequence Alignment of the Rho-binding domain of the Rho-kinase

The RhoBD(69) region used for the present crystallographic study is underlined. The *a-g* heptad repeats of helices are displayed above the sequence in the coiled-coil domain of RhoBD(69). Mutated residues that weaken or abolish the Rho-binding is colored in yellow and pink, respectively. Residues of which substitution leads to no effect are boxed by thin lines. Added Kinectin 1177-1199, ROCK-I/Kinctin homology region, conserved residues are colored in green.

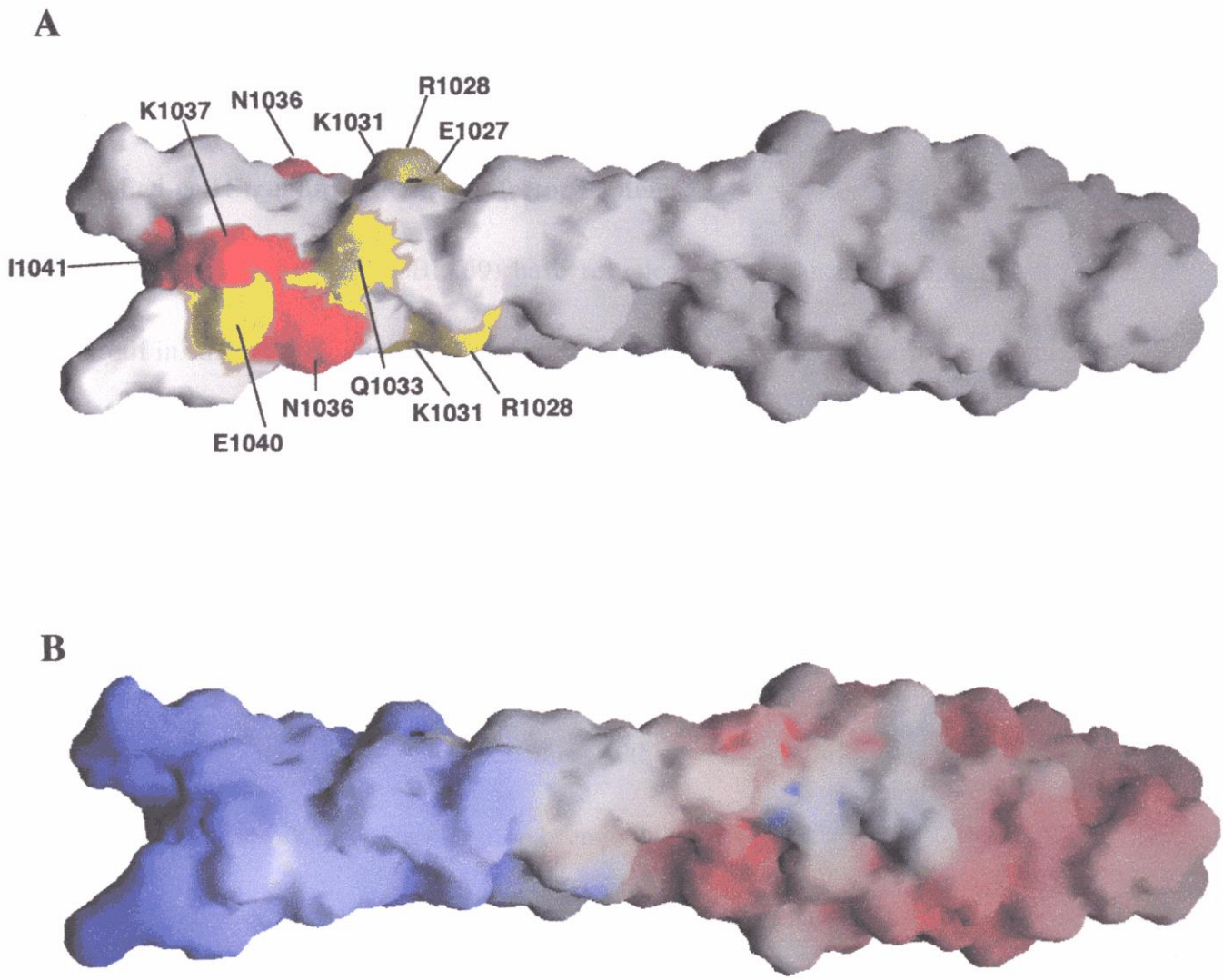

Fig.36. Accessible surface area of RhoBD(69)

(A) Residues critical for Rho binding mapped onto the solvent accessible surface. Residues that weaken or abolish the Rho-binding is colored yellow and red, respectively.

(B) Electrostatic surface potentials of the RhoBD(69) with negative potentials in red and positive potentials in blue. The region critical for Rho binding is mainly positively charged.

3. Discussion

Coiled-coil Structure in Other Effector Proteins

Crystal structure of RhoBD(69) have revealed the existence of parallel coiled-coil motif in Rho-binding domain of Rho-kinase, as is predicted from the primary sequence. The coiled-coil and leucine zipper motifs are increasingly recognized as an important element of numerous proteins. These motifs stabilize subunit associations and facilitate oligomerizaion. It is noteworthy that the defined Rho-binding regions among many Rho effector proteins such as ROCKs, citron and kinectin are all found in regions of extended α-helical coiled-coil structures although no significant sequence motifs common to these RhoA effectors have been identified.

MRCK, closely related to Rho-kinase, have an extended coiled-coil domain and forms a tetramer or dimer in solution. Moreover, it is strongly suggested that the coiled-coil domain of MRCK entwines to form parallel structure that drive MRCK oligomerization (Tan et al., 2001). It is shown that kinectin is present in dimer by hydrodynamic studies (Kumar et al, 1998). Two Rho molecules could bind to these coiled-coil domains from both sides since the parallel coiled-coil structure contains symmetric surfaces. In fact, two antibodies raised against kinectin attached at the same region on opposite sides of the kinectin molecule (Kumar et al, 1998). This suggests that the coiled-coil is not anti-parallel but parallel, and the molecule having affinity for

the coiled-coil domain can attach on the both sides. To clarify this, further experiment will be required.

RhoA binding Mode of Rho-kinase and PKN

It is interesting whether the binding mode observed in PKN is distinct from that of Rho-kinase, as proposed by Fujisawa et al. (1996, 1998) according to the sequence homology and binding experiment. The helical wheel diagram of the C-terminal region RhoBD(69) reveals that some residues, which would be critical for RhoA-binding, coincide with the PKN ACC-finger residues which participate in the Contact-1 interactions with RhoA in the RhoA/PKN complex crystal. Especially, RhoBD(69) Lys-1031, Lys-1037 and Glu-1040 correspond to PKN Lys-53, His-88 and Asp-85, respectively (Fig.37). It suggests that if Rho-kinase exist as dimer, some interactions similar to those found in the PKN Contact-1 could be observed at the C-terminal region of the RhoBD(69).

Interestingly, RhoBD(69) dose not preserve exposed hydrophobic residues corresponding to those forming a surface hydrophobic patch in the PKN ACC-finger domain to participate in the Contact-2 interactions with RhoA in the RhoA/PKN complex. These differences, which must perturb the interactions at the PKN Contact-2, is consistent with the reported results that rat ROKα dose not interfere the GAP-activated GTPase activity of RhoA (Leung et al., 1995).

The ROCK-I/Kinectin homology region (residues 980-1002 for Rho-kinase) may be involved in RhoA binding (Alberts et al., 1998) (Fig.35). A mutational analysis shows that a region (residues 934-945 in $p160^{ROCK}$, residues 964-975 for Rho-kinase) near ROCK-I/Kinectin homology region may be involved in Rho binding (Fujisawa et al., 1996). This region corresponds to the N-terminal region of the current structure with negative electrostatic potentials. This second possible binding site for RhoA may be related to the multiple proposed binding determinants of Rho (Fujisawa et al., 1998).

These observations suggest the RhoA binding mode of Rho-kinase may be different from that of PKN, while these two binding modes involving α-helical domain, which is distinct from the CRIB domains for Cdc42 and Rac.

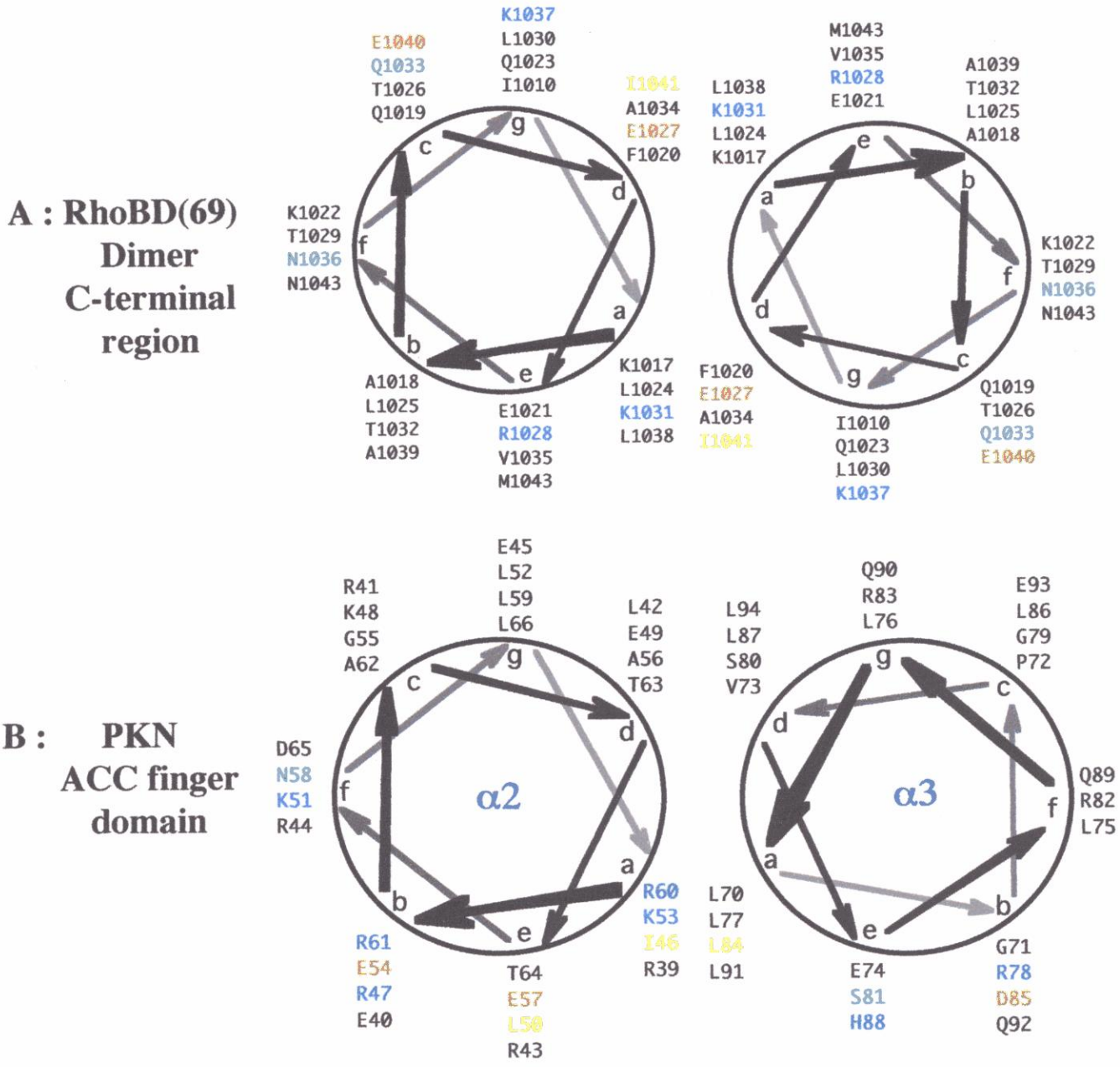

Fig.37. Axial helical projections of the RhoBD(69) and PKN ACC finger domain

(A) Axial helical projections looking down the helices of the RhoBD(69) dimer from C termini. The residues that would be important for RhoA binding are colored in red (acidic), blue (basic), yellow (hydrophobic) and green (others), respectively.

(B) Axial helical projections looking down the helix bundle from the N and C termini of helices α2 and α3, respectively. The residues participate in the interactions with RhoA at the RhoA/PKN complex shown Fig.9 (contact-1) are colored same as (A).

IV. Conclusions

The RhoA/PKN complex structure presented reveals that PKN has a novel effector domain for Rho, which is distinct from the CRIB domains for Cdc42 and Rac. This PKN ACC-finger domain binds RhoA at the RhoDRs containing Switch I, β-strands B2/B3, and the C-terminal α-helix A5. The specificity determinant residues of Rho are located at all the RhoDRs and are different from the specificity determinant residues of Cdc42 and Rac. Thus, the present structure illustrates the various ways that the Rho family members of small G proteins interact with their effector proteins. We have also shown that the ACC-finger domain is widely conserved in rhotekin and rhophilin. Sequence analysis based on the structure suggests that PKN has tandemly-repeated ACC-finger domains at the N-terminal regulatory region. The present structure provides a clue to the analysis of the multiple RhoA-PKN interactions in its utilization of multiple effector domains and, possibly, different binding surfaces on the G protein.

The most common mechanism of effector activation by small G proteins is thought to be the disruption of intramolecular autoinhibitory interactions, to expose functional domains (Bishop et al., 2000). PKN and Rho-kinase have also been reported to contain autoinhibitory domains. A region of the Rho-kinase autoinhibitory domain includes the RhoBD and PH domains (Amano et al., 1999, 2000). In the case of PKN, the binding of Rho appears to co-operate with binding of lipids such as arachidonic acid and with auto-phosphorylation to remove an auto-inhibitory interaction. These interactions fully activate its protein kinase C-

like kinase domain (Kitagawa et al., 1996, Yoshinaga et al., 1999, Palmer et al., 1995b). The present structure could provide a clue to the activation mechanism of PKN, as unmasking and activating catalytic domain.

Recently, the structure of p21-activated kinase 1 (PAK1) that is regulated by Cdc42 or Rac has been solved (Lei et al., 2000) in an auto-inhibited state. Its structure suggests that auto-inhibitory state is achieved by dimerization. The small GTPase binding may trigger a series of conformational changes, beginning with disruption of the PAK1 dimer. It is of interest whether conformational changes involving dimer dissociation would occur in Rho-kinase or not. Further crystallographic investigation of RhoBD complexed with Rho will be required to understand detailed molecular recognition mechanism of Rho by Rho-kinase.

V. Acknowledgements

The present studies and thesis have been performed under the direction of Professor Toshio Hakoshima (Division of structural biology, Nara Institute of Science and Technology). I would like to express my gratitude to Professor Hakoshima. I am deeply grateful to his cordinal guidance, discussions and encouragement. I wish to express my sincere gratitude to Dr. T. Shimizu (Science of Biological Supramolecular Systems, Yokohama-city University), Dr. K. Ihara (Department of Biochemistry, The University of Texas Southwestern Medical Center) for teaching me from basic handling of *E.coli* to practical computer works, and to Dr. K. Okada for teaching me to practical computer works. I wish to express my thanks to Dr. S. Kuroda (Computer Science, Graduate School of Information Science and Technology, Tokyo University), Dr. M. Amano (Department of Cell Pharmacology, Graduate School of Medicine, Nagoya University) and Prof. K.Kaibuchi (Department of Cell Pharmacology, Graduate School of Medicine, Nagoya University) for the gifts of many plasmid for RhoA, PKN, and RhoBD expression, and helpful discussions. I am grateful to Ms. J. Tsukamoto and Dr. S. Takayama, for their assistance with the mass spectroscopy and the N-terminal sequencing. I also would like to thank to Dr. N. Igarashi, Dr. M. Suzuki, Dr. N. Watanabe, and Dr. N. Sakabe, for their assistance on the MAD data collection at PF, Tsukuba.

Thanks to Professor Masahiro Shirakawa for his helpful discussion. Thanks also to Dr. T. Ikegami, Dr. C. Kojima, and Dr. M. Mishima for helpful discussion, and to all members of laboratory for their help and valuable discussion.

This work was partly supported by a research fellowship from the Japan Society for the Promotion of Science to me.

VI. References

Abrahams, J. P. and Leslie, A. G. W. (1996) Methods used in the structure determination of bovine mitochondrial F1 ATPase *Acta Cryst.* **D52**, 30-42

Abdul-Manan, N., Aghazadeh, B., Liu, G. A., Majumdar, A., Ouerfelli, O., Siminovitch, K. A., Rosen, M. K. (1999) Structure of Cdc42 in complex with the GTPase-binding domain of the 'Wiskott-Aldrich syndrome' protein. *Nature*. **399**, 379-83

Alberts, A. S., Bouquin, N., Johnston, L. H., Treisman, R. (1998) Analysis of RhoA-binding proteins reveals an interaction domain conserved in heterotrimeric G protein beta subunits and the yeast response regulator protein Skn7. *J. Biol. Chem.* **273**, 8616-22

Amano, M., Chihara, K., Nakamura, N., Kaneko, T., Matsuura, Y., Kaibuchi, K. (1999) The COOH terminus of Rho-kinase negatively regulates rho-kinase activity. *J. Biol. Chem.* **274**, 32418-24

Amano, M., Fukata, Y., Kaibuchi, K. (2000) Regulation and functions of Rho-associated kinase. *Exp. Cell. Res.* **261**, 44-51

Amano, M., Ito, M., Kimura, K., Fukata, Y., Chihara, K., Nakano, T., Matsuura, Y., Kaibuchi, K. (1996b) Phosphorylation and activation of myosin by Rho-associated kinase (Rho-kinase). *J. Biol. Chem.* **271**, 20246-9

Amano, M., Mukai, H., Ono, Y., Chihara, K., Matsui, T., Hamajima, Y., Okawa, K., Iwamatsu, A., Kaibuchi, K. (1996a) Identification of a putative target for Rho as the serine-threonine kinase protein kinase N. *Science*. **271**, 648-50

Biou, V., Yaremchuk, A., Tukalo, M., Cusack, S. (1994) The 2.9 A crystal structure of T. thermophilus seryl-tRNA synthetase complexed with tRNA(Ser). *Science*. **263**, 1404-10

Bishop, A.L., Hall, A. (2000) Rho GTPases and their effector proteins. *Biochem. J.* **348**, 241-55

Blundell, T., Barlow, D., Borkakoti, N., Thornton, J. (1983) Solvent-induced distortions and the curvature of alpha-helices. *Nature*. **306**, 281-3

Brunger, A. T. Adams, P. D. Clore, G. M. DeLano, W. L. Gros, P. R. Grosse-Kunstleve, W. Jiang, J. S. Kuszewski, J. Nilges, M. Pannu, N. S. Read, R. J. Rice, L. M. Simonson, T. and Warren Warren, G. L. (1998) *Crystallography & NMR System*: A New Software Suite for Macromolecular Structure Determination. *Acta. Cryst.* **D54**, 905-921

Bush, E. W., Helmke, S. M., Birnbaum, R. A., Perryman, M. B. (2000) Myotonic dystrophy protein kinase domains mediate localization, oligomerization, novel catalytic activity, and autoinhibition. *Biochemistry.* **39**, 8480-90

Chook, Y. M., Blobel, G. (1999) Structure of the nuclear transport complex karyopherin-beta2-Ran x GppNHp. *Nature.* **399**, 230-7

Crowther, R.A. (1972) *The molecular replacement.* In "Int. Sci. Rev. No. 13", Rossmann, M. G. ed. (Gordon and Breach, New York) pp.173-178

Crowther, R. A. and Blow, D. M. (1967) A method of positioning a known molecule in an unknown crystal structure. *Acta Cryst.* **23**, 544-548

Cusack, S., Berthet-Colominas, C., Hartlein, M., Nassar, N., Leberman, R. (1990) A second class of synthetase structure revealed by X-ray analysis of Escherichia coli seryl-tRNA synthetase at 2.5 A. *Nature.* **347**, 249-55

Day, C. L., Alber, T. (2000) Crystal structure of the amino-terminal coiled-coil domain of the APC tumor suppressor. *J. Mol. Biol.* **301**, 147-56

De La Fortelle, E. and Bricogne, G. (1997) Maximum-Likelihood Heavy-Atom Parameter Refinement for Multiwavelength Anomalous Diffraction Methods. Methods Enzymol. 276, 472-494

Drugan, J. K., Khosravi-Far, R., White, M. A., Der, C. J., Sung, Y. J., Hwang, Y. W., Campbell, S. L. (1996) Ras interaction with two distinct binding domains in Raf-1 may be required for Ras transformation. *J. Biol. Chem.* **271**, 233-7

Emerson, S. D., Madison, V. S., Palermo, R. E., Waugh, D. S., Scheffler, J. E., Tsao, K. L., Kiefer, S. E., Liu, S. P., Fry, D.C. (1995) Solution structure of the Ras-binding domain of c-Raf-1 and identification of its Ras interaction surface. *Biochemistry.* **34**, 6911-8

Fabian, J.R., Vojtek, A.B., Cooper, J.A., Morrison, D.K. (1994) A single amino acid change in Raf-1 inhibits Ras binding and alters Raf-1 function. *Proc. Natl. Acad. Sci. U S A.* **91**, 5982-6

Flynn, P., Mellor, H., Palmer, R., Panayotou, G., Parker, P. J. (1998) Multiple interactions of PRK1 with RhoA. Functional assignment of the Hr1 repeat motif. *J. Biol. Chem.* **273**, 2698-705

Fujisawa, K., Fujita, A., Ishizaki, T., Saito, Y., Narumiya, S. (1996) Identification of the Rho-binding domain of p160ROCK, a Rho-associated coiled-coil containing protein kinase. *J. Biol.*

Chem. **271**, 23022-8

Fujisawa, K., Madaule, P., Ishizaki, T., Watanabe, G., Bito, H., Saito, Y., Hall, A., Narumiya, S. (1998) Different regions of Rho determine Rho-selective binding of different classes of Rho target molecules. *J. Biol. Chem.* **273**, 18943-9

Geyer, M., Herrmann, C., Wohlgemuth, S., Wittinghofer, A., Kalbitzer, H. R. (1997) Structure of the Ras-binding domain of RalGEF and implications for Ras binding and signalling. *Nat. Struct. Biol.* **4**, 694-9

Hall, A. (1998) Rho GTPases and the actin cytoskeleton. *Science.* **279**, 509-14

Herrmann, C., Horn, G., Spaargaren, M., Wittinghofer, A. (1996) Differential interaction of the ras family GTP-binding proteins H-Ras, Rap1A, and R-Ras with the putative effector molecules Raf kinase and Ral-guanine nucleotide exchange factor. *J. Biol. Chem.* **271**, 6794-800

Holm, L., Sander, C. (1995) Dali: a network tool for protein structure comparison. *Trends. Biochem. Sci.* **20**, 478-80

Hotta, K., Tanaka, K., Mino, A., Kohno, H., Takai, Y. (1996) Interaction of the Rho family small G proteins with kinectin, an anchoring protein of kinesin motor. Biochem. *Biophys. Res. Commun.* **225**, 69-74

Huang, L., Weng, X., Hofer, F., Martin, G. S., Kim, S. H. (1997) Three-dimensional structure of the Ras-interacting domain of RalGDS. *Nat. Struct. Biol.* **4**, 609-15

Hubbard, S. J. and Thornton, J. M. (1993) 'NACCESS', Computer Program, Department of Biochemistry and Molecular Biology, University College London.

Ihara,K. Muraguchi,S. Kato,M. Shimizu,T. Shirakawa,M. Kuroda,S. Kaibuchi,K. and Hakoshima,T. (1998) Crystal structure of human RhoA in a dominantly active form complexed with a GTP analogue. *J.Biol.Chem.* **27**, 9656-9666

Joneson, T., McDonough, M., Bar-Sagi, D., Van, Aelst. L. (1996) RAC regulation of actin polymerization and proliferation by a pathway distinct from Jun kinase. *Science.* **274**, 1374-6

Jones,T.A. Zou, J.Y. Cowan,S.W. and Kjeldgaad,M. (1991) Improved methods for building protein models in electron density maps and the location of errors in these models. *Acta Cryst.* **A47**, 110-119

Kaibuchi, K., Kuroda, S., Amano, M. (1999) Regulation of the cytoskeleton and cell adhesion

by the Rho family GTPases in mammalian cells. *Annu. Rev. Biochem.* **68**, 459-86

Kawamata, T., Taniguchi, T., Mukai, H., Kitagawa, M., Hashimoto, T., Maeda, K., Ono, Y., Tanaka, C. (1998) A protein kinase, PKN, accumulates in Alzheimer neurofibrillary tangles and associated endoplasmic reticulum-derived vesicles and phosphorylates tau protein. *J. Neurosci.* **18**, 7402-10

Kikuchi, A., Demo, S. D., Ye, Z. H., Chen, Y. W., Williams, L. T. (1994) ralGDS family members interact with the effector loop of ras p21. *Mol. Cell Biol.* **14**, 7483-91

Kimura, K., Ito, M., Amano, M., Chihara, K., Fukata, Y., Nakafuku, M., Yamamori, B., Feng, J., Nakano, T., Okawa, K., Iwamatsu, A., Kaibuchi, K. (1996) Regulation of myosin phosphatase by Rho and Rho-associated kinase (Rho-kinase). *Science.* **273**, 245-8

Kishida, S., Shirataki, H., Sasaki, T., Kato, M., Kaibuchi, K., Takai, Y. (1993) Rab3A GTPase-activating protein-inhibiting activity of Rabphilin-3A, a putative Rab3A target protein. *J. Biol. Chem.* **268**, 22259-61

Kitagawa, M., Shibata, H., Toshimori, M., Mukai, H., Ono, Y. (1996) The role of the unique motifs in the amino-terminal region of PKN on its enzymatic activity. *Biochem. Biophys. Res. Commun.* **220**, 963-8

Kitagawa, M., Mukai, H., Shibata, H., Ono, Y. (1995) Purification and characterization of a fatty acid-activated protein kinase (PKN) from rat testis. *Biochem. J.* **310**, 657-64

Kozma, R., Ahmed, S., Best, A., Lim, L. (1995) The Ras-related protein Cdc42Hs and bradykinin promote formation of peripheral actin microspikes and filopodia in Swiss 3T3 fibroblasts. *Mol. Cell. Biol.* **15**, 1942-52

Kraulis, P. J. (1991) MOLSCRIPT - A program to produce both detailed and schematic plots of protein structures. *J. Appl. Crystallogr.* **24**, 946-950

Kumar, J., Erickson, H. P., Sheetz, M. P. (1998) Ultrastructural and biochemical properties of the 120-kDa form of chick kinectin. *J. Biol. Chem.* **273**, 31738-43

Lamarche, N., Tapon, N., Stowers, L., Burbelo, P. D., Aspenstrom, P., Bridges, T., Chant, J., Hall, A. (1996) Rac and Cdc42 induce actin polymerization and G1 cell cycle progression independently of p65PAK and the JNK/SAPK MAP kinase cascade. *Cell.* **87**, 519-29

Laskowski, R.A. MacArthur,M.W. Moss,D.S. and Thornton,J.M. (1993) Programs to check the Stereochemical Quality of Protein Structures. *J.App.Cryst.* **26**, 283

Lei, M., Lu, W., Meng, W., Parrini, M. C., Eck, M. J., Mayer, B. J., Harrison, S. C. (2000) Structure of PAK1 in an autoinhibited conformation reveals a multistage activation switch. *Cell.* **102**, 387-97

Leung, T., Chen, X. Q., Manser, E., Lim, L. (1996) The p160 RhoA-binding kinase ROK alpha is a member of a kinase family and is involved in the reorganization of the cytoskeleton. *Mol. Cell. Biol.* **16**, 5313-27

Leung, T., Manser, E., Tan, L., Lim, L. (1995) A novel serine/threonine kinase binding the Ras-related RhoA GTPase which translocates the kinase to peripheral membranes. *J. Biol. Chem.* **270**, 29051-4

Lu, Y., Settleman, J. (1999) The Drosophila Pkn protein kinase is a Rho/Rac effector target required for dorsal closure during embryogenesis. *Genes. Dev.* **13**, 1168-80

Madaule P, Eda M, Watanabe N, Fujisawa K, Matsuoka T, Bito H, Ishizaki T, Narumiya S. (1998) Role of citron kinase as a target of the small GTPase Rho in cytokinesis. *Nature.* **394**, 491-4

Manser, E., Leung, T., Salihuddin, H., Tan, L., Lim, L. (1993) A non-receptor tyrosine kinase that inhibits the GTPase activity of p21cdc42. *Nature.* **363**, 364-7

Manser, E., Leung, T., Salihuddin, H., Zhao, Z.S., Lim, L. (1994) A brain serine/threonine protein kinase activated by Cdc42 and Rac1. *Nature.* **367**, 40-6

Matsui, T., Amano, M., Yamamoto, T., Chihara, K., Nakafuku, M., Ito, M., Nakano, T., Okawa, K., Iwamatsu, A., Kaibuchi, K. (1996) Rho-associated kinase, a novel serine/threonine kinase, as a putative target for small GTP binding protein Rho. *EMBO. J .* **15**, 2208-16

Matsuzawa, K., Kosako, H., Inagaki, N., Shibata, H., Mukai, H., Ono, Y., Amano, M., Kaibuchi, K., Matsuura, Y., Azuma, I., Inagaki, M. (1997) Domain-specific phosphorylation of vimentin and glial fibrillary acidic protein by PKN. *Biochem. Biophys. Res. Commun.* **234**, 621-5

Matthews, B. W. (1968) Solvent content of protein crystals. *J. Mol. Biol.* **33**, 491-7

Merritt, E. A. and Murphy M. E. P. (1994) *Raster3D* Version 2.0. A program for photorealistic molecular graphics. *Acta Cryst.* **D50**, 869-873

Milburn, M. V., Tong, L., deVos, A. M., Brunger, A., Yamaizumi, Z., Nishimura, S., Kim, S. H. (1990) Molecular switch for signal transduction: structural differences between active and

inactive forms of protooncogenic ras proteins. *Science*. **247**, 939-45

Morii, N., Sekine, A., Ohashi, Y., Nakao, K., Imura, H., Fujiwara, M., Narumiya, S. (1988) Purification and properties of the cytosolic substrate for botulinum ADP-ribosyltransferase. Identification as an Mr 22,000 guanine nucleotide-binding protein. J. *Biol. Chem.* **263**, 12420-6

Mott HR, Owen D, Nietlispach D, Lowe PN, Manser E, Lim L, Laue ED.
(1999) Structure of the small G protein Cdc42 bound to the GTPase-binding domain of ACK. *Nature*. **399**, 384-8

Mukai, H., Kitagawa, M., Shibata, H., Takanaga, H., Mori, K., Shimakawa, M., Miyahara, M., Hirao, K., Ono, Y. (1994) Activation of PKN, a novel 120-kDa protein kinase with leucine zipper-like sequences, by unsaturated fatty acids and by limited proteolysis. *Biochem. Biophys. Res. Commun.* **204**, 348-56

Mukai, H., Ono, Y. (1994) A novel protein kinase with leucine zipper-like sequences: its catalytic domain is highly homologous to that of protein kinase C. *Biochem. Biophys. Res. Commun.* **199**, 897-904

Mukai H, Toshimori M, Shibata H, Kitagawa M, Shimakawa M, Miyahara M, Sunakawa H, Ono Y. (1996) PKN associates and phosphorylates the head-rod domain of neurofilament protein. *J. Biol. Chem.* **271**, 9816-22

Mukai, H., Toshimori, M., Shibata, H., Takanaga, H., Kitagawa, M., Miyahara, M., Shimakawa, M., Ono, Y. (1997) Interaction of PKN with alpha-actinin. *J. Biol. Chem.* **272**, 4740-6

Murzin, A. G., Brenner, S. E., Hubbard, T., Chothia, C. (1995) SCOP: a structural classification of proteins database for the investigation of sequences and structures. *J. Mol. Biol.* **247**, 536-40

Nassar, N., Horn, G., Herrmann, C., Scherer, A., McCormick, F., Wittinghofer, A. (1995) The 2.2 A crystal structure of the Ras-binding domain of the serine/threonine kinase c-Raf1 in complex with Rap1A and a GTP analogue. *Nature*. **375**, 554-60
Navaza,J. (1994) Amore: an Automated package for molecular replacement. *Acta Cryst.* **A50**, 157-163

Nicholls, A. Bharadwaj, R. and Honig, B. (1993) GRASP - graphical representation and analysis of surface properties. *Biophys. J.* **64**, A166

Nishizuka, Y. (1995) Protein kinase C and lipid signaling for sustained cellular responses.

FASEB. J. **9**, 484-96

Nobes, C.D., Hall, A. (1995) Rho, rac, and cdc42 GTPases regulate the assembly of multimolecular focal complexes associated with actin stress fibers, lamellipodia, and filopodia. *Cell.* **81**, 53-62

Ostermeier C, Brunger AT. (1999) Structural basis of Rab effector specificity: crystal structure of the small G protein Rab3A complexed with the effector domain of rabphilin-3A. *Cell.* **96**, 363-74

Otwinowski, Z. and Minor, W. (1996) Processing of X-ray diffraction data collected in oscillation mode. *Methods Enzymol.* **276**, 307-326

Palmer, R. H., Dekker, L. V., Woscholski, R., Le Good, J. A., Gigg, R., Parker, P. J. (1995b) Activation of PRK1 by phosphatidylinositol 4,5-bisphosphate and phosphatidylinositol 3,4,5-trisphosphate. A comparison with protein kinase C isotypes. *J. Biol. Chem.* **270**, 22412-6

Palmer, R. H., Dekker, L. V., Woscholski, R., Le Good, J. A., Gigg, R., Parker, P. J. (1995a) Activation of PRK1 by phosphatidylinositol 4,5-bisphosphate and phosphatidylinositol 3,4,5-trisphosphate. A comparison with protein kinase C isotypes. *J. Biol. Chem.* **270**, 22412-6

Palmer, RH., Ridden, J., Parker, P.J. (1995) Cloning and expression patterns of two members of a novel protein-kinase-C-related kinase family. *Eur. J. Biochem.* **227**, 344-51

Peng, B., Morrice, N. A., Groenen, L. C., Wettenhall, R. E. (1996) Phosphorylation events associated with different states of activation of a hepatic cardiolipin/protease-activated protein kinase. Structural identity to the protein kinase N-type protein kinases. *J. Biol. Chem.* **271**, 32233-40

Reid, T., Furuyashiki, T., Ishizaki, T., Watanabe, G., Watanabe, N., Fujisawa, K., Morii, N., Madaule, P., Narumiya, S. (1996) Rhotekin, a new putative target for Rho bearing homology to a serine/threonine kinase, PKN, and rhophilin in the rho-binding domain. *J. Biol. Chem.* **271**, 13556-60

Ridley, A.J., Hall, A. (1992) The small GTP-binding protein rho regulates the assembly of focal adhesions and actin stress fibers in response to growth factors. *Cell.* **70**, 389-99

Ridley, A. J., Paterson, H. F., Johnston, C. L., Diekmann, D., Hall, A. (1992) The small GTP-binding protein rac regulates growth factor-induced membrane ruffling. *Cell.* **70**, 401-10

Rittinger, K., Walker, P. A., Eccleston, J. F., Smerdon, S. J., Gamblin, S. J. (1997) Structure at 1.65 A of RhoA and its GTPase-activating protein in complex with a transition-state

analogue. *Nature.* **389**, 758-62

Rossmann, M. G. and Blow, D. M. (1962) The detection of sub-units within the crystallographic asymmetric unit. *Acta. Cryst.* **15**, 24-31

Sahai, E., Alberts, A. S., Treisman, R. (1998) RhoA effector mutants reveal distinct effector pathways for cytoskeletal reorganization, SRF activation and transformation. *EMBO. J.* **17**, 1350-61

Schurr, J. M. (1977) Dynamic light scattering of biopolymers and biocolloids. *CRC. Crit. Rev. Biochem.* **4**, 371-431

Sekine, A., Fujiwara, M., Narumiya, S. (1989) Asparagine residue in the rho gene product is the modification site for botulinum ADP-ribosyltransferase. *J. Biol. Chem.* **264**, 8602-5

Shibata, H., Mukai, H., Inagaki, Y., Homma, Y., Kimura, K., Kaibuchi, K., Narumiya, S., Ono, Y. (1996) Characterization of the interaction between RhoA and the amino-terminal region of PKN. *FEBS. Lett.* **385**, 221-4

Stebbins, C. E., Borukhov, S., Orlova, M., Polyakov, A., Goldfarb, A., Darst, S. A. (1995) Crystal structure of the GreA transcript cleavage factor from Escherichia coli. *Nature.* **373**, 636-40

Takahashi, M., Mukai, H., Toshimori, M., Miyamoto, M., Ono, Y. (1998) Proteolytic activation of PKN by caspase-3 or related protease during apoptosis. *Proc. Natl. Acad. Sci. U S A.* **95**, 11566-71

Takanaga, H., Mukai, H., Shibata, H., Toshimori, M., Ono, Y. (1998) PKN interacts with a paraneoplastic cerebellar degeneration-associated antigen, which is a potential transcription factor. *Exp. Cell. Res.* **241**, 363-72

Tan, I., Seow, K. T., Lim, L., Leung, T. (2001) Intermolecular and intramolecular interactions regulate catalytic activity of myotonic dystrophy kinase-related Cdc42-binding kinase alpha. *Mol. Cell. Biol.* **21**, 2767-78

Tarricone, C., Xiao, B., Justin, N., Walker, P. A., Rittinger, K., Gamblin, S. J., Smerdon, S. J. (2001) The structural basis of Arfaptin-mediated cross-talk between Rac and Arf signalling pathways. *Nature* **411**, 215-9

Tesmer, J. J., Sunahara, R. K., Gilman, A. G., Sprang, S. R. (1997) Crystal structure of the catalytic domains of adenylyl cyclase in a complex with Gsa.GTPgS. *Science.* **278**, 1907-16

Van Aelst, L., D'Souza-Schorey, C. (1997) Rho GTPases and signaling networks. *Genes. Dev.*

11, 2295-322

Vetter, I. R., Nowak, C., Nishimoto, T., Kuhlmann, J., Wittinghofer, A. (1999) Structure of a Ran-binding domain complexed with Ran bound to a GTP analogue: implications for nuclear transport. *Nature.* **398**, 39-46

Vetter, I. R. and Wittinghofer, A. (2001) The guanine nucleotide-binding switch in three dimensions. *Science.* **294**, 1299-304

Walshaw, J., Woolfson, D. N. (2001) Socket: a program for identifying and analysing coiled-coil motifs within protein structures. *J. Mol. Biol.* **307**, 1427-50

Warne, P. H., Viciana, P. R., Downward, J. (1993) Direct interaction of Ras and the amino-terminal region of Raf-1 in vitro. *Nature.* **364**, 352-5

Watanabe, G., Saito, Y., Madaule, P., Ishizaki, T., Fujisawa, K., Morii, N., Mukai, H., Ono, Y., Kakizuka, A., Narumiya, S. (1996) Protein kinase N (PKN) and PKN-related protein rhophilin as targets of small GTPase Rho. *Science.* **271**, 645-8

Weeks, C. M., Miller, R. (1999) Optimizing Shake-and-Bake for proteins. *Acta. Crystallogr.* **D55**, 492-500

Wei, Y., Zhang, Y., Derewenda, U., Liu, X., Minor, W., Nakamoto, R. K., Somlyo, A. V., Somlyo, A. P., Derewenda, Z. S. (1997) Crystal structure of RhoA-GDP and its functional implications. *Nat. Struct. Biol.* **4**, 699-703

Whitby, F. G., Phillips, G. N. Jr. (2000) Crystal structure of tropomyosin at 7 Angstroms resolution. *Proteins.* **38**, 49-59

Wolf, E., Kim, P. S., Berger, B. (1997) MultiCoil: a program for predicting two- and three-stranded coiled coils. *Protein. Sci.* **6**, 1179-89

Yamamoto, K., Kondo, J., Hishida, T., Teranishi, Y., Takai, Y. (1988) Purification and characterization of a GTP-binding protein with a molecular weight of 20,000 in bovine brain membranes. Identification as the rho gene product. *J. Biol. Chem.* **263**, 9926-32

Yan, Y., Winograd, E., Viel, A., Cronin, T., Harrison, S. C., Branton, D. (1993) Crystal structure of the repetitive segments of spectrin. *Science.* **262**, 2027-30

Yoshinaga, C., Mukai, H., Toshimori, M., Miyamoto, M., Ono, Y. (1999) Mutational analysis of the regulatory mechanism of PKN: the regulatory region of PKN contains an arachidonic acid-sensitive autoinhibitory domain. *J. Biochem.* **126**, 475-84

Zhang, X. F., Settleman, J., Kyriakis, J. M., Takeuchi-Suzuki, E., Elledge, S. J., Marshall, M. S., Bruder, J. T., Rapp, U. R., Avruch, J. (1993) Normal and oncogenic p21ras proteins bind to the amino-terminal regulatory domain of c-Raf-1. *Nature*. **364**, 308-13